North Atlantic multidecadal to centennial variability in a model and a marine proxy dataset

Dissertation
zur Erlangung des Doktorgrades
der Mathematisch Naturwissenschaftlichen Fakultät
der Christian-Albrechts-Universität zu Kiel
vorgelegt von

Jennifer Veronika Mecking

Department of Meteorology,
Research Division of Ocean Circulation and Climate Dynamics
Helmholtz Centre for Ocean Research Kiel
Kiel University, Kiel, Germany

May 2013

Contents

Abstract

Variability on decadal and longer timescales is of great interest in climate research due to it's socio-economic impacts, potential for predictability and masking of anthroprogenic global warming. Observational evidence of multidecadal variability in the North Atlantic exists in the sea surface temperature (SST), often referred to as the Atlantic Multidecadal Variability (AMV), and also in the atmosphere, for example seen in sea level pressure variations associated with the North Atlantic Oscillation (NAO). Observational oceanic data on these timescales is mainly restricted to the surface, does not extend past the last 145 years and becomes quite sparsely sampled in the higher latitudes in the earlier years. Hence, to increase our understanding of climate variability on these timescales it is essential to turn to both proxy and model data.

The first part of this thesis focuses on an annually-resolved proxy record (1818-1967) of Mg/Ca variations from a North Pacific/ Bering Sea coralline alga. Not only does the algal Mg/Ca have a very strong connection to the local winter SST and a lagged relation to the Aleutian Low it also it has a correlation of -0.87 with the winter NAO and 0.60 with the AMV index on decadal timescales. The link can explain the coherence of decadal North Pacific and AMV, as suggested by earlier studies using climate models and in the limited observational data.

The second part of the thesis focuses on the ocean general circulation model, NEMO to better understand AMV. For this purpose the model was forced only with the atmospheric patterns associated with the NAO, both from the observed NAO index and from a 2000 year long white NAO index. Focusing on key ocean circulation patterns, we show that the Atlantic Meridional Overturning Circulation (AMOC) and sub-polar gyre (SPG) strength have a red noise response but no dominant timescale, providing no evidence for a oscillatory ocean-only mode of variability. The time derivative of both the AMOC at 30°N and SPG strength

show a strong, almost linear relation to the NAO for timescales longer than 86 and 15 years, respectively. The different response characteristics are confirmed by constructing simple statistical models that show AMOC and SPG variability can be reconstructed by integrating the NAO index by the previous 53 and 10 winters, respectively. Alternatively, the AMOC and the SPG strength can be reconstructed with auto-regressive (AR) models of order seven and five, respectively. A closer look at the ocean model response of the 2000 year long ocean model integration shows three distinct timescales of variability. The first, an interannual timescale with variability shorter than 15 years, can be mainly related to Ekman dynamics. Secondly, the multidecadal timescale, 15-65 years, is mainly concentrated in the SPG and is controlled by temperature variability. Finally, the centennial timescales, with variability longer than 65 years, can be attributed to the ocean being in a series of quasi-equilibrium with the forcing. The statistical models presented in this thesis to reconstruct the AMOC and SPG strength on multidecadal and longer timescales can be useful for prediction and model inter-comparision.

Zusammenfassung

Variabilität auf dekadischen und längeren Zeitskalen ruft in der Klimaforschung aufgrund sozioökonomische Auswirkungen und dem Potential zur Vorhersagbarkeit groβes Interesse hervor. Beobachtungen ergeben, dass die Temperatur der Meeresoberfläche (SST) im Nord-Atlantik multidekadische Variabilität aufweist. Diese wird häufig als Atlantische Multidekadische-Variabilität (AMV) bezeichnet. In der Atmosphäre zeigt sich im Oberflächenluftdruck ebenfalls eine multidekadische Variabilität, die Nord-Atlantik-Oszillation (NAO). Die Beobachtungsdaten dieser Zeitskalen über Ozeane beschränken sich hauptsächlich auf die Oberfläche. Sie sind nur für die letzten 145 Jahre vorhanden und in den höheren Breiten für die frühen Jahre auch nur spärlich. Klimaproxy- und Modelldaten sind für unser Verständnis der Klimavariabilität dieser Zeitskalen unerläβlich.

Der erste Teil dieser Arbeit konzentriert sich auf eine jährlich aufgelöste Klima-Proxy (1818-1967) von Mg/Ca-Variationen einer korallinen Alge aus dem Nord-Pazifik/ Beringsee. Das Algen-Mg/Ca hat nicht nur eine sehr starke Verbindung zum lokalen Winter SST und eine zeitlich verzögerte Beziehung zum Aleutischen Tief; es besteht auch eine Korrelation von -0,87 mit der Winter NAO und eine Korrelation von 0,60 mit dem AMV-Index auf dekadischen Zeitskalen. Wie bereits frühere Studien unter Verwendung von Klimamodellen und durch begrenzte Beobachtungsdaten andeuten, könnte diese Verbindung die Kohärenz des dekadischen Nord-Pazifiks und der AMV erklären.

Der zweite Teil der Arbeit beschäftigt sich mit dem allgemeinen Ozean- Zirkulationsmodell NEMO, das durch das atmosphärische Muster der NAO angetrieben wird. Der zweite Teil der These konzentriert sich auf das allgemeine Ozean Zirkulationsmodell, NEMO, der mit dem atmosphärischen Muster die NAO angetrieben wird, vom beobachteten NAO-Index und von einem 2000-Jahre langen Weiβengeräusch NAO-Index. Durch Untersuchung der relevanten Zirkulationsmuster im

Ozean wird gezeigt, dass die Atlantische Meridionale Umwälzbewegung (AMOC) und die Stärke des Subpolarwirbels (SPG) mit rotem Rauschen reagieren, aber keine dominanten Zeitskalen aufweisen. Somit stellen sie keinen Nachweis für einen Ozean-Schwingungsmodus der Variabilität dar.Die Zeitableitung des AMOC bei 30°N und die SPG-Stärke zeigen eine starke, fast lineare Beziehung zur NAO für Zeiträume von jeweils mehr als 86 und 15 Jahren. Die abweichenden Charakteristika der Reaktionen werden durch einfache statistische Modelle, bestätigt. Diese Modelle zeigen dass AMOC und SPG Variabilität durch Integration des NAO-Index der vorrausgehenden 53, beziehungsweise 10 Winter rekonstruiert werden kann. Alternativ können die AMOC und die SPG-Stärke mit autoregressiven Modellen (AR) der Ordnung 7 beziehungsweise 5 rekonstruiert werden. Ein näherer Blick auf die Reaktion des Ozeans auf die 2000-jährige Ozeanmodellintegration ergibt drei eindeutig verschiedene Zeitskalen der Variabilität. Es hat sich gezeigt, dass Variabilität einer interannualer Zeitskala von weniger als 15 Jahren hauptsächlich mit Ekman-Dynamik zusammenhängt. Des Weiteren konzentriert sich die multidekadische Zeitskala von 16- 65 Jahren hauptsächlich im SPG und wird durch Temperaturvariabilität gesteuert. Schlieβlich können die hundertjährigen Zeitskalen, mit Variabilität von mehr als 65 Jahren, dem Ozean zugeschrieben werden, der in einer Reihe von Quasi-Equilibrium Zuständen ist. Die statistischen Modelle, die in dieser Arbeit dargestellt werden, um die AMOC- und SPG-Stärke auf den multidekadischen und längeren Zeitskalen zu rekonstruieren, können für Vorhersage sowie für Modellvergleiche nützlich sein.

Chapter 1

Introduction

With the current concern about anthroprogenic induced climate change and the inevitable socio-economical impacts, it is becoming increasingly important to be able to understand and predict climate variability on decadal timescales. The North Atlantic is considered to be a region with a high potential for predictability on decadal timescales (*Boer* [2004]), in particular, the subpolar region have been shown to be successful on decadal timescales (*Keenlyside et al.* [2008], *Yeager et al.* [2012] and *Doblas-Reyes et al.* [2013]). The North Atlantic Ocean contains an important thermohaline overturning circulation that transports the majority of the oceanic heat transport in the North Hemisphere (*Wunsch* [2005]). In particular, the Gulf Stream/North Atlantic Current system transports warm, saline waters northwards where the waters then cool and sink in the Labrador and Greenland Seas (*Wunsch et al.* [2002]). Understanding the variability of the North Atlantic component of the thermohaline circulation will be examined in this thesis.

A clear multidecadal signal can be seen in the observed North Atlantic sea surface temperature (SST) variability with a timescale of approximately 70-80 years (*Kerr* [2000]). This signal is often referred to as the Atlantic Multidecadal variability (AMV) or the Atlantic Mutlidecadal Oscillation (*Kerr* [2000], *Enfield et al.* [2001], *Knight et al.* [2005]). A common example of an index for AMV is defined in *Dima*

and Lohmann [2007], section 3a, as the detrended, annual mean SST, computed over the region 0° to 60°N and 75° to 7.5°W (Figure 1.1b). Correlation between this AMV index and the annual mean SST shows a signal that is of the same sign over the entire North Atlantic region. However, a small region of positive correlation is also found along the Aleutian Islands in the North Pacific (Figure 1.1a), suggesting a possible link between the interdecadal variability of the North Atlantic and North Pacific Oceans (more details in Chapter 2). The SST pattern associated with the AMV index is thought to be a surface fingerprinting of climate variability originating in the North Atlantic ocean basin (*Zhang* [2008]).

Observations and model data link the AMV index to several natural phenomena, for example, the frequency of North Atlantic hurricanes, rainfall in the Sahel region and North America, as well as, the river outflow of the Mississippi river (*Goldenberg et al.* [2001],*Zhang and Delworth* [2006],*Enfield et al.* [2001]). Understanding the AMV, as well as the physics behind it, is very desirable due to it's links to climate signals in the surrounding continents. Unfortunately, the observational SST record only extends back to 1870 which is not long enough to confirm whether the AMV index is truly oscillatory or if it is more like a random white or red noise process. Despite more subsurface observational data starting to become available through, for example, the RAPID array (*Cunningham et al.* [2007]), these datasets all have a very short record. To extend our knowledge of the AMV it is essential to turn to both proxy records and modelling studies.

Several types of proxy records reconstructing the variability in the North Atlantic region have been studied. Among these records are ice core data from Greenland and Ellesmere Island which describes North Atlantic variability with a dominant timescale of 20 years (*Chylek et al.* [2011]). Coral data analyzing annual growth rates or $\delta^{18}O$, from the Caribbean, can also be used as a proxy for the AMV and show multidecadal timescales similar to the observed AMV index (*Kilbourne et al.*

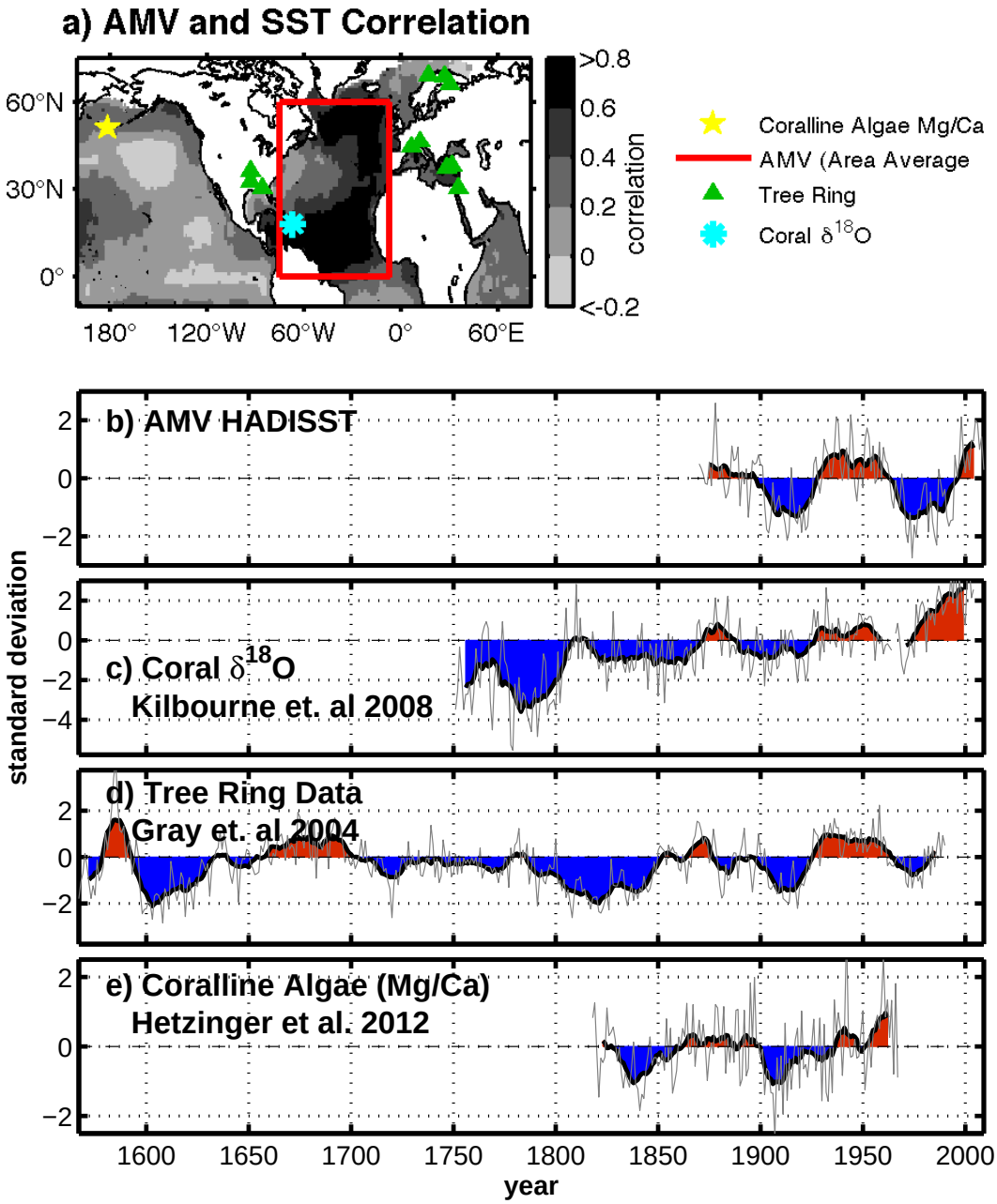

Figure 1.1: a) Correlation of the AMV index with SST from HadiSST (*Rayner et al.* [2003]) (shading), locations of various proxy data (star, triangles and asterisk) and the area used to compute the AMV index (red box). b) AMV index from observed SSTs, c) Coral δ^{18} data from a Caribbean coral (*Kilbourne et al.* [2008]), d) Tree ring data (*Gray et al.* [2004]) and e) the Coralline Algae Mg/Ca record (*Hetzinger et al.* [2012]). The grey lines are annual values and black lines with shading show 11 year running means. All timeseries are detrended over the time period 1870 to 1967.

[2008]/Figure 1.1c, *Hetzinger et al.* [2008] and *Saenger et al.* [2009]). In the study by *Gray et al.* [2004], tree ring data from several trees surrounding the North Atlantic Ocean (Figure 1.1a & d) were used to reconstruct an AMV index with an explained variance of 94% of the observed AMV index in the 20th century on decadal timescales. The available proxy data however show discrepancies before the 20th century (Figure 1.1). Some of these proxy records also indicate multiple timescales in the North Atlantic (*Saenger et al.* [2009] and *Chylek et al.* [2012]). Recently high latitude marine based coralline algae have been shown to be a useful proxy for local SSTs (*Hetzinger et al.* [2009]). A coralline algae sample from the Aleutian islands has shown a strong relation to the AMV index as well as the dominate atmospheric signal in the North Atlantic, the North Atlantic Oscillation (NAO) (Figure 1.1e, more details in Chapter 2).

The NAO is the dominate signal in the North Atlantic atmosphere explaining up to 31% of the variance in the winter mean air temperature anomalies over the North Atlantic (*Hurrell* [1995]). The NAO pattern was first described by Sir Gilbert Walker in 1924 when he examined station recorded sea level pressure (SLP) data from around the world (*Walker* [1924]). The NAO index measures the difference in pressure between the area of high SLP over the Azores and the low SLP over Iceland (Figure 1.2a). There are several ways to define the NAO index, some based on differences in winter station based SLP measurements and others based on the the first empirical orthogonal function of the winter mean SLP over the North Atlantic, all of which give a very similar signal (*Jones et al.* [2003]). Instrumental records of the NAO index go back to the early 1820's (*Jones et al.* [1997]) and show that the NAO has undergone multidecadal variations giving it a weakly red spectrum (*Wunsch* [1999], Figure 1.2b). Several northern hemispheric weather phenomena can be linked to variations in the NAO index (*Greatbatch* [2000] and *Hurrell et al.* [2003]), hence understanding NAO related variability would be very beneficial. Similar to the AMV index, several proxy records attempt to reconstruct the NAO index with

some success where instrumental data are available (*Cook* [2003]). Several studies have shown that the NAO can influence the variability in the North Atlantic Ocean (*Dickson et al.* [1996], *Visbeck et al.* [1998], *Curry and McCartney* [2001], *Eden and Jung* [2001], *Eden and Willebrand* [2001], *Visbeck et al.* [2003], *Köller et al.* [2010], and *Latif and Keenlyside* [2011]). In particular convection in the Labrador Sea is thought to be controlled by the NAO (*Dickson et al.* [1996], *Eden and Willebrand* [2001], *Eden and Jung* [2001] and *Latif et al.* [2006]). The NAO is not the only pattern that can drive to variability in the North Atlantic Ocean. The East Atlantic Pattern and the Scandinavian Pattern (*Barnston and Livezey* [1987]) can contribute to ocean variability (*Msadek and Frankignoul* [2009] and *Medhaug et al.* [2012]), at least in models, although their importance in the real world is not clear.

In the North Atlantic branch of the thermohaline circulation, there is a clear northward transport in the upper layers of the ocean with sinking in the Labrador Sea and Greenland Sea and a deeper return flow. This meridional transport in the North Atlantic is referred to as the Atlantic Meridional Overturning Circulation (AMOC) and can be computed as follows:

$$MOC(y,z,t) = \int_{-H}^{z} \int_{west}^{east} v(x,y,z',t)dxdz', \tag{1.1}$$

where v are the meridional currents and H is the ocean depth (described in section 6 of *Wunsch* [2012]). The AMOC plays an important role in the dynamics of multi-decadal variability in the Atlantic in several modelling studies (e.g. *Delworth et al.* [1993], *Delworth and Greatbatch* [2000], *Vellinga and Wu* [2004] and *Dijkstra et al.* [2006]). Observations of the AMOC is very limited; the RAPID array provides the AMOC strength at 26.5°N since 2004 and shows a mean value of 18.7 Sv (1Sv = 10^6 m^3/s) (*Cunningham et al.* [2007]). This record is unfortunately too short to be able to gain an insight into the multidecadal nature of the AMOC, suggesting that one needs to turn to modelling studies. Large uncertainties exist in past changes in the

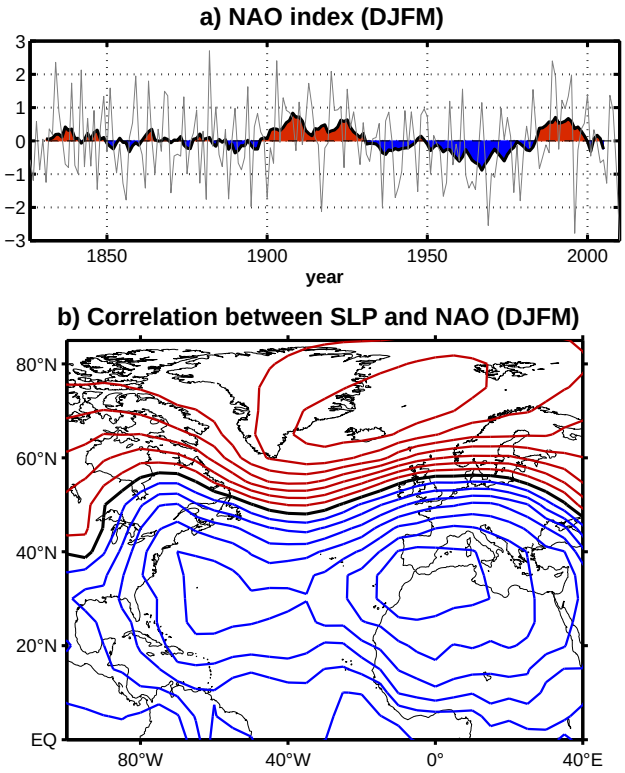

Figure 1.2: a) December, January, February and March (DJFM) mean NAO index, computed from SLP difference between Gibraltar and Iceland (*Jones et al.* [1997]). Grey lines are annual values and shaded lines are filtered with 11 year running mean. b) Correlation between the DJFM mean HADSLP2 sea level pressure data (1850 - 2004, *Allan and Ansell* [2006]) and the DJFM NAO index. Contours are spaced 0.1 apart, thick black line is 0 correlation, red positive correlation and blue negative correlation.

AMOC (*Bryden et al.* [2005] and *Latif et al.* [2006]), and large disagreement among ocean reanalysis (*Keenlyside and Ba* [2010]). The AMOC computed from several model studies shows variability ranging from 20 years (e.g. *Danabasoglu* [2008]) to centennial timescales (e.g., *Menary et al.* [2012]). Despite the differences among the various models, there is often a clear connection between the model AMOC and AMV index, with the AMOC leading the AMV index by approximately 5 years (*Latif et al.* [2004] and Ba et al., in preparation). Several mechanisms have been suggested for explaining AMOC variability, involving convection (e.g. *Delworth et al.* [1993], *Eden and Jung* [2001], *Latif and Keenlyside* [2011] and *Medhaug et al.* [2012]), a role for subpolar gyre dynamics (e.g. *Delworth et al.* [1993]), signals from the Arctic (*Jungclaus et al.* [2005]) and coupled atmosphere-ocean dynamics (e.g. *Timmermann et al.* [1998] and *Vellinga and Wu* [2004]).

Not only is the vertical circulation of the North Atlantic important but also the horizontal circulation. The barotropic streamfunction of the vertically averaged transport in the North Atlantic shows two main regions of circulation, the subtropical gyre, a clockwise ocean gyre centered in the tropics, and the subpolar gyre (SPG), a counter-clockwise circulation centered at 60°N. These two ocean gyres are separated by the Gulf Stream/North Atlantic Current and their underlying dynamics was first explained by *Sverdrup* [1947], *Stommel* [1948] and *Munk* [1950]. The strength of the SPG can be measured through the sea surface height, which can be measured by altimetry data going back to 1994, or in models through taking and area mean of the barotropic streamfunction in the subpolar gyre region (*Lohmann et al.* [2009]). The study by *Curry and McCartney* [2001] showed that the NAO can be linked to the zonal transport across the Atlantic (southern part of the SPG; northern part of the subtropical gyre). The modelling study by *Langehaug et al.* [2012] showed that the strength of the SPG can be connected to the Labrador Sea water thickness, Greenland-Scotland overflow and the East Atlantic Pattern (*Barnston and Livezey* [1987]). A mechanism, involving the changes in density in the

center of the SPG caused by changes in convection and leading to a SPG variability of around 20 years, was described in *Born and Mignot* [2012]. In several studies the SPG also plays a role in the mechanism driving variability in the AMOC (e.g. *Delworth et al.* [1993] and *Böning et al.* [2006]) as well as northwards heat transport North of 45°N (e.g. *Häkkinen* [1999] and *Gulev et al.* [2003]).

This thesis focuses on the connection between the NAO, the AMV and ocean circulation. Chapter 2 examines a marine proxy record from the North Pacific that shows strong connections to both the NAO index and the AMV index, as well an inter-basin connection between the North Atlantic and North Pacific. The main concern of the remainder of the thesis is to what extent can AMV be explained by a stochastically forced ocean model. Chapter 3 analyzes the results from an ocean general circulation model (OGCM) forced using a stochastically varying NAO index and builds statistical relationships between the NAO index and the AMOC at 30°N and the SPG strength. Chapter 4 goes further into results from the stochastically forced NAO model run and describes some of the mechanisms behind the various timescales of variability. Finally, the last chapter provides a summary of the results shown and a brief outlook.

Chapter 2

Marine proxy evidence linking decadal North Pacific and Atlantic climate

S. Hetzinger (1,2*), J. Halfar (1), **J. V. Mecking** (3), N. S. Keenlyside (3), A. Kronz (4), R. S. Steneck (5), W. H. Adey (6), P. A. Lebednik (7)

Published in Climate Dynamics[1]

(1) CPS-Department, University of Toronto Mississauga, 3359 Mississauga Rd. N, Mississauga, ON, L5L 1C6, Canada
(2) IFM-GEOMAR, Leibniz Institute of Marine Sciences, Wischhofstr. 1-3, 24148 Kiel, Germany
(3) IFM-GEOMAR, Leibniz Institute of Marine Sciences, Dsternbrooker Weg 20, 24105 Kiel, Germany
(4) Geowissenschaftliches Zentrum, University of Gttingen, Goldschmidtstr. 1, 37077 Göttingen, Germany
(5) Darling Marine Center, University of Maine, 193 Clarks Cove Road, Walpole, ME 04573, USA
(6) Department of Botany, Smithsonian Institution, 10th and Constitution Ave, NW, Washington, DC 20560-0166, USA
(7) ARCADIS U.S. Inc., 2033 North Main Street, Suite 340, Walnut Creek, CA 94596, USA

*corresponding author: shetzinger@ifm-geomar.de, phone: +49-431-600-2314, fax: +49-431-600-2925.

[1]S. Hetzinger, J. Halfar, **J. V. Mecking**, N. S. Keenlyside, A. Kronz, R. S. Steneck, W. H. Adey, P. A. Lebednik 2012: Marine proxy evidence linking decadal North Pacific and Atlantic climate, Climate Dynamics, doi:10.1007/s00382-011-1229-4

2.1 Abstract

Decadal- to multidecadal variability in the extra-tropical North Pacific is evident in 20th century instrumental records and has significant impacts on Northern Hemisphere climate and marine ecosystems. Several studies have discussed a potential linkage between North Pacific and Atlantic climate on various time scales. On decadal time scales no relationship could be confirmed, potentially due to sparse instrumental observations before 1950. Proxy data are limited and no multi-centennial high-resolution marine geochemical proxy records are available from the subarctic North Pacific.

Here we present an annually-resolved record (1818-1967) of Mg/Ca variations from a North Pacific/ Bering Sea coralline alga that extends our knowledge in this region beyond available data. It shows for the first time a statistically significant link between decadal fluctuations in sea-level pressure (SLP) in the North Pacific and North Atlantic. The record is a lagged proxy for decadal-scale variations of the Aleutian Low. It is significantly related to regional sea surface temperature (SST) and the North Atlantic Oscillation (NAO) index in late boreal winter on these time scales. Our data show that on decadal time scales a weaker Aleutian Low precedes a negative NAO by several years. This atmospheric link can explain the coherence of decadal North Pacific and Atlantic Multidecadal Variability (AMV), as suggested by earlier studies using climate models and limited instrumental data.

Keywords: Aleutian Low, North Atlantic Oscillation, North Pacific, Atlantic Multidecadal Variability, Mg/Ca, coralline algae

2.2 Introduction

A better knowledge of past decadal to interdecadal surface ocean variability in the North Pacific/Bering Sea is crucial in order to predict the impacts of anthropogenic climate change on the diverse Bering Sea ecosystem. The Bering Sea, a region transitional between the Subarctic and Arctic, is particularly sensitive to warming due to its seasonal ice cover (*Sigler et al.* [2010]). A continuing trend to warmer temperatures, as reported for the past decade (*Overland and Stabeno* [2004]), would have major impacts on commercial and subsistence fisheries and sea-bird and marine mammal populations (*Grebmeier et al.* [2006]).

North Pacific climate exhibits significant decadal- to interdecadal variability (*Trenberth and Hurrell* [1994]; *Mantua et al.* [1997]) that may be unrelated to externally forced climate change. These variations have been linked to ocean dynamics (*Latif and Barnett* [1994]), air-sea interaction with the subtropical Pacific (*Liu et al.* [2002]), and extra-tropical - tropical interactions (*Deser et al.* [2004]). Models suggest that AMV can contribute to North Pacific variability (*Zhang and Delworth* [2007]). This is supported by the analysis of observational SST data (*dOrgeville and Peltier* [2007]). However, debate continues on the mechanisms and physical processes driving multidecadal SST variability in the North Pacific, and it is not clear whether Pacific decadal variability and AMV are related or independent (*Park and Latif* [2010]).

On shorter time scales atmospheric variability in the North Pacific and North Atlantic are linked in winter by the annular mode, the leading pattern of Northern Hemisphere wintertime atmospheric circulation (*Thompson and Wallace* [1998]). This connection describes an out-of-phase relationship between the Aleutian and Icelandic lows, particularly evident during recent decades (*Honda et al.* [2001]). The Aleutian and Icelandic lows are semipermanent wintertime low-pressure systems centered over the North Pacific and North Atlantic oceans that are closely

related to the Pacific/North American pattern (*Wallace and Gutzler* [1981]) and the NAO (*Hurrell* [1995]), respectively. These low-pressure systems strongly affect extra-tropical Northern Hemisphere climate, particularly influencing winter weather conditions over North America and Europe (*Trenberth and Hurrell* [1994]; *Honda et al.* [2005]). On decadal time scales, however, little is known about interbasin linkages, as available observational data are very limited in length and results are sensitive to the methods used (*Müller et al.* [2008]; *Schwing et al.* [2003]). In the North Pacific/ Bering Sea region observational data are only available starting 1900 with reasonably good measurement coverage for SST existing from the mid-1950s (Fig. 2.1a).

Although decadal and multidecadal variability, such as the Pacific Decadal Oscillation (PDO) (*Mantua et al.* [1997]), has been detected in paleo-proxy archives, most high-resolution climate reconstructions for the North Pacific were inferred from terrestrial archives (*MacDonald and Case* [2005]). However, these records, often derived from tree-ring chronologies, do not provide the corresponding SST patterns (*dOrgeville and Peltier* [2007]). Recent studies have shown that encrusting coralline algae are well suited as recorders of extra-tropical paleoclimatic signals because of their (1) common occurrence in mid- to high-latitude oceans, (2) multicentury lifespan (*Halfar et al.* [2011]), and (3) ability to produce annual incremental growth patterns in a high Mg-calcite framework that can be targeted for high-resolution geochemical sampling (*Halfar et al.* [2007]; *Williams et al.* [2010]). Past SST variations have previously been reconstructed from the coralline species Clathromorphum nereostratum (*Hetzinger et al.* [2009]), which is widely distributed on rocky substrate along central northern Pacific coastlines (*Adey et al.* [2008]).

Using annually resolved climate data derived from a coralline alga, we show that an interbasin link exists between the North Pacific and North Atlantic on decadal time scales. Specifically, we use annually-resolved skeletal Mg/Ca variations in a 150-

year old coralline alga (Clathromorphum nereostratum; 1818-1967; Amchitka Island, Aleutians, Alaska; Supplementary Figure 2.6) as a proxy for past SST variability.

2.3 Materials and Methods

2.3.1 Sample collection

A 5 cm thick crust of the crustose coralline alga Clathromorphum nereostratum was collected live in August 1969 from 25 m water depth off Amchitka Island, Alaska (Kirlof Point; 51°24.936'N, 179°17.976'E; specimen AM-KR-80 8-69-14B, Supplementary Figure 2.6) in the western Bering Sea-Aleutian Island region (Fig. 2.1). The sample is part of a collection of coralline algae that was obtained for an extensive systematic study of the coralline flora of the Pacific Coast in the late 1960s and early 1970s (*Lebednik* [1977]) and was provided by the U.S. National Herbarium of the Smithsonian Institution, Washington DC. In an earlier study using the upper portion of this long-lived plant (1902-1967), it was shown that algal Mg/Ca ratios are suitable as a proxy for paleotemperature variations (*Hetzinger et al.* [2009]). Here, Mg/Ca ratios of individual growth increments were analyzed by measuring single-point electron microprobe transects, yielding a 150-year record (1818-1967) with a temporal resolution of ca. 15 samples/year. Detailed description of sample preparation procedures was presented in *Hetzinger et al.* [2009].

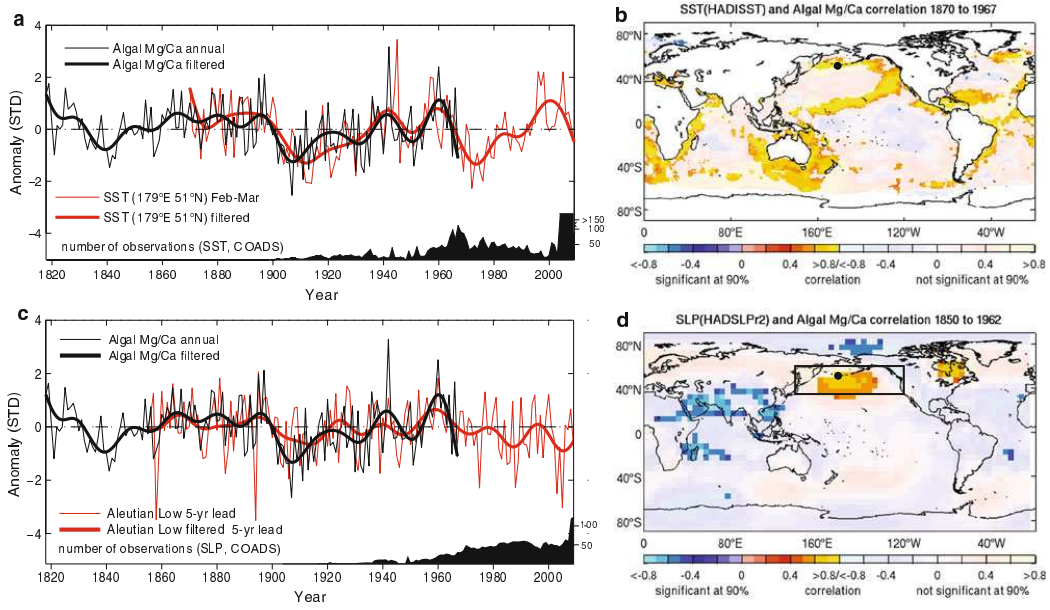

Figure 2.1: Algal Mg/Ca time series and its relation to sea surface temperature and sea level pressure. (a) Unfiltered (thin lines) and filtered (15-year low-pass, thick lines) variations in algal Mg/Ca from Amchitka Island (black) and local SST (Feb-Mar; red). Correlation between filtered data is r = 0.85 (significant at 96%, 1870-1967). Average number of monthly observations in instrumental SST data for the study site (shaded). No data are available before 1900, before 1960 number of monthly observations decreases markedly (often <15/month), after 2004 it is greater than 150/month. (b) Correlation map between filtered algal Mg/Ca and global SST anomalies (Feb-Mar; 1870-1967). (c) Unfiltered (thin lines) and filtered (15-year low-pass, thick lines) variations in algal Mg/Ca (black) and the Aleutian Low index leading by 5 years (Feb-Mar; red). Correlation between filtered data is r = 0.75 (significant at 99%, 1870-1967). Number of available observations (35-60°N and 140-240°E region; shaded) show that prior to the 1970s there are less than 50/month on average. (d) Lag-correlation map between filtered algal Mg/Ca (annual) and global sea level pressure (SLP; Feb-Mar) leading by 5 years. Black dot indicates location of study site. Area used to calculate the Aleutian Low index is highlighted by black rectangle (35°N-60°N, 140°E-120°W). All available SLP data are shown (1850-1962) overlapping with the algal record. The correlation patterns do not change significantly when using the period common to all time series (as in Table 1). Number of monthly observations in (a) and (c) derived from COADS, http://www.esrl.noaa.gov/psd/. Data in (a) and (c) were normalized to unit variance for comparison by subtracting the mean and dividing by standard deviation (STD). Data shown in maps were detrended and filtered prior to correlation analysis. Filtering was done with a 15-year low-pass butterworth filter. Significant (90% significance level, bold colors) and insignificant (shaded) correlations are displayed separately in maps (b, d)

2.3.2 Chronology

High-resolution photomosaics produced by an automated reflected-light microscope system (*Hetzinger et al.* [2009]) enabled the identification and lateral mapping of growth patterns over the entire sample. Easily identifiable lines demarcating annual growth increments are generated by seasonal fluctuation in cell wall calcification (i.e. large and poorly calcified cells form in the spring, whereas short and heavily calcified cells develop in summer, fall, and winter) (*Moberly Jr* [1968]). A chronology was generated by counting annual growth increments on the mapped and digitized image of the specimen. The sample was collected live in August 1969, hence the top layer was assigned the year of collection. Based on the number of annual growth increments, the sample comprises an archive that extends continuously from 1818-1967 (Supplementary Figure 2.6). Annual growth rates were determined by measuring individual growth increment thickness perpendicular to the growth lines. The average growth rate is 295 m/yr (range was 140-540 μm/yr). Areas of high Mg values within the skeleton typically occur during the summer. Hence, the maximum (minimum) Mg/Ca values were tied to August (March), which is on average the warmest (coolest) month in the study area. The algal Mg/Ca time series was linearly interpolated between these anchor points using the AnalySeries software (*Paillard et al.* [1996]) to obtain an equidistant proxy time series with monthly resolution. The uncertainty of the age model is $\sim$1-2 months in any given year. The developed chronology was refined and thoroughly cross checked for possible errors in the age model by comparing annual extreme values in the Mg/Ca ratio time series to mapped growth increment patterns for each individual year of algal growth.

2.3.3 Electron Microprobe Analysis

Elemental composition of the algal sample was analyzed by subsampling individual growth increments using a JEOL JXA 8900 RL electron microprobe at the Univer-

sity of Gttingen, Germany. For quantitative wavelength dispersive measurements, an acceleration voltage of 15 kV, a spot diameter of 3 m, and a beam current of 12 nA were used. Subsamples were obtained at 20 m intervals on transect lines that were oriented perpendicular to the plane (i.e. sequence) of calcite accretion. At each interval the specific subsample location was selected manually by moving the stage no more than 20 m laterally from the transect line to avoid unsuitable sample locations (i.e. conceptacles (uncalcified reproductive structures) and uncalcified cell interiors). The mean standard deviations of the multiple standard measurements (dolomite standard Dolomite USNM 10057 (*Jarosewich and MacIntyre* [1983]) were found to be no larger than 0.2 mass % for MgO and 0.4 mass % for CaO (2-sigma). Errors of counting statistics vary between 1.8-2.2 relative % for MgO and 0.76-0.84 relative % for CaO. The detection limit of Mg calculated from the background noise was found to be 0.02% (2-sigma). Elemental composition (Mg and Ca) of the Amchitka sample obtained by electron microprobe analysis was validated by measuring a bulk sample manually removed parallel to the electron microprobe transect using the ICP-OES (Inductively Coupled Plasma-Optical Emission Spectrometer) technique (*Hetzinger et al.* [2009]). More details on electron microprobe analysis of algal Mg and Ca are presented in *Hetzinger et al.* [2009].

2.3.4 Definition of indices and data analysis

The following indices are used throughout the study and are defined as follows:

Local SST (1870-2009) Observed February-March mean SST from HADISST (*Rayner et al.* [2003]) at 179E, 51N, the grid-point closest to the algal sample.

Aleutian Low (1850-2009) Minimum sea level pressure (SLP) in the region covering 35N-60N and 140E-120W in February and March from HADSLP2r observations (*Allan and Ansell* [2006]). This is a similar definition to that used by *Honda et al.* [2001].

North Pacific Index (NPI) (1851-2009) SLP averaged over the region 30N-65N and 160E-140W from November-March from the observation-based dataset HADSLP2r (*Allan and Ansell* [2006]), as defined by *Trenberth and Hurrell* [1994].

AMO reconstruction (Gray) (1567-2004) Reconstruction of the Atlantic Multidecadal Oscillation (AMO) based on tree-ring chronologies from land regions surrounding the North Atlantic (*Gray et al.* [2004]).

Atlantic Multidecadal Variability (AMV) (1870-2009) The area average of annual mean detrended SST anomalies from HADISST (*Rayner et al.* [2003]) in the region 0-60N, 75W-7.5W.

Coral δ^{18}O (Kilbourne) (1751-2004) Reconstruction of Caribbean SST anomalies based on coral δ^{18}O from a sample in the Tropical Atlantic Ocean near Puerto Rico (*Kilbourne et al.* [2008]).

North Atlantic Oscillation (NAO) (1850-2009) First empirical orthogonal function (EOF) of January to March mean SLP over the North Atlantic (20N-70N, 70W-40E), using HADSLP2r (*Allan and Ansell* [2006]).

Pacific Decadal Oscillation (PDO) (1870-2008) First empirical orthogonal function (EOF) of annual mean SST over the North Pacific between 20N and 60N, using HADISST (*Rayner et al.* [2003]) (data available 1870-2008).

All data are linearly detrended based on the period common to all time series (1870-1967). Significance was computed using a two-sided Student's t-test with the degrees of freedom determined using the autocorrelation of the individual time series. Thus we account for the reduction in degrees of freedom when filtering the data.

2.4 Results

As previously shown skeletal Mg/Ca variations in this coralline alga are a proxy for past SST variability (*Hetzinger et al.* [2009]). Cross-spectral and correlation analyses indicate that algal Mg/Ca ratios are a reliable estimator of North Pacific SST on time scales longer than 10 years with highest correlations in winter (February-March; Supplementary Figures 2.7 and 2.8). Hence, in the following comparisons among proxy data, SST, and climate variables, we use 15-year low-pass filtered data for February-March. However, our results are qualitatively similar when using winter (Jan-Mar) or annual mean values (Supplementary Figure 2.8). A direct comparison of the algal Mg/Ca record to SST variability at the study site yields a significant positive relationship (Figs. 2.1a, 2.2a and Table 2.1; r = 0.85, sign. at 96%, filtered data), confirming that algal Mg/Ca records local decadal-scale SST variability. The degrees of freedom used to estimate significance account for filtering (see Methods). Correlating algal Mg/Ca with instrumental SST data on a global scale (Fig. 2.1b) reveals the relation of the algal proxy with large-scale SST variability. Significant positive relationships exist between algal Mg/Ca and northern North Pacific/ Bering Sea SSTs, confirming the ability of algal Mg/Ca to archive local and regional SST changes (Fig. 2.1b). There are also relationships to other parts of the global oceans, including the Atlantic. However, the PDO is not significantly related to either algal Mg/Ca or SST at the study site (Table 2.1). Despite the PDO being the dominant mode of decadal variability in the North Pacific, it explains little variability along the central Aleutian Island chain, where the study site is located (Figure 2.3a).

2.4.1 Lagged proxy for decadal Aleutian Low

A highly significant lagged relationship is evident between algal Mg/Ca and the Aleutian Low in late winter (February-March, r = 0.75, Aleutian Low leading by 5 years, sign. at 99%, filtered data; Figs. 2.1c, 2.2a and 2.8, Table 2.2) when this low

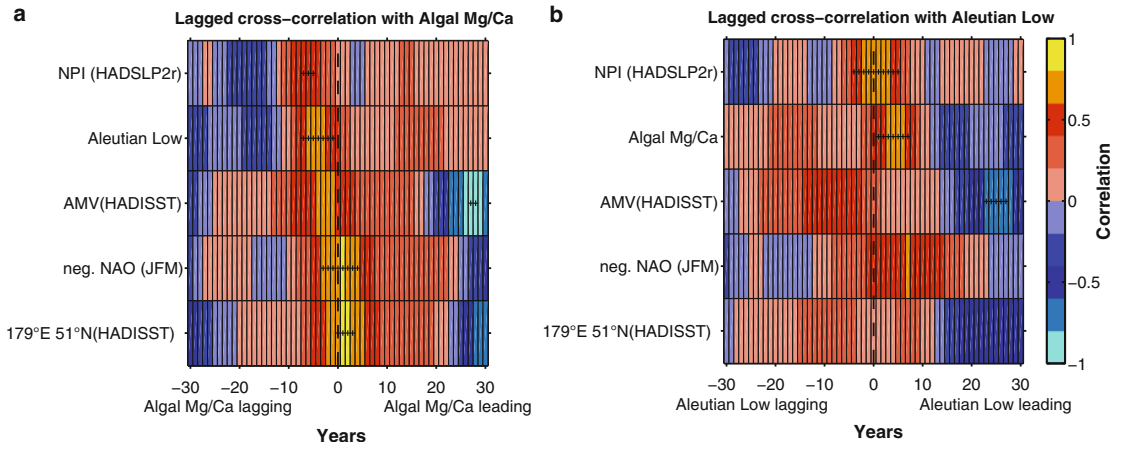

Figure 2.2: Lagged cross-correlations among algal Mg/Ca, North Pacific Index (NPI), Aleutian Low, AMV-index, NAO-index, and local SST. (a) Cross-correlation of algal Mg/Ca with climate indices, positive lags (years) indicate algal Mg/Ca leads. (b) As in (a), but for the Aleutian Low index. Data shown are linearly detrended and 15-year low-pass filtered. Cross correlations significant at 90% level indicated by crosses. Correlations apply to the period common to all time series (1870-1967)

pressure system dominates the atmospheric variability. The relation of the algal data to the North Pacific Index (NPI), another index for the Aleutian Low (*Trenberth and Hurrell* [1994]), is less significant (November-March, r = 0.38, NPI leading by 5 years, sign. at 75%, filtered data; Fig. 2.2a, Table 2.2). Significant spatial SLP correlation patterns are detected in the North Pacific, with positive correlations located in the northern North Pacific/Bering Sea region and negative correlations in the Arctic (Fig. 2.1d). This relationship shows that a weakening of the Aleutian Low precedes warm SSTs at the study site by several years. The lag between SST and SLP potentially indicates the ocean's response to the atmosphere, and the time scale is consistent with previous modelling studies (*Schneider et al.* [2002]), although these focused on the PDO. However, the mechanism for this is not investigated here. Instrumental observations also show that the Aleutian Low influences SST at the study site, but the relation is less significant (Fig. 2.2, Supplementary Figure 2.9).

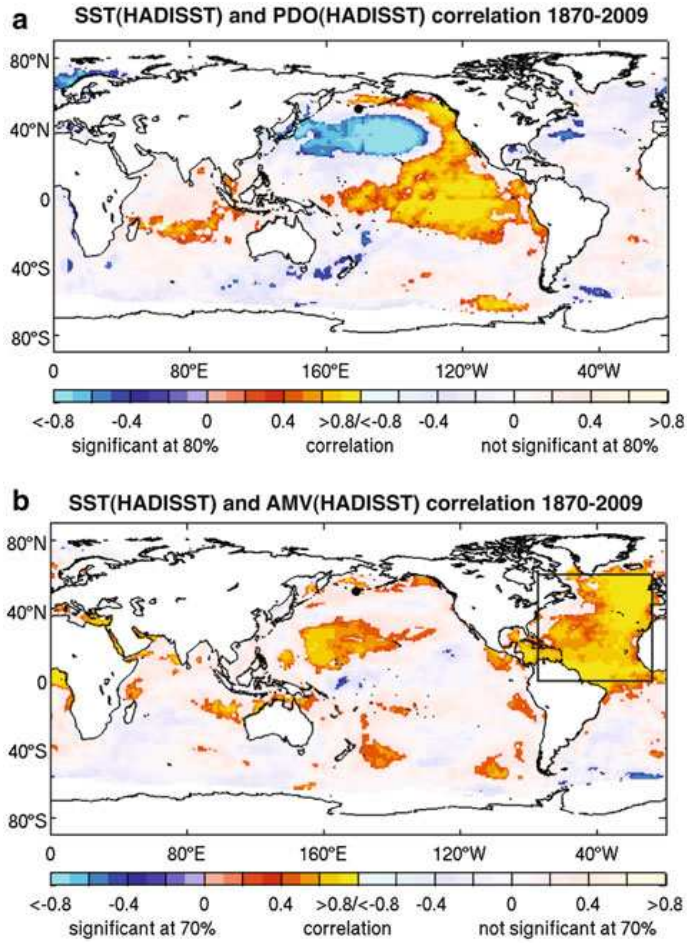

Figure 2.3: Relation of observed Pacific and Atlantic decadal/interdecadal climate variability to SST. (a) Correlation of the PDO-index and Feb-Mar SST anomalies. (b) Correlation map of the AMV-index and Feb-Mar SST anomalies. Location of study site indicated by black dot. Area used to calculate the AMV-index is highlighted by black rectangle (0-60°N, 7.5-75°W). Significant (bold colors) and insignificant (shaded) correlations displayed separately. Shading indicates the 80% (a) and 70% (b) significance levels. All data detrended prior to correlation analysis. Correlation maps were computed for the length of available SST data (1870-2009). The correlation patterns do not change significantly when using the period common to all time series (1870-1967)

2.4.2 Decadal atmospheric bridge: North Pacific - North Atlantic

Moreover, a significant instantaneous relation of algal Mg/Ca to SLP in the North Atlantic is detected resembling the pattern of the NAO (Fig. 2.4). A highly signifi-

cant negative relationship is found between the algal time series and the NAO-index on decadal time scales (Figs. 2.2a, 2.5, and 2.8), with the NAO explaining 76% of the variance in algal Mg/Ca (January-March, r = -0.87, sign. at 99.8%, filtered data; Table 2.1). As skeletal Mg/Ca of the alga is a lagged proxy for the Aleutian Low (Figs. 2.1c,d and 2.2), these correlations suggest that a weaker Aleutian Low precedes a negative NAO by several years. A similar relation is found in instrumental observations (Figs. 2.2b and 2.4), although instrumental observations reveal lower and statistically insignificant correlation (90% confidence) between the NAO-index and the Aleutian Low (Fig. 2.2b). This could be due to limited instrumental data (e.g., number of observations for the Aleutian Low decreases significantly before 1960, see Fig. 2.1c).

2.4.3 Relation between AMV and PDV

Since the NAO is a key driver of ocean circulation in the North Atlantic on decadal time scales (*Eden and Jung* [2001]), its relation to the North Pacific could link SST in both basins. In fact, the algal time series is related to the AMV (Figs. 2.2a, 2.5 and Table 2.1), which is responsible for climate and ocean changes across much of the Northern Hemisphere (*McCabe et al.* [2004]). The correlation between grid-SST for the study site and the AMV-index is high and statistically significant (r = 0.8, sign. at 94%, filtered data; Table 2.1). However, the relation of AMV to most of the northern North Pacific is not highly significant (Figure 2.3b). A comparison of the algal time series with proxy data from the Atlantic indicates that this teleconnection may have persisted prior to the instrumental record (*Gray et al.* [2004]; *Kilbourne et al.* [2008]) (Fig. 2.5d,e; Table 2.1). When examining the positive/negative phases in the AMV-index and in the proxy records (Fig. 2.5), distinct similarities between all time series on decadal- to interdecadal time scales can be recognized. Positive phases prevailed between approximately the 1860s-1900, 1930s-1960s, and negative phases between around 1820-1860, 1900-1930s, 1970-1990s. The correlation among

algal Mg/Ca and Atlantic AMV proxies is low, however, the correlation of algal Mg/Ca to observed AMV is comparable with other AMV proxy records (Table 2.1).

2.5 Discussion and Summary

Here we introduce a new proxy for decadal-scale variations of the Aleutian Low based on an algal record from the subarctic North Pacific. Previous proxy-based reconstructions of the NPI (an index of the Aleutian Low) have so far been based on terrestrial archives (e.g., tree ring chronologies (*D'Arrigo et al.* [2005])). The correlation among different NPI and Aleutian Low indices (tree ring, coralline algae and instrumental data) on decadal time scales are similar (Table 2.2), although the correlation of algal Mg/Ca to the Aleutian Low index is the highest. Thus, geochemical records from subarctic North Pacific coralline algae offer alternative possibilities to extend NPI/Aleutian Low records back before reliable instrumental data.

The alga provides the first marine proxy evidence for a statistically significant linkage between decadal variations in atmospheric circulation over the extra-tropical North Pacific and Atlantic, with a weaker Aleutian Low tending to precede a negative NAO. This relationship has been uncertain owing to a sparseness of instrumental data, particularly in the North Pacific (Fig. 2.1a,c) and could not be confirmed (*Müller et al.* [2008]; *Schwing et al.* [2003]). This link could also change over time. After about 1970 instrumental SST and the Aleutian Low Index show different trends (Fig. 2.1a,c). The underlying reasons for this divergence in instrumental data are unclear. As our proxy record ends in 1967, this could not be investigated.

There are various possible explanations for the extra-tropical North Pacific-Atlantic link. The simplest might be that the annular mode's (*Thompson and Wallace* [1998]) interaction with the ocean leads to a different response in the North

Pacific and North Atlantic than on interannual time scales (Fig. 2.4), such that decadal fluctuations of the Aleutian Low and NAO are anticorrelated with a several year lag. Alternative explanations may be that the atmospheric pattern is a response to the AMV (*Zhang and Delworth* [2007]; *dOrgeville and Peltier* [2007]) or a hemispheric mode of variability (*Timmermann et al.* [1998]).

The atmospheric bridge between the North Pacific and North Atlantic on decadal time scales may explain the observed coherence between observed SST and proxy records (Table 2.1, Fig. 2.5) in both basins. Hence, our results provide evidence for the existence of an atmospherically-modulated connection between northern North Pacific/ Bering Sea SST and AMV on low-frequencies. However, the mechanism behind the North Pacific - North Atlantic teleconnection remains unclear. Models and longer proxy reconstructions (e.g. *D'Arrigo et al.* [2005]; *Luterbacher et al.* [2001]; *Gray et al.* [2004]) are required to help understand it as well as the differences between interannual and decadal time scales.

This record represents the longest annually-resolved marine geochemical proxy record from the subarctic North Pacific to date, complementing very sparse instrumental data. Moreover, it is so far the longest continuous geochemical proxy record from the coralline alga C. nereostratum, extending to the early 19th century. Coralline algal longevity may extend to several hundred years, enabling these plants to serve as an important and only recently utilized marine archive for the subarctic oceans where only few high-resolution archives are available. In fact, live specimens of Clathromorphum nereostratum collected from the North Pacific Ocean can reach ages of up to 850 years exhibiting continuous growth (*Halfar et al.* [2007]), making this species one of the longest-lived marine organisms on record.

Table 2.1: Correlation analysis among North Pacific algal Mg/Ca, climate indices and Atlantic proxy data. From top to bottom: Amchitka algal Mg/Ca (1818-1967, annual average), North Alantic Oscillation (NAO) index (JFM), Atlantic Multidecadal Variability (AMV), reconstructed Atlantic Multidecadal Oscillation (AMO) based on tree-ring chronologies (*Gray et al.* [2004]), reconstructed Caribbean SST anomalies based on coral δ^{18}O (*Kilbourne et al.* [2008]), local SST (179°E, 51°N, Feb-Mar), Pacific Decadal Oscillation (PDO) index. Correlations for unfiltered (lower left) and low-pass filtered (15-year cut off; shaded grey) data are shown. Significance levels shown in brackets (90% significance in bold). All data were detrended from 1870-1967 prior to comparison. Correlations apply to the period common to all time series (1870-1967)

	Algal Mg/Ca	NAO-index (JFM)	AMV-index	AMO-reconstr. (Gray)	coral δ^{18}O (Kilbourne)	SST (179°E 51°N)	PDO-index
Algal Mg/Ca	**1.00 (100.0)**	**−0.87 (99.8)**	0.60 (79.9)	0.49 (77.0)	0.15 (27.0)	**0.85 (96.4)**	0.00 (0.4)
NAO-index (JFM)	**−0.34 (98.4)**	**1.00 (100.0)**	−0.68 (87.4)	**−0.63 (90.6)**	−0.22 (39.2)	**−0.90 (98.6)**	0.08 (15.7)
AMV-index	0.31 (76.6)	−0.34 (80.8)	**1.00 (100.0)**	**0.87 (98.5)**	0.67 (86.6)	**0.80 (94.0)**	0.05 (6.9)
AMO-reconstr. (Gray)	0.18 (31.3)	−0.20 (33.8)	0.64 (89.6)	**1.00 (100.0)**	0.61 (88.6)	0.71 (86.7)	0.02 (3.4)
coral δ^{18}O (Kilbourne)	0.04 (15.2)	0.14 (48.9)	0.39 (87.1)	0.37 (60.0)	**1.00 (100.0)**	0.29 (38.9)	−0.33 (56.4)
SST (179°E 51°N)	0.35 (86.8)	−0.37 (88.5)	**0.55 (97.6)**	0.38 (61.0)	0.11 (36.7)	**1.00 (100.0)**	0.03 (3.8)
PDO-index	0.07 (25.2)	−0.22 (70.2)	0.09 (27.6)	0.05 (8.3)	−0.17 (57.6)	0.14 (44.9)	**1.00 (100.0)**

Unfiltered annual data

Low-pass filtered (15-year cut off)

Table 2.2: Correlation analysis among North Pacific algal Mg/Ca, Aleutian Low index, reconstructed North Pacific Index (NPI) (tree ring based (*D'Arrigo et al.* [2005])), and the instrumental NPI index (*Trenberth and Hurrell* [1994]). (*) Algal Mg/Ca is lagging other indices by 5 years. Correlations for unfiltered (lower left) and low-pass filtered (15-year cut off; shaded grey) data are shown. Significance levels shown in brackets (90% significance in bold). All data were detrended from 1870-1967 prior to comparison. Correlations apply to the period common to all time series (1870-1967)

	Algal Mg/Ca*	Aleutian Low index	NPI-reconstr. (D'Arrigo)	NPI-index
Algal Mg/Ca*	**1.00 (100.0)**	**0.75 (99.3)**	0.35 (67.8)	0.38 (74.9)
Aleutian Low index	**0.40 (99.6)**	**1.00 (100.0)**	0.44 (80.2)	**0.71 (98.8)**
NPI-reconstr. (D'Arrigo)	0.21 (69.3)	0.28 (82.5)	**1.00 (100.0)**	0.54 (89.5)
NPI-index	0.25 (83.8)	**0.64 (100.0)**	**0.38 (93.6)**	**1.00 (100.0)**

Low-pass filtered (15-year cut off)

Unfiltered annual data

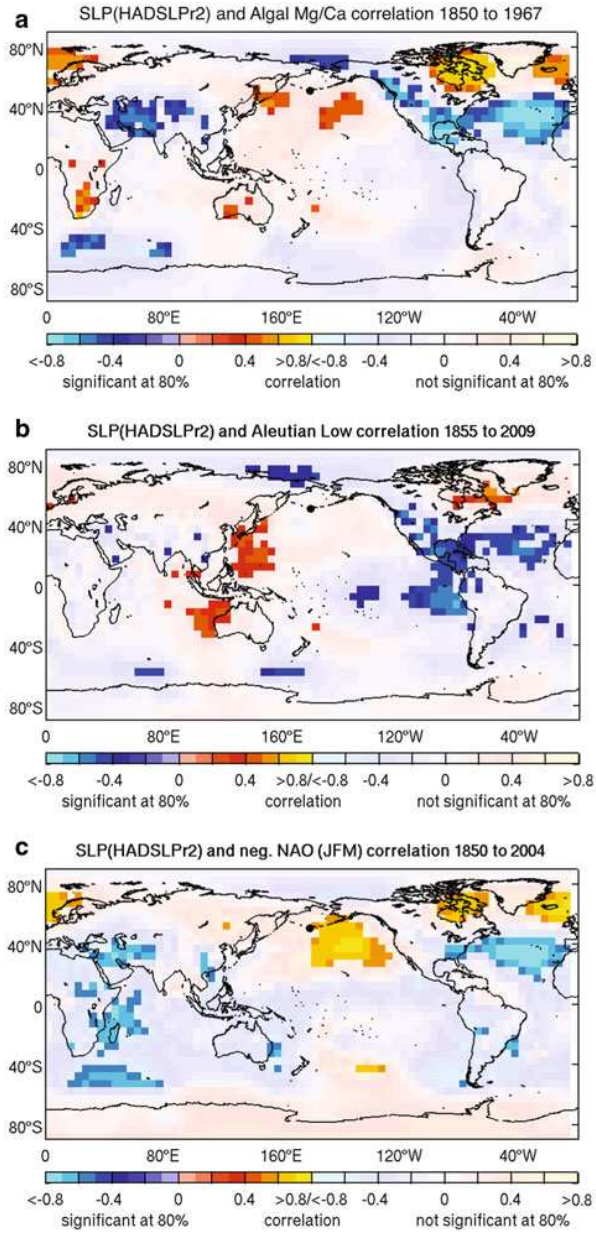

Figure 2.4: (a) Correlation map between global SLP (Feb-Mar) and algal Mg/Ca (annual average). A significant instantaneous relation of algal Mg/Ca to SLP in the North Atlantic is detected resembling the pattern of the NAO. (b) Lag-correlation map between global SLP (Feb-Mar) and the Aleutian Low index. The Aleutian Low index is leading global SLP by 5 years. (c) Lag-correlation map between global SLP (Feb-Mar) and the NAO-index (Jan-Mar) lagging by 5 years. Note that a negative NAO-index was used. Significant (80% significance level, bold colors) and insignificant (shaded) correlations displayed separately. All data low-pass filtered and detrended prior to correlation analysis. Correlation patterns are very similar when using the period common to all time series (1870-1967)

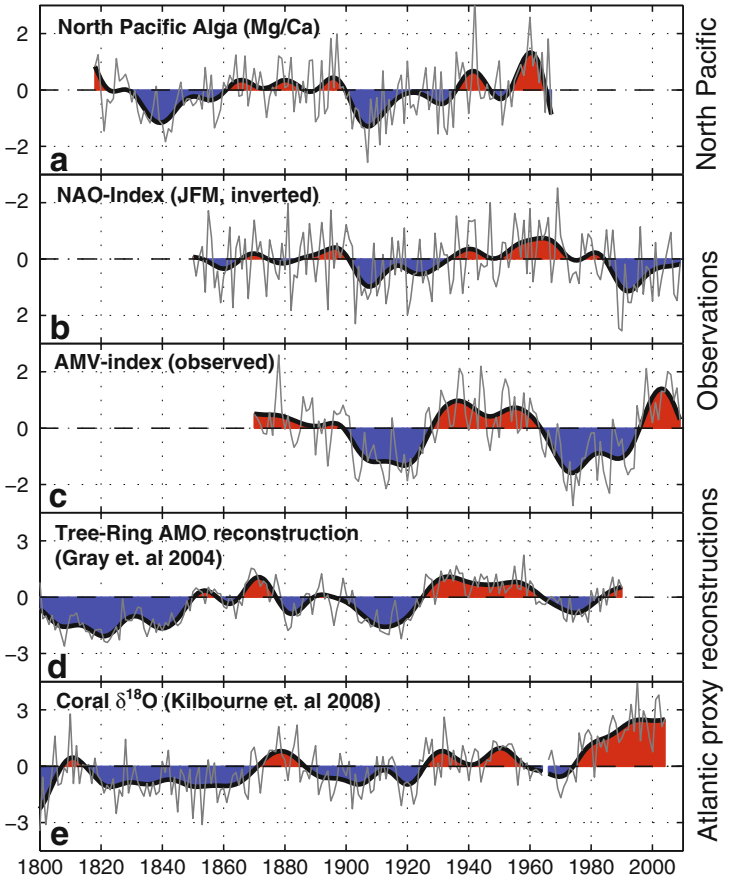

Figure 2.5: Algal Mg/Ca record compared to the NAO-index, AMV-index, and Atlantic proxy records for AMV. Atlantic proxy records were derived from land-based (tree-ring (*Gray et al.* [2004])) and marine (coral (*Kilbourne et al.* [2008])) archives. Annual (thin lines) and 15 year low-pass filtered data (bold lines) are shown. All data were linearly detrended and normalized. Note that the NAO-index is inverted

2.6 Acknowledgements

We thank B. Williams, R. Greatbatch, and M. Latif for discussion and helpful comments. This research was funded by the Alexander von Humboldt Foundation (Feodor Lynen Fellowship to S.H.), the Deutsche Forschungsgemeinschaft (grant HA 3238/2-1. 2-2 to J.H. and A.K.; and Emmy Noether grant KE 1471/2-1 to N.S.K and J.V.M), a Natural Sciences and Engineering Research Council of Canada Discovery Grant and a Canadian Foundation for Innovation and Research and Ontario Research Fund Grant (all J.H.). Two anonymous reviewers are thanked for their valuable comments that greatly improved this manuscript.

2.7 Supplementary Figures

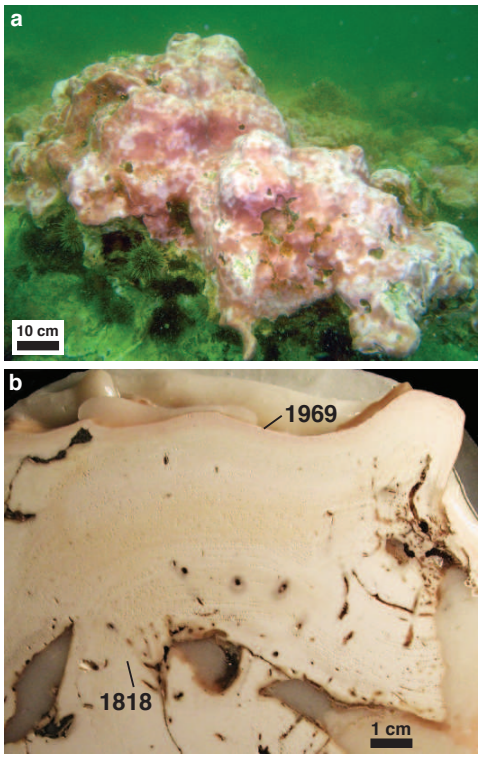

Figure 2.6: Coralline alga Clathromorphum nereostratum: (a) Live crustose coralline alga plant (Clathromorphum nereostratum) growing attached to the seafloor. Image taken at around 10 m water depth near Amchitka Island, Aleutian Islands. (b) Sectioned algal sample collected live in August 1969 from 25 m water depth off Amchitka Island, Alaska, used in this study. Annual growth increments are clearly visible. The record extends from 1969 (uppermost layer of growth, pinkish color) to 1818

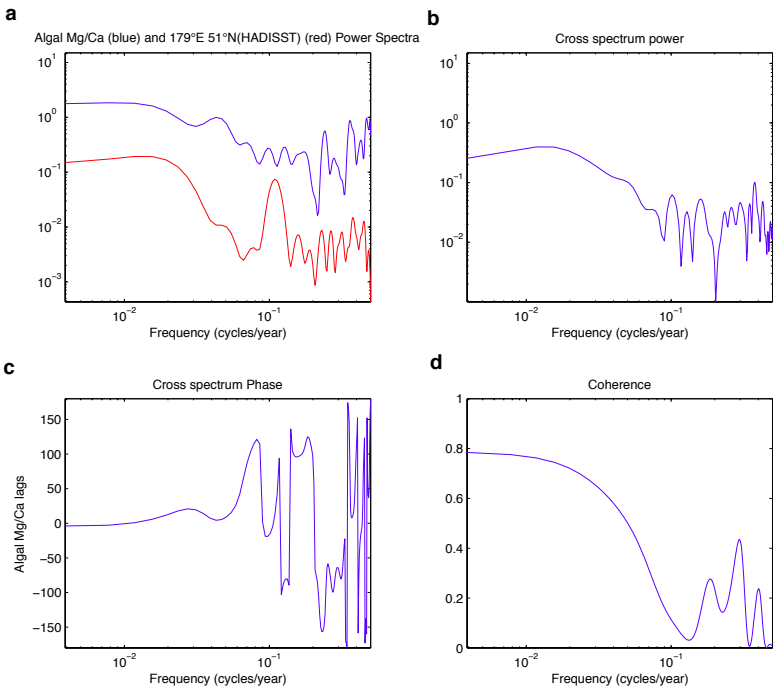

Figure 2.7: Cross-spectral analysis between local SST (Feb-Mar; red) and algal Mg/Ca (blue). (a) Power spectra, cross spectrum (b) power, (c) phase, and (d) coherence. Highest coherence is found on time scales longer than 10 years, with in phase variations of algal and SST data. However, this may also be due to sparse instrumental SST data. Cross spectra were computed using a 65-year window

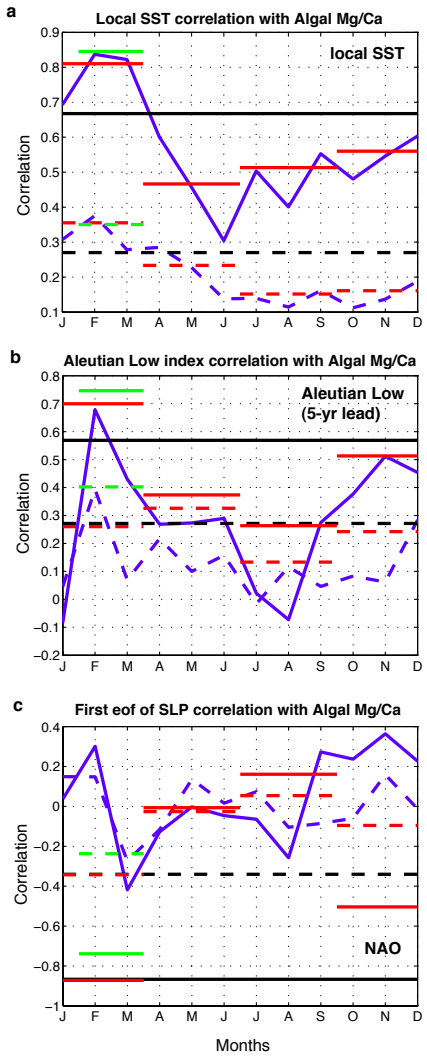

Figure 2.8: Algal Mg/Ca correlated to local SST, Aleutian Low index, and NAO-index for various seasons. Dashed lines mark unfiltered data, solid lines are 15-year low-pass filtered. Blue curve denotes monthly values. Red markers display three-month means, green markers two-month means, and black solid line annual average SST/SLP, respectively. (a) Correlations between local SST and algal Mg/Ca. Highest correlation is found in Feb-Mar, but there is little difference to the annual or Jan-Mar average. (b) Correlations between algal Mg/Ca and the Aleutian Low index leading by five years. The highest correlation is in Feb- Mar. (c) Correlations between NAO-index and algal Mg/Ca. Highest correlation is found in Jan-Mar. Mean SLP values calculated before EOF analysis. Correlations apply to the period common to all time series (1870-1967)

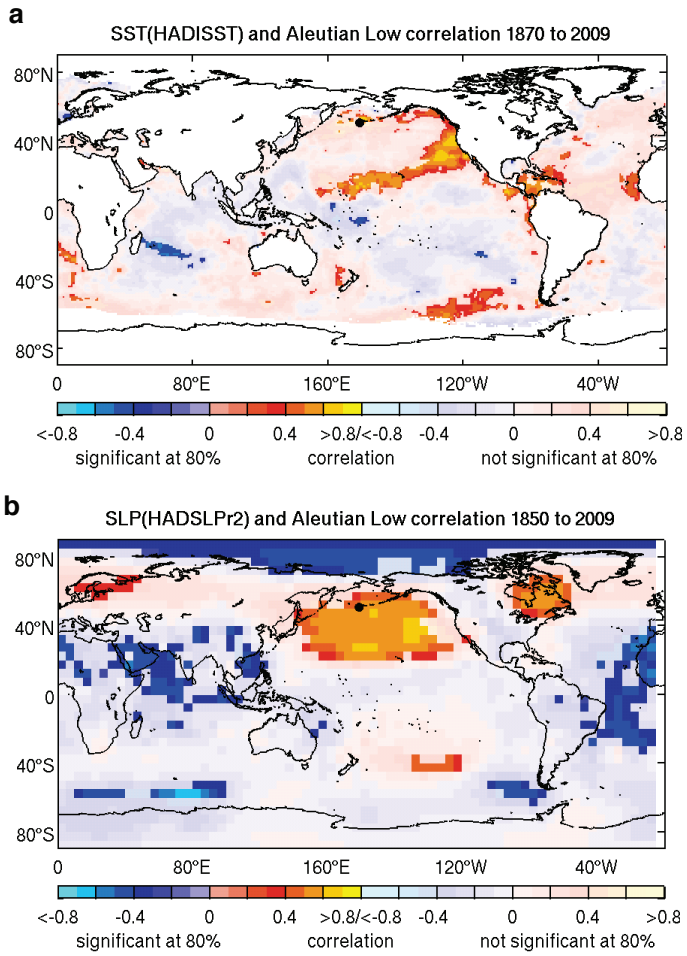

Figure 2.9: Relation of instrumental Aleutian Low index with SST and SLP; i.e., supplementing Figure 1b,d, where algal proxy data were shown: (a) Lag-correlation map between Aleutian Low index and SST anomalies; Aleutian Low index leading SST by 5 years. (b) Correlation map between Aleutian Low index and SLP (no lag). SST and SLP data shown for Feb-Mar. Significant (80% significance level, bold colors) and insignificant (shaded) correlations displayed separately. All data low-pass filtered and detrended prior to correlation analysis. Correlation maps were computed for the length of available (a) SST data (1870-2009) and (b) SLP data (1850-2009), respectively. The correlation patterns do not change significantly when using the period common to all time series 1870-1967

Chapter 3

Stochastically-forced multidecadal variability in the North Atlantic: A model study

J. V. Mecking (1*), N. S. Keenlyside (2), R. J. Greatbatch (1)

Submitted to Climate Dynamics

(1) Helmholtz Centre for Ocean Research Kiel (GEOMAR), Dsternbrooker Weg 20, 24105 Kiel, Germany
(2) Geophysical Institute and Bjerknes Centre, University of Bergen, Bergen, Norway

*corresponding author: jmecking@geomar.de.

3.1 Abstract

Observations show a multidecadal signal in the North Atlantic ocean, but the underlying mechanism and cause of its timescale remain unknown. Previous studies have suggested that it may be driven by the North Atlantic Oscillation (NAO), which is the dominant pattern of winter atmospheric variability. To further address this issue, the global ocean general circulation model, NEMO, is driven using a 2000 year long white noise forcing associated with the NAO. Focusing on key ocean circulation patterns, we show that the Atlantic Meridional Overturning Circulation (AMOC) and Sub-polar Gyre (SPG) strength both have enhanced power at low frequencies but no dominant timescale, and thus provide no evidence for a oscillatory ocean-only mode of variability. Instead, both indices respond linearly to the NAO forcing, but with different response times. The variability of the AMOC at 30°N is strongly enhanced on timescales longer than 90 years, while that of the SPG strength starts increasing at 15 years. The different response characteristics are confirmed by constructing simple statistical models that show AMOC and SPG variability can be related to the NAO variability of the previous 53 and 10 winters respectively. Alternatively, the AMOC and the SPG strength can be reconstructed with Auto-regressive (AR) models of order seven and five, respectively. Both statistical models reconstruct interannual and multidecadal AMOC variability well, while on the other hand, the AR(5) reconstruction of the SPG strength only captures multidecadal variability. Using these methods to reconstruct ocean variables can be useful for prediction and model intercomparision.

Keywords: North Atlantic, NAO, Atlantic Multidecadal Variability, Sub-polar gyre, Stochastic and OGCM

3.2 Introduction

The North Atlantic Ocean is a very important component of the climate system, being the main source of poleward heat transport in the Northern Hemisphere ocean. A large part of the variability in the North Atlantic Ocean sea surface temperature (SST) is associated with the Atlantic Multidecadal Variability (AMV), also referred to as the Atlantic Multidecadal Oscillation(*Kerr* [2000], *Enfield et al.* [2001], *Knight et al.* [2005]). An index for the AMV is typically computed as the detrended, area average, SST over the region 0° to 60°N and 75°W to 7.5°E (following section 3a from *Dima and Lohmann* [2007], Figure 3.1a). The AMV can be linked to major climatic impacts, for example, there is a strong relationship to the frequency of North Atlantic hurricanes, rainfall in the Sahel region and North America, as well as, the river outflow of the Mississippi river (*Goldenberg et al.* [2001],*Zhang and Delworth* [2006],*Enfield et al.* [2001]). The SST pattern associated with the AMV is considered to be a surface signature of multidecadal variability in the North Atlantic ocean (*Knight et al.* [2005]). The AMV index, as constructed from historical SSTs has an oscillatory character with a period of approximately 70 years (Figure 3.1a), but the instrumental record is relatively short. Tree ring data (*Gray et al.* [2004]), coral (*Kilbourne et al.* [2008]), ice core records (*Chylek et al.* [2011]) and coralline algae (*Hetzinger et al.* [2012]) can be used to gain insight into the character of modes of multidecadal variability in the North Atlantic before the observational record. However, there are disagreements among these proxy data. Furthermore, not only is it of great interest to identify the time scales of multidecadal variability in the North Atlantic but also to understand the underlying physics. For these reasons it is important to turn to models to gain a better insight into interdecadal variability of the North Atlantic Ocean.

Many modeling studies have looked into the variability of the North Atlantic Ocean using either ocean models driven by specified atmospheric forcing or coupled

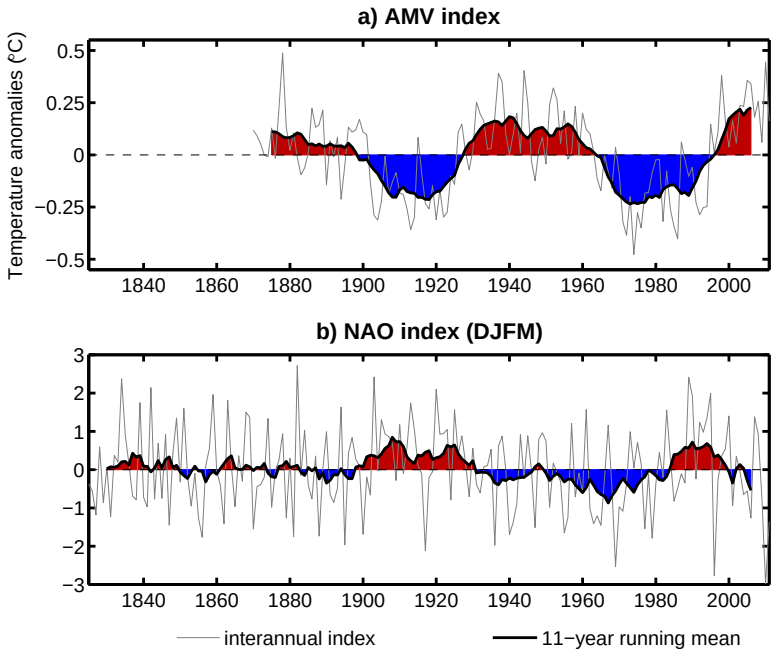

Figure 3.1: (a) The AMV index computed as the detrended annual mean SST in the region 0° to 60°N and 75°W to 7.5°E (following method outlined in section 3a of *Dima and Lohmann* [2007]) using SST data from HADISST [*Rayner et al.*, 2003]. (b) The NAO index computed from the difference of the normalized SLP anomalies, Gibraltar minus Iceland (*Jones et al.* [1997]) averaged over December, January, February and March (DJFM). The thin gray lines are inter-annual data and the thick black and shaded lines are 11-year runnings means of the data.

ocean/atmosphere models. These modeling studies have produced a wide range of timescales of variability from 20 years (e.g., *Born and Mignot* [2012]) to centennial (e.g., *Menary et al.* [2012]) in ocean circulation patterns. A focus of these studies is often on the Atlantic Meridional Overturning Circulation (AMOC), since it is important for transporting heat and often has a pronounced multidecadal signal (e.g., *Delworth et al.* [1993]). In many model studies variability in the AMOC is closely related to the AMV (e.g., *Knight et al.* [2005]). These studies all involve slightly different mechanisms for the AMOC variability, several of which involve the interaction between convection and sub-polar gyre dynamics (e.g. *Delworth et al.* [1993] and *Born and Mignot* [2012]) or influences from the Arctic (*Jungclaus et al.* [2005]), some of them coupled atmosphere-ocean mechanisms (e.g. *Timmermann*

et al. [1998] and *Vellinga and Wu* [2004]) and others having an ocean-only mechanism (e.g. *Greatbatch and Zhang* [1995] and *Dijkstra et al.* [2006]). In several cases it is not always clear which multi-decadal timescales are excited, in some cases more than one timescale is found (*Park and Latif* [2011], *Delworth and Zeng* [2012]) while in others different timescales of variability are present at different times in the model simulation (*Kwon and Frankignoul* [2012]).

Atmospheric forcing plays an important role in exciting the multidecadal variability in the ocean (e.g., *Delworth and Greatbatch* [2000] and *Eden and Jung* [2001]). The North Atlantic Oscillation (NAO), a measure of the sea level pressure difference between the Azores High and Icelandic Low (Figure 3.1b), is the dominate mode of atmospheric variability over the North Atlantic (*Hurrell* [1995]) explaining up to 31% of the northern hemisphere winter mean temperature variability (*Hurrell* [1996]). During the short instrumental period the NAO index has undergone multidecadal variations, giving it a weakly red spectrum (*Wunsch* [1999]). As with the AMV index, the NAO index has an important impact on the northern hemisphere climate with significant socio-economical impacts (*Greatbatch* [2000], *Hurrell et al.* [2003] and *Drinkwater et al.* [2003]). Several studies have looked at the impact that the NAO has on the ocean (*Dickson et al.* [1996], *Visbeck et al.* [1998], *Curry and McCartney* [2001], *Eden and Jung* [2001], *Eden and Willebrand* [2001], *Visbeck et al.* [2003], and *Köller et al.* [2010]). In particular, the study by *Eden and Willebrand* [2001] showed, that the ocean responds rapidly to the wind stress component of the NAO but has a slower response to the heat flux anomalies associated with the NAO. *Eden and Jung* [2001] forced an ocean model with the variability associated with the NAO index added to climatology, which reproduced some of the observed multidecadal variability in the North Atlantic SST (see their Figure 4). Their study also demonstrated that ocean dynamics is important in determining the SST response as suggested by *Bjerknes* [1964]. In the study by *Curry and McCartney* [2001] a connection between the zonal transport across the North Atlantic Ocean and the

NAO index was shown. *Dickson et al.* [1996] link convection in the Labrador Sea to the positive phase of the NAO, which can then be linked to the variability in the North Atlantic (*Eden and Willebrand* [2001], *Eden and Jung* [2001]and *Latif et al.* [2006]). In the coupled climate modeling study of *Medhaug et al.* [2012], the NAO directly affects the convection in the Labrador Sea, which then leads to a change in the AMOC two years later. It is also important to note that the NAO is not the only important atmospheric forcing pattern that can lead to multidecadal ocean variability in the North Atlantic in models. For example, the East Atlantic Pattern and the Scandinavian Pattern (*Barnston and Livezey* [1987]) can contribute to ocean variability (*Msadek and Frankignoul* [2009] and *Medhaug et al.* [2012]).

Beginning with the ideas from *Hasselmann* [1976], the ocean response to forcing in modelling studies is often described in terms of a response to a stochastic or white noise atmosphere (*Delworth and Greatbatch* [2000], *Kwon and Frankignoul* [2012] and *Born and Mignot* [2012]). *Delworth and Greatbatch* [2000], for example, were able to excite a multidecadal response in an ocean model through forcing the ocean using only a white noise atmosphere. Furthermore, the multidecadal variability in the AMOC was reproduced by driving the model only by the low-frequency (20 year and longer) part of the forcing spectrum. In *Delworth and Greatbatch* [2000] low frequency variability in the AMOC can be interpreted as a linear response to the low frequency variability in the atmospheric (flux) forcing.

Simple statistical models can be useful tools to interpret the complex behaviour of reality and coupled climate models. Such models are able to describe a link between the atmosphere and the ocean. Through integrating the heat flux over the Labrador Sea region for the past 10 years, *Ortega et al.* [2011] were able to reproduce 74.5% of the AMOC in their coupled model. Similarly, *Langehaug et al.* [2012] were able to reproduce 43.6% of the variance in the sub-polar gyre (SPG) strength in their coupled climate model using a multiple linear regression model based on

Labrador Sea water thickness, Greenland-Scotland overflow and the atmospheric East Atlantic Pattern (*Barnston and Livezey* [1987]). *Curry and McCartney* [2001] were able to reproduce approximately 60% of the variance of their North Atlantic Ocean transport index through integrating the NAO index over the past 10 years. The study by *Eden et al.* [2002] used a fifth order auto-regressive (AR(5)) process to represent an ocean model that was driven by the NAO which, in turn, was modelled as a stochastic white noise process with a weak feedback from the ocean.

The aim of this study is to gain a deeper understanding of the North Atlantic response to stochastic atmospheric variability, as a null hypothesis for multidecadal variability in the North Atlantic. Motivated by previous work, our approach is to drive a global ocean general circulation model (OGCM) using forcing associated with stochastic variability of the NAO. As discussed above, multidecadal variability in the Atlantic Ocean is thought to be associated with ocean circulation changes, so most of the analysis focuses on AMOC and SPG indices. The results indicate that ocean variables, such as the strength of the AMOC, show a red noise response but not a simple AR(1) response to the NAO forcing. However, this response can be explained through higher order AR processes forced by the NAO index. Novel aspects of this work are firstly, the use of a more realistic OGCM that has a global domain and relatively high resolution, and an active sea-ice component; and secondly, the application of the simple statistical methods to interpret the results. The paper is structured as follows. Section 3.3 gives a description of the model and the experimental setup. Section 3.4 describes the results of the OGCM integrations and section 4 develops statistical models linking the NAO to the AMOC and the sub-polar gyre strength. Finally, section 4.8 contains a summary as well as a brief discussion of the results.

3.3 Model set-up

For this study, the Nucleus for European Modelling of the Ocean (NEMO) Ocean General Circulation model (OGCM) version 3.1 is used (*Madec et al.* [1998]). The parameter set-up is taken from the Drakkar configuration (*The Drakkar Group* [2007]). This configuration has been used successfully in several studies (see *Barnier et al.* [2006]). The OGCM uses the global ORCA05 grid, a tri-polar grid with poles over Antarctica, Siberia and Canada and horizontal resolution of approximately 0.5°, with slightly higher meridional resolution towards the poles. There are 46 vertical levels of varying thickness, highly resolved near the surface (6 m level thickness) but with coarser resolution at depth (up to 550 m level thickness). To get a more accurate representation of the ocean bottom the OGCM uses partial steps. The ocean model set-up also includes the interactive sea ice model, LIM2. To keep the OGCM from drifting, surface salinity is restored to climatology on a time scale of 150 days. This set-up also uses the *Gent and McWilliams* [1990] eddy parameterization.

3.3.1 Atmospheric forcing

The atmospheric forcing for this study comes from the COREv2 dataset (*Large and Yeager* [2004], *Large and Yeager* [2009]). The ocean model is provided with the 10 m atmospheric temperature, winds, humidity, longwave radiation, shortwave radiation, and snow and rain from both the normal year and the inter-annual (1948 to 2007) datasets (*Griffies et al.* [2004]). The forcing data are of varying temporal resolution with the temperature, winds and humidity available 6 hourly, long and short wave radiation daily and precipitation values as monthly means. The normal year dataset assumes a year of typical synoptic variability which can then be used repeatedly as a climatological forcing (*Griffies et al.* [2009]). The atmospheric fields are read in by the OGCM and then interpolated onto the model grid and the fluxes are computed by the ocean model code directly. In addition to a climatologically

Model Integration	Short Name	Years	Description
Fully-Forced	FF	1948 - 2007	Model integration using the complete COREv2 forcing
NAO-Forced	NF	1826 - 2010	Model integration using the normal year forcing plus anomalies based on the observed NAO
Stochastic-Forced	SF	2000 years	Model integration using the normal year forcing plus anomalies from the stochastic NAO

Table 3.1: Details of the various model integrations used in this study.

forced spin-up (see section 3.3.4) a model integration was performed using the inter-annual COREv2 data from 1948-2007, referred to as the fully forced (FF) integration (Table 3.1).

3.3.2 NAO forcing

For the experiments forced by the NAO index, atmospheric forcing used by the OGCM was restricted to that based only on the NAO, similar to the procedure used in *Eden and Jung* [2001]. In contrast to *Eden and Jung* [2001], where air-sea fluxes are used as forcing fields, we use the following atmospheric variables: 10 m winds, temperature and humidity, short and long wave radiation and precipitation. The NAO index used in this study is a difference in normalized (mean set to zero and standard deviation set to one) sea level pressure anomalies, Gibraltar minus Iceland (*Jones et al.* [1997]) (Figure 3.1b). This index was chosen due to the length of the record, with monthly data available from 1825 to the present (only data up to 2010 is used in this study). To produce the NAO-based forcing data, the NAO index is regressed onto the monthly means of the 8 required forcing fields from the inter-annual COREv2 dataset, using data from 1948 until 2006, for each month separately. These forcing patterns show a strong signal in the Northern Hemisphere,

especially over the North Atlantic, and a weaker signal elsewhere (Figure 3.2). In summer, the forcing patterns are considerably weaker by at least a factor of 2 in most locations (Figure 3.2)[1]. These patterns are then multiplied by the NAO index for each month and added to the normal year COREv2 data to create an atmospheric forcing dataset from 1825 to 2010. A model integration, referred to as NAO-forced (NF), is performed using the NAO forcing patterns together with the time series of the observed NAO index from 1826 to 2010 (Table 3.1). A drawback of our method, as opposed to using a flux based forcing dataset as in *Eden and Jung* [2001], that is since the forcing anomalies are added to the model year forcing, the storm track is in the same location throughout the entire model integration irrespective of the applied NAO index. In reality both the storm track and the storminess in the Atlantic region are affected by the NAO index (*Hurrell et al.* [2003]).

3.3.3 Stochastic forcing

In the stochastically-forced (SF) integration, the NAO index used to drive the model (referred to as the stochastic NAO) has a white spectrum in each month by construction, and is normally distributed, with the same mean and standard deviation as the observed NAO index for each month separately. In Figure 3.3a, the JFM mean of the stochastic NAO index is shown along with a wavelet spectrum of this index (for more details see section 3.4). Apart for the NAO index used to drive the model, the SF and NF integrations are performed similarly.

[1]The station based NAO index of *Jones et al.* [1997] is not ideal for the summer since the centers of action of the NAO are shifted to be centered over Greenland and the United Kingdom, as opposed to Iceland and the Azores, based on an EOF analysis (*Hurrell et al.* [2003],*Greatbatch and Rong* [2006]). We ignore this issue here since it is the winter NAO that matters for forcing the AMOC (*Eden and Willebrand* [2001]).

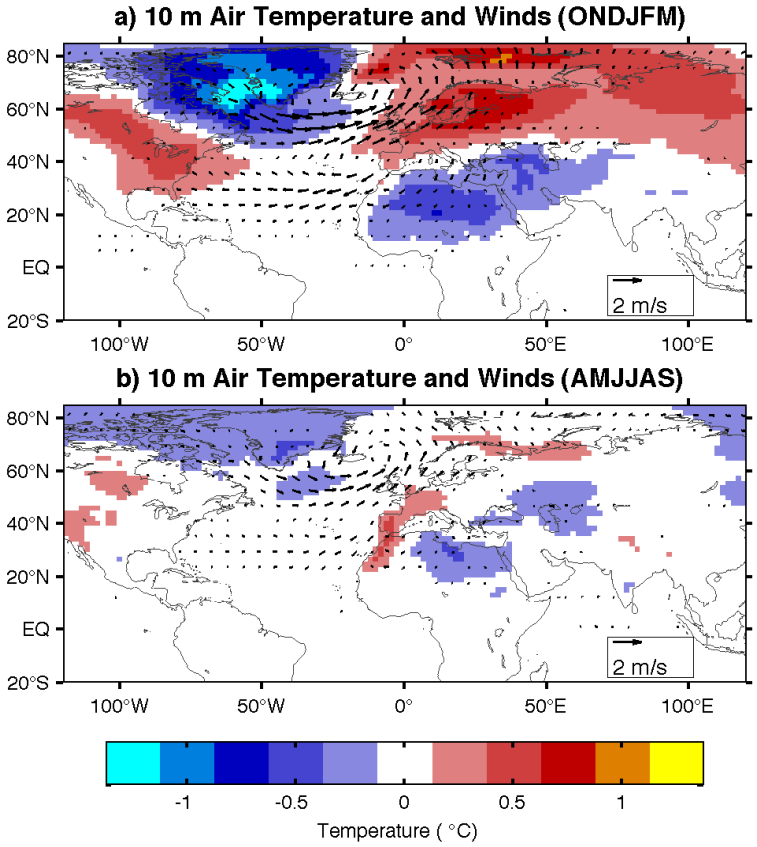

Figure 3.2: The mean of one standard deviation of the 10 m temperature and 10 m wind NAO-regressed fields (a) averaged over the colder months (ONDJFM) and (b) averaged over the warmer months (AMJJAS). The shading shows the 10 m temperature and the vectors show the 10 m winds. Winds below 0.1 m/s are not shown and wind vectors are only shown for every third grid box.

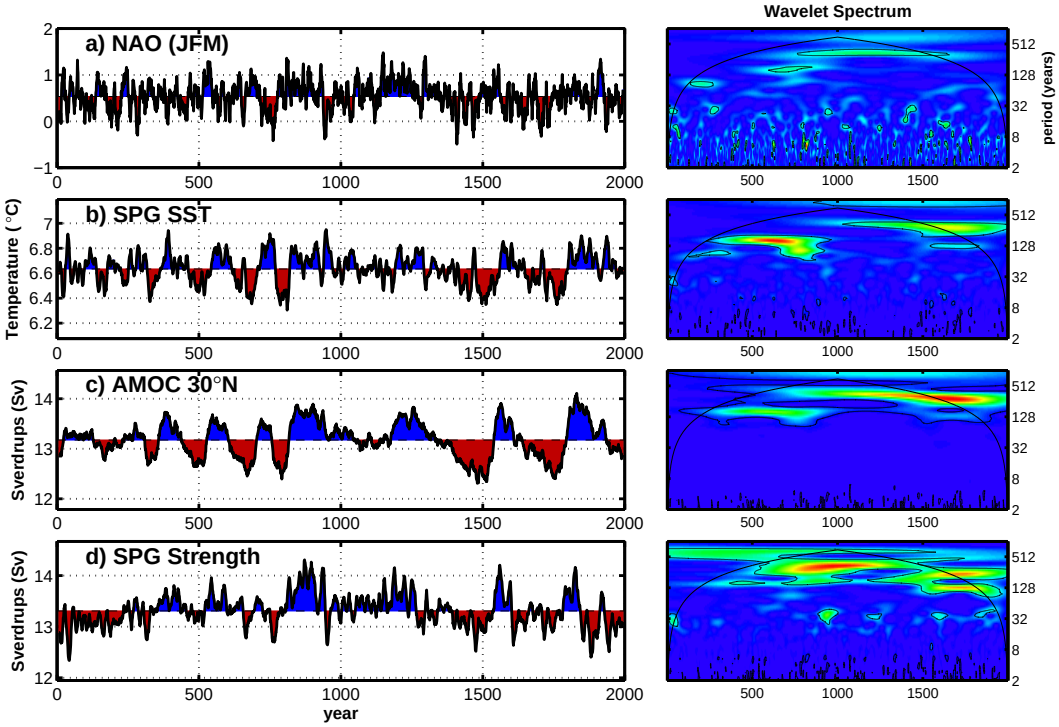

Figure 3.3: (a) The stochastic NAO index averaged over the winter (JFM), (b) the annual mean SST in the SPG region (defined as 60°W to 15°W, 48°N to 65°N), (c) the AMOC at 30°N, defined as the maximum annual mean meridional overturning at 30°N and (d) the SPG strength, defined as the negative mean barotropic stream-function in the sub-polar gyre region, from the stochastic model integration (left) along with the wavelet analysis (right). Before plotting all the time-series have been filtered with an 11 year running mean. Prior to the calculations shown, the linear trend was removed from the time-series.

3.3.4 Model spin-up

A 900 year long spin-up was performed using the normal year COREv2 forcing alone. All experiments using inter-annually varying forcing were then started from year 725 of the spin-up model integration. When changing from normal year to inter-annually varying forcing it takes the model several years to adjust to the change. To avoid problems associated with the change, in the cases of using observation-based forcing (FF and NF), the forcing cycle is repeated twice and the second iteration is then analyzed. When stochastic forcing (SF) is used, the first 150 years are considered as model adjustment and are not analyzed.

3.4 Model results

3.4.1 NAO-forced integration

With the NAO being the main source of atmospheric variability over the North Atlantic, a natural question is: How much of the ocean variability can be explained through the NAO alone? This question was previously addressed in the paper by *Eden and Jung* [2001] where they show that important features of the multi-decadal variability in the North Atlantic SST can be reproduced only using inter-annually varying NAO forcing. Here we compare the NAO-forced (NF) model integration to the fully-forced (FF) model integration and observations (where available). Overall, the NF model integration reproduces the variability in the FF integration particularly in the Atlantic at higher latitudes, especially north of 45°N (not shown).

For the annually averaged sea surface temperature (SST) in the sub-polar gyre (SPG) region (defined as 60°W to 15°W, 48°N to 65°N and denoted SPG SST) the correlation between the FF and NF model integrations is 0.73 (Figure 3.4b). However, the variability in NF has approximately half the amplitude of that from

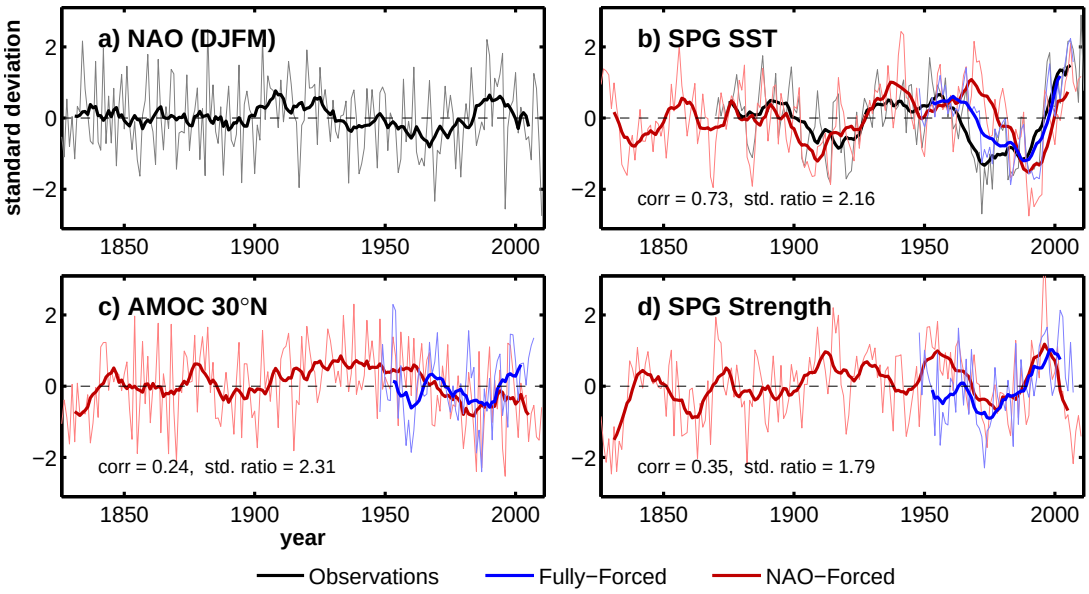

Figure 3.4: (a) The JFM NAO index, (b) the annual mean SST anomalies in the SPG region, (c) the AMOC at 30°N and (d) the SPG strength from observations where available in black, the FF model shown in blue and the NF integration in red. All time-series are normalized by the standard deviation of the time-series. The fine lines are inter-annual values and the thick lines are filtered with an 11 year running mean. The correlations between the two time-series and the ratio of the standard deviation of the FF integration to the NF integration are shown when applicable.

the FF integration (measured as the ratio of the standard deviation of the time series of annual means). When the entire North Atlantic is considered (the AMV region, not shown) the signal is a factor of 6 weaker, due to the atmospheric forcing being concentrated in the northern North Atlantic. The observed time-series of SPG SST (*Rayner et al.* [2003]) shows a multi-decadal signal with minima around 1920 and 1975, a maximum around 1950 and increasing SST from the late 1990s to the present (Figure 3.4b). This index is representative of the northern component of the SST pattern associated with the AMV index. This signal is also present in the NF and FF integrations with some significant differences in timing of the events (Figure 3.4b). Similarities with the observed SST, particularly in FF, are expected since the ocean model forcing includes the 10 m atmospheric temperature.

In the study by *Eden and Jung* [2001] the AMOC was measured using the meridional overturning at 48°N, which they showed to have a multi-decadal signal. The annual mean AMOC at 48°N from the NF integration compares to the *Eden and Jung* [2001] AMOC quite well with a correlation of 0.73 on inter-annual timescales and 0.86 on decadal timescales (running mean of 11 years applied to the two time-series). However, in this study we measure the AMOC using the maximum value of the annual mean meridional overturning streamfunction at 30°N as it has a more prominent multi-decadal component. The AMOC from the NF model integration exhibits multi-decadal variability with minima around 1890 and 1990 and a broad maximum around 1940 (Figure 3.4c). The AMOC at 30°N shows some similarity between the FF and the NF integrations especially in the trend seen in the filtered data from 1960 until 1975 as well as the slight upward trend there-after (Figure 3.4c) with the trend in the NF integration being weaker. The variability of the AMOC in the NF integration is a factor of 2.3 weaker than the FF integration when measured as the ratio of the standard deviation of annual means.

The strength of the subpolar gyre (SPG) in this study is measured as the negative of the annual mean barotropic streamfunction averaged over the SPG region (60°W to 15°W, 48°N to 65°N, as in *Lohmann et al.* [2009]). SPG in the NF integration shows some variability with timescales on the order of 2-3 decades, which is shorter than that seen in the AMOC (Figure 3.4d). When looking at the SPG on the longer timescales (11 year running mean) there is a similar signal in both the FF and the NF integrations during the time of their overlap (Figure 3.4d), with a minimum at approximately 1975 and a maximum at 1995 (Figure 3.4d). In the case of the SPG strength the ratio of variability from FF to NF is 1.8.

3.4.2 Stochastic integration results

In the Stochastically Forced (SF) model integration, the OGCM was forced for 2000 years using a white noise NAO index (Figure 3.3a). Detrended time-series of SPG SST, AMOC at 30°N and the SPG strength, along with their wavelet spectra (following the technique in *Torrence and Compo* [1998]) are shown in Figure 3.3. The wavelet spectra and spectral analyses (not shown) show that there is enhanced variability at low frequencies in the ocean response, however, there does not seem to be a particular frequency of variability that stands out, as one would expect if an internal ocean/sea-ice mode of variability were being excited (e.g., as suggested by *Griffies and Tziperman* [1995]). Moreover, the striking thing from the wavelet spectra in Figure 3.3 is that the structure of the model response in frequency space is very similar to that in the forcing; see, for example, the strong signal of approximately 150 year variability between years 500 and 1000, and the approximately 300 year variability from year 1000 to 1750. These similarities suggest that the ocean has a linear response to variability in the atmospheric forcing, as seen in the study by *Delworth and Greatbatch* [2000]. The SPG SST, AMOC at 30°N and SPG strength all have the property that variability at lower frequencies is stronger than at higher frequencies, as one would expect for a red noise process. In the case of the SPG SST index, the SST follows a simple red spectrum [2] quite closely (not shown) while the AMOC at 30°N and the SPG strength do not follow the simple red noise spectrum. The wavelet spectrum for the AMOC at 30°N shows a strong signal at periods above approximately 90 years that mirrors the signal in the NAO, but with much weaker variability on shorter time-scales (Figure 3.3c). The behavior of the sub-polar gyre (SPG) strength is similar to the AMOC at 30°N with lower frequency variability highlighted. However, for the SPG, the enhanced response starts at a considerably lower period of approximately 15 years (Figure 3.3d). In particular, variability at

[2] A simple red spectrum is defined in *Gilman et al.* [1963] to be a first order Auto-Regressive process, AR(1), process.

periods around 32 years is enhanced in the SPG time-series. An exception to this in the SPG strength is that the variability seems to completely disappear around 60 years while periods above and below 60 years exist.

3.5 Statistical Models

We now turn to statistical models to explain the characteristic responses of the AMOC at 30°N and the SPG strength variability.

3.5.1 Relation between the AMOC and the NAO

In the wavelet spectrum from the previous section it appears that there may be a linear relationship between the NAO and the AMOC at 30°N on time-scales longer than approximately 90 years. After applying a low pass filter with a cut off frequency of 86 years (86 years gives the highest correlation values in the following analysis) the annual mean AMOC and winter NAO time-series show similar peaks and troughs, slightly shifted from each other (Figure 3.5a), with peaks (troughs) of the NAO index coinciding with an increase(decrease) in the AMOC. This result suggests that the NAO influences the rate of change of the AMOC, $dAMOC/dt$, rather than the AMOC itself (Figure 3.5a). This implies that the AMOC may be modelled as the integral of the NAO index. Thus, following *Curry and McCartney* [2001] and *Ortega et al.* [2011], we try to model the AMOC at 30°N using a weighted summation of the winter NAO index (JFM), an index we refer to as an "integrated NAO", in the following way:

$$AMOC(t) = \alpha_0 + \sum_{k=1}^{q} \alpha_k NAO(t-k+1) + \xi(t), \tag{3.1}$$

where q is the number of years of the NAO used to compute the AMOC, with the

α_k's computed using a linear regression method. The correlation between simulated and NAO reconstructed AMOC increases with q, leveling off at 50 years with a value of approximately 0.7 (Figure 3.6). We use 53 coefficients in the remainder of our analysis giving a correlation of 0.68 for monthly means and 0.67 for decadal timescales (here decadal timescales is defined as an 11 year running mean) (Figure 3.5b). The coefficients are computed by linear regression and can be divided into two groups. The first 2-3 coefficients are responsible for the inter-annual timescales and the remaining coefficients produce the multi-decadal signal (Figure 3.5c). The later coefficients are all relatively small, positive and of similar value, allowing us to draw parallels between the AMOC reconstruction and applying a 53 year long running mean to the NAO. Furthermore, applying a 53 year long running mean is similar to low-pass filtering data with a cut off frequency approximately twice that of the order of the running mean, giving some insight into the apparent cut off of 86 years mentioned earlier.

As an alternative to integration over 50 years of the NAO index, the AMOC at 30°N may be modeled as an AR processes (see the Appendix). From theory, an autoregressive (AR) process of order p,

$$AMOC(t) = \sum_{h=1}^{p} \phi_h AMOC(t-h) + w(t), \tag{3.2}$$

where $w(t)$ is white noise, and ϕ_h are the AR coefficients, can be rewritten as an infinite sum of the white noise, $w(t)$ (*Shumway et al.* [2000]). Integrating the NAO, as done above, is similar to having an infinite sum of white noise. In the integrated NAO above 53 years of the NAO index are used and increasing the number of previous years makes very minor improvements to the fit, suggesting that it is worthwhile to consider an AR fit. The power spectrum of the AMOC (Figure 3.7a) shows that it does not satisfy the simple definition of a red noise process (an AR(1) process) which is often used as a null hypothesis test when looking for the

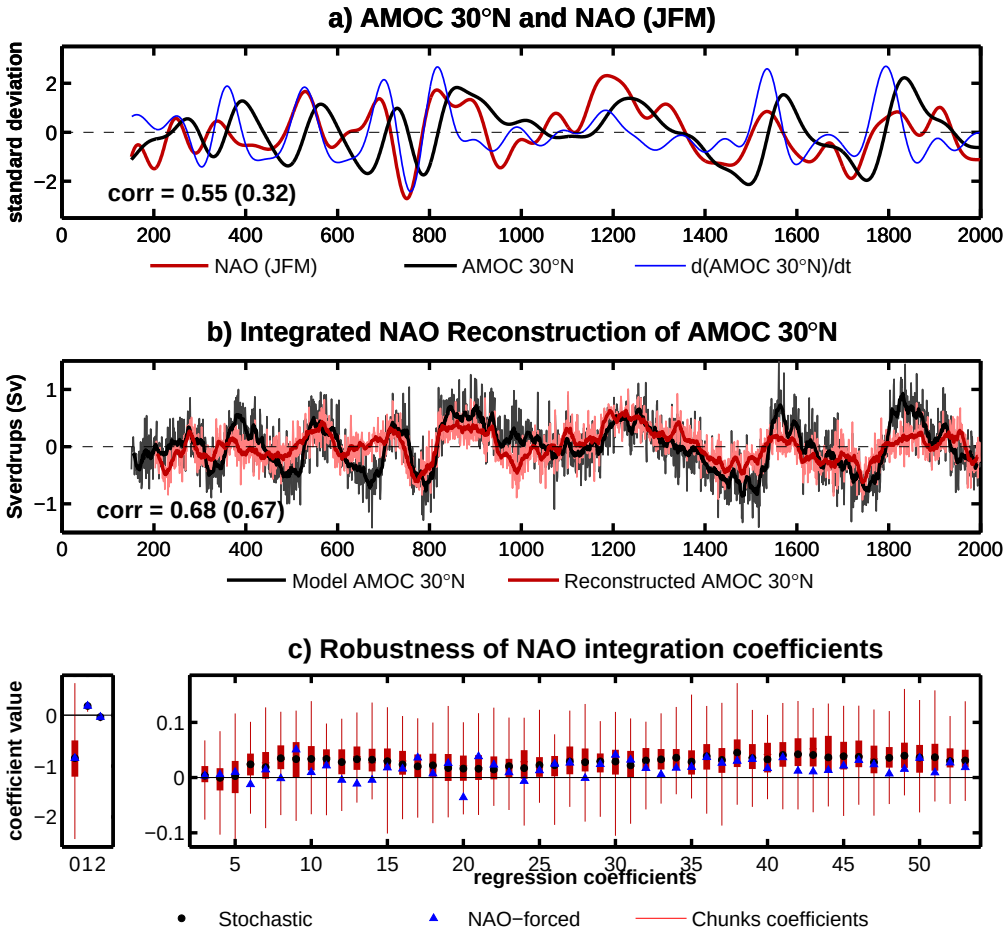

Figure 3.5: (a) Comparison of the time-series of the JFM Stochastic NAO index (red), with the AMOC at 30°N (black) and the time derivative of the AMOC at 30°N (blue). All the time-series are displayed filtered with a 86 year low pass Butterworth filter. The correlations in the lower left corner are the correlation between the NAO and the time derivative of the AMOC at 30°N and the correlation between the NAO and the AMOC at 30°N in brackets. (b) Reconstruction of the model AMOC at 30°N using a weighted moving average (see Eqn. 3.1) of the NAO (red) compared to the model AMOC at 30°N. The fine lines are inter-annual values and the thick lines are filtered with an 11 year running mean. Correlations for inter-annual data are shown in the left corner, and for filtered data in brackets. (c) The coefficients computed for the reconstruction (black circles), coefficients estimated from the NF integration (blue triangles) and the range of the coefficients when 185 year long chunks are used is shown as a thin red line with the 25th to 75th percentile shown as a thick red line. Note the different scales used for coefficients 0 to 2 and 3 to 53.

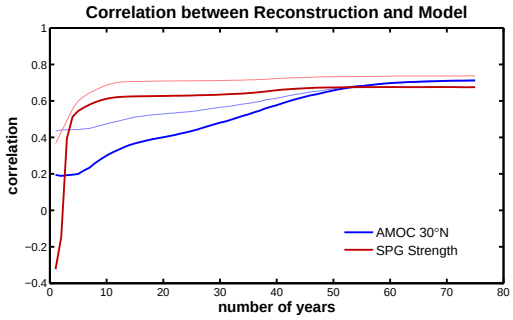

Figure 3.6: Correlations between model AMOC at 30°N and the integrated NAO reconstruction of the AMOC at 30°N (blue) as a function of the number of years of the NAO index used in the moving average and similarly for the SPG strength (red). The thin lines are constructed using inter-annual varying data and the thick lines use data filtered with an 11 year running mean.

possibility of an oscillation of the AMOC internal to the climate system. In SF there is no pronounced oscillatory peak in the spectrum which would have been consistent with the existence of an internal mode of oscillation in the ocean/sea-ice model as noted earlier.

In *Eden et al.* [2002] an AR(5) process was successfully used to represent the ocean model in their study. The partial auto correlation (PACF) function is often used to help determine the order of AR process that gives the best fit (see the Appendix). In our study, the PACF of the AMOC at 30°N from the SF model integration has significant correlations at the 5% level up to 7 years lag, whereas the auto correlation function (ACF) does not have a clear point where it no longer is significant (Figure 3.7b). This suggests that the best fit to the AMOC for the SF integration is an AR(7) process (directly testing AR processes with orders higher and lower than 7 also does not improve the fit). The coefficients, ϕ_h of the AR(7) process computed using the Yule-Walker equations (detailed in *Shumway et al.* [2000]) are shown in Figure 3.7d. The theoretical power spectrum of the AR(7) process using the computed ϕ_h's shows a very good fit to the power spectrum from the AMOC from the SF integration, consistent at the 5% significance level (Figure 3.7a).

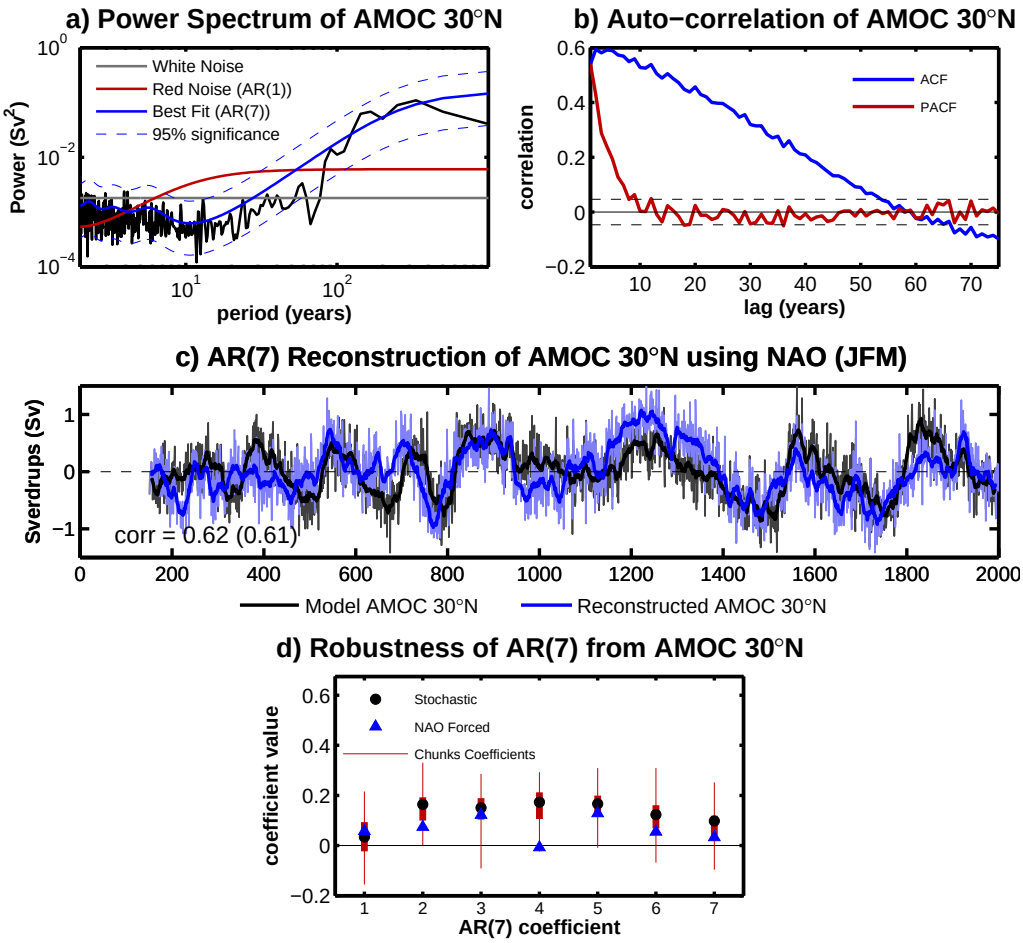

Figure 3.7: (a) The power spectrum of the AMOC at 30°N (black) along with the theoretical white noise spectrum (gray), red noise (AR(1)) spectrum (red) and the best fit AR(7) spectrum (blue) along with the 95% confidence interval (dashed blue). (b) The ACF (blue) and the PACF (red) of the AMOC at 30°N with the dashed black lines indicating 95% significance when comparing with white noise. (c) Reconstruction of the model AMOC at 30°N using an AR(7)process with the NAO as the forcing data (blue) compared to the model AMOC at 30°N. The thin lines are inter-annual values and the thick lines are filtered with an 11 year running mean. Correlations for inter-annual data are shown in the left corner, and for filtered data in brackets. (d) The coefficients computed for the reconstruction (black circles), coefficients estimated from the NF integration (blue triangles) and the range of the coefficients when 185 year log chunks are used is shown as a thin red line with the 25th to 75th percentile shown as a thick red line.

We reconstruct the AMOC as an AR(7) process, with the NAO index used as the white noise in the AR(7) process (Figure 3.7). The best estimate for the noise, $w(t)$, in the AR process is the winter mean of the NAO index over the months January, February and March (JFM), which is not surprising since it is only during the late months that deep convection, the mechanism linking the NAO to variability in the AMOC, occurs. The AR(7) reconstruction of the AMOC produces a strong correlation with the SF model AMOC with a correlation of 0.62 on inter-annual and 0.61 on multi-decadal timescales (11 year running mean). This statistical method performs only slightly worse than assuming that the AMOC can be reconstructed by integrating the NAO index as discussed earlier, but to achieve a similar correlation as with the integrated NAO reconstruction requires at least 45 previous years of the NAO index (Figure 3.6).

3.5.2 Relation between the SPG strength and the NAO

In contrast to the AMOC at 30°N, the SPG strength has variability on shorter time scales, highlighted by the variability present around the 32 year period evident in the wavelet analysis (Figure 3.3d). Applying a low-pass filter with a 15 year cut off to both the JFM NAO index and the SPG strength from the SF model integration shows a relationship similar to that with the AMOC at 30°N, where the peaks (troughs) in the NAO aline with an increasing (decreasing) SPG strength, giving a correlation between $d(SPG)/dt$ and the NAO index of 0.57 (Figures 3.8a). Performing a similar analysis on the SPG strength as with the AMOC gives different results. The ACF of the SPG strength time-series decreases rapidly up to 10 years lag and remains stable thereafter (Figures 3.9b). Fewer coefficients are required for a skillful integrated NAO reconstruction of SPG strength (i.e., analogous to Equation 3.1), as compared to the AMOC at 30°N (Figure 3.6 and 3.8b). Using 10 previous years of the JFM NAO index gives a correlation of 0.69 between reconstructed and full timeseries on inter-annual timescales, and 0.61 on decadal timescales. However, the

reconstruction continues to gradually improve up to the inclusion of approximately 45 years (Figure 3.6). Figure 3.8b shows the integrated NAO reconstruction of the SPG strength using 10 years of the NAO index with the coefficients shown in Figure 3.8c. As before, the first few coefficients represent the inter-annual variability and the remaining coefficients reproduce decadal timescales. However, while the reconstruction captures variability on decadal timescales, variability on timescales longer than approximately 50 years are not properly reconstructed (this can be clearly seen in the power spectrum of the reconstructed SPG strength (not shown)). To capture the variability on timescales longer than 50 years, it is necessary to extend the number of years used in the NAO integration to 46 or more, giving a correlation of 0.71 on inter-annual timescales and 0.65 on decadal timescales.

The PACF analysis of the SPG strength shows that the best fit for the SPG strength would be an AR(5) process (Figure 3.9b). Again, using the winter (JFM) NAO index as the white noise in the AR process the SPG strength is reconstructed reasonably well for the longer timescales with a correlation of 0.59 but fails at representing the inter-annual variability with a correlation near zero (Figure 3.9c). The study by *Eden and Willebrand* [2001] shows that positive NAO wind stress forcing creates a positive anomaly in the barotropic streamfunction in the SPG region and hence decreases the strength of the SPG in phase with the NAO. However, only 3 years later the barotropic streamfunction has the opposite sign in the SPG region, due to the delayed ocean response to the heat flux forcing. From this it follows that the internal variability of the SPG strength is likely to have different dynamics from the longer time-scale variability, probably explaining the failure of the AR(5) model on inter-annual timescales.

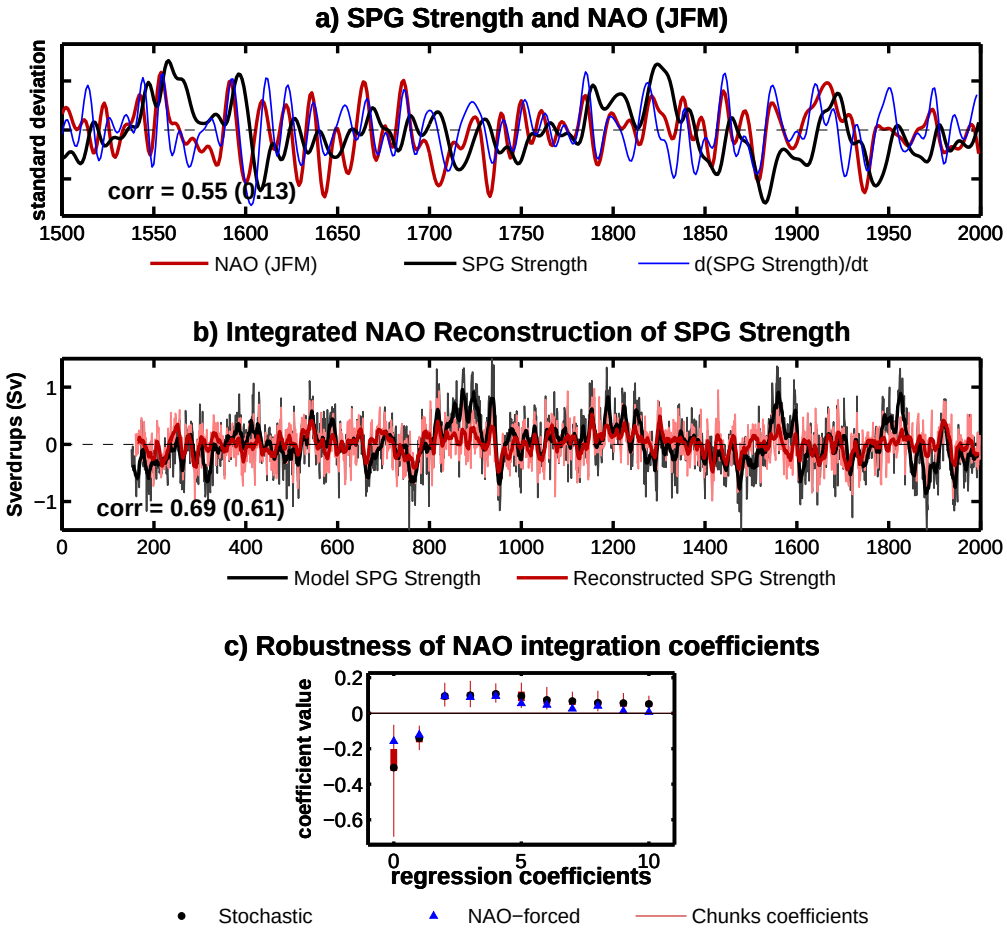

Figure 3.8: Same as Figure 3.5 for the SPG strength with the exception of using a cut off of 15 years and the different scale in (a). Note that even though only a subsection of the timeseries is shown in (a) all the calculations are done on the full timeseries.

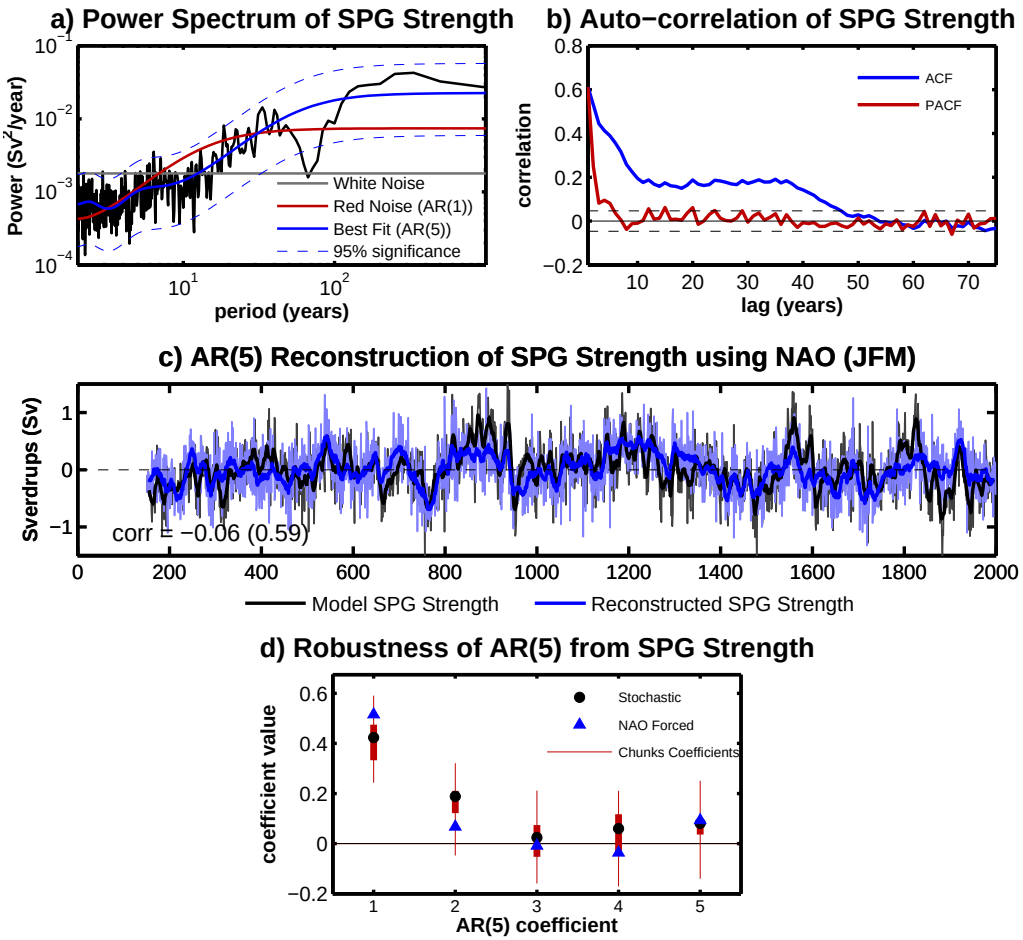

Figure 3.9: Same as Figure 3.7 for the SPG strength.

3.5.3 Reconstruction of the NAO-forced integration

Returning to the NAO forced (NF) integration mentioned in section 3.4.1, we can use this model integration to test the statistical models developed in the previous sections. Reconstructing the AMOC at 30°N using the integrated NAO approach with the coefficients computed in section 3.5.1 from the stochastically forced (SF) integration gives a reconstruction that is on par with the reconstruction of the SF integration (Figure 3.10), with correlation values almost identical on the inter-annual scale and even slightly higher on the multi-decadal scale (Figure 3.10a). Similarly, for the SPG strength, the integrated NAO statistical model using coefficients computed from the SF integration performs quite well, with correlations only marginally lower than those from the long stochastic model integration (Figure 3.10b). Similar results are also seen with the AR statistical models using the coefficients computed from the SF integration, however, in this case the correlations are slightly lower than the reconstruction of the full stochastically forced model integration on decadal time-scales (Figure 3.10c&d). As noted in sections 3.5.1 and 3.5.2, the AR(7) reconstruction of the AMOC was able to capture the variability on inter-annual time-scales but the AR(5) reconstruction of the SPG strength failed at capturing the inter-annual variability, as indeed, is also the case here. These statistical models do not work as well for the FF integrations (not shown). However, this is not unexpected given that the FF integration is forced with more than just the NAO index.

3.5.4 Robustness of the coefficients

In this study we based our statistical models on 1850 years of data. However, over a thousand years of observational data are not available. Here we test the robustness of our statistical models to fitting using a similar length of data available from instrumental observations, and we divide the SF model integration into 185 year long chunks. The coefficients for the statistical models are then computed for each of the

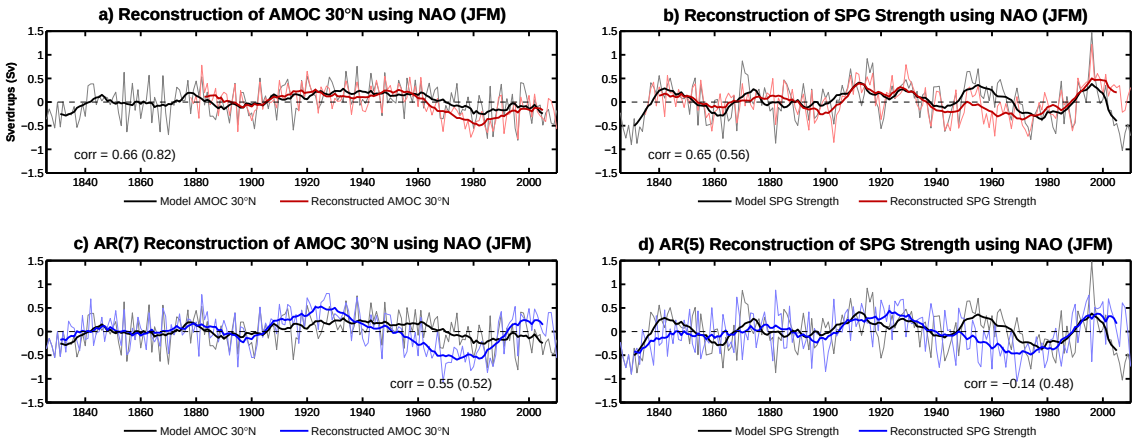

Figure 3.10: Reconstructions of i) the AMOC at 30°N from the NAO-forced model integration using (a) integrated NAO and (c) the AR(7) process and ii) the SPG strength from the NAO-forced model integration using the (b) the integrated NAO and (d) the AR(5) process. The time series from the NF model integration is shown in black and the integrated NAO reconstruction shown in red and the AR reconstruction shown in blue. The thin lines are inter-annual values and the thick lines are filtered with an 11 year running mean.

185 year long chucks. For the integrated NAO reconstructions the first coefficient (α_0) has a vary large range in values (Figures 3.5c and 3.8c). However, this large range is due to the differences in the mean of the 185 year long chunks, since the first coefficient is just a constant (Equation 3.1). The remaining coefficients in the NAO integrated reconstructions of both the SPG strength and AMOC tend to keep the same sign for the majority of the chucks. When the number of coefficients used in the NAO integration are increased the coefficients become extremely small and vary about zero (not shown). When recomputing the integrated NAO coefficients for the NF integration we get values that all fall within the range of values computed from the 185 year long chunks (Figures 3.5c and 3.8c). The range of the AR coefficients when computed from 185 year long chunks from the SF integration show for some coefficients that they can have a change of sign (Figures 3.7d and 3.9d). However, as for the integrated NAO, the AR coefficients computed from the NF model integration fall within the range of the coefficients computed from the 185 year chunks from the SF integration.

3.6 Conclusions and Discussion

The main question we wished to address was: What is the nature of multidecadal variability of the North Atlantic that is excited by stochastic atmospheric forcing associated with the NAO? Thus our analysis is concentrated on the two dominant ocean circulation patterns linked with Atlantic multidecadal variability: the AMOC at 30°N and the SPG strength. This study looked at the response of an OGCM to stochastic NAO forcing in a 2000 year long simulation (i.e., forcing with a spatial NAO structure scaled by a white noise time series). The global OGCM, NEMO, is used with a horizontal resolution of approximately 0.5°, which compared to previous studies (i.e. *Eden and Jung* [2001]) is higher and includes interactions with the high latitudes. A potential drawback to the model set-up used in this study is that the model is forced using bulk formula as opposed to the flux forcing directly, as a result variations in storm track position associated with the NAO are not properly represented and surface variations are damped. However, given that the focus is on ocean circulation and that the NAO forced (NF) integration can capture a significant part of the variability in the fully forced (FF) integration we believe these do not compromise our results too much.

Our results provide no evidence for a preferred frequency response to the stochastic forcing, with the strength of the response increasing with period until it reaches a cutoff frequency at which it saturates. The AMOC at 30°N and the SPG strength, show the characteristics of a red spectrum in which the low frequency variability is stronger than the high frequency variability, but do not satisfy the null hypothesis of a simple red noise spectrum (defined as the spectrum of an AR(1) process). Furthermore, wavelet spectral analysis, and comparison of filtered timeseries and time derivatives, clearly show that the AMOC at 30°N and the SPG strength are a simple linear response to the atmospheric forcing.

We applied simple statistical models in order to understand the different char-

acteristic response of the AMOC at 30°N and the SPG strength. First, we model AMOC and SPG strength as the integral of the proceeding winter NAO index with different weights for different lags. With this method we can skillfully reconstruct the AMOC and SPG strength in the stochastically forced (SF) integration with a correlation of approximately 0.65 using 53 years and 10 years of the winter NAO index, respectively. Upon investigation of the coefficients computed for the integrated NAO it becomes clear that the first 2-3 coefficients are responsible for reconstructing the inter-annual variability of the AMOC and the SPG strength, while the remaining coefficients reconstruct the decadal to multidecadal variability. Reconstructing the SPG strength using only 10 years of the NAO index misses some of the multidecadal timescales, which are captured when we extend the integration to include 46 years of the winter NAO index. The coefficients beyond the first 2-3, for the AMOC and the first 10-15 for the SPG strength are all of similar value, and thus the integration is similar to applying a running mean to the NAO index of approximately 50 years, which leads to having signals longer than about 90 years amplified.

Alternatively, the AMOC at 30°N and the SPG strength can be reconstructed using AR processes, using previous years of the indices themselves and only one year of the winter NAO index. For the AMOC at 30°N, an AR(7) process is able to produce a fit with a strong correlation ($\sim$0.68) on both inter-annual and multidecadal timescales. For the SPG strength an AR(5) process gives the best fit to represent multidecadal timescales but fails to capture the variability on interannual timescales probably because of different dynamics operating on the inter-annual and decadal timescales (*Eden and Willebrand* [2001]). Neither the AMOC nor the SPG strength follow the simple AR(1) spectrum or show pronounced spectral peaks at a single frequency. This analysis concludes that using AR processes (in the case of the AMOC at 30°N) or integrating the NAO (in the case of the SPG strength) are nice simple methods to reconstruct and interpret the results from an OGCM.

The higher order AR processes give insight into the internal dynamics and predictability of the ocean, with higher order AR processes suggesting more predictability. Comparing the AR process fittings among various models can be quite useful for model inter-comparison studies. For instance, Figure 3.11 shows the spectrum of the AMOC at 30°N from several coupled climate models along with the spectrum from the best fit AR process. Half of these coupled models show that an AR process of order 7 is the best fit while the remaining models all have a best fit of at least order 4. The results show that the AMOC is not as simple as a red noise (AR(1)) process and supports using a higher order AR process to represent the AMOC. In the paper by *Timmermann et al.* [1998], it was already pointed out that it is not possible to fit an AR(1) or AR(2) process to the AMOC, and in the paper by *Eden et al.* [2002], the authors successfully used an AR(5) process to represent ocean variability and make future projections about the likely behavior of the NAO.

Further investigation using atmosphere-ocean coupled models can help gain further insight towards the potential for using integrated NAO and AR fits as a method for prediction. *Ortega et al.* [2011] make a first attempt at this type of analysis. In our case only the winter NAO index was used. However, there is additional variability present in the atmosphere that could be included in the analysis: for example, *Medhaug et al.* [2012] showed that both the Scandinavian Pattern and the NAO is important for driving the AMOC in their model and *Langehaug et al.* [2012] showed that the East Atlantic Pattern is important for controlling the SPG strength in their model. Other oceanic variables, with a strong connection to the NAO for example, the Barents Sea inflow (*Dickson et al.* [2000]), could also be represented using simple statistical models. Finally, the analysis used in this paper demonstrates that simple statistical models can potentially be very useful for representing climate variables on both interannual to interdecadal timescales both efficiently and inexpensively, with a potential use as predictive tools.

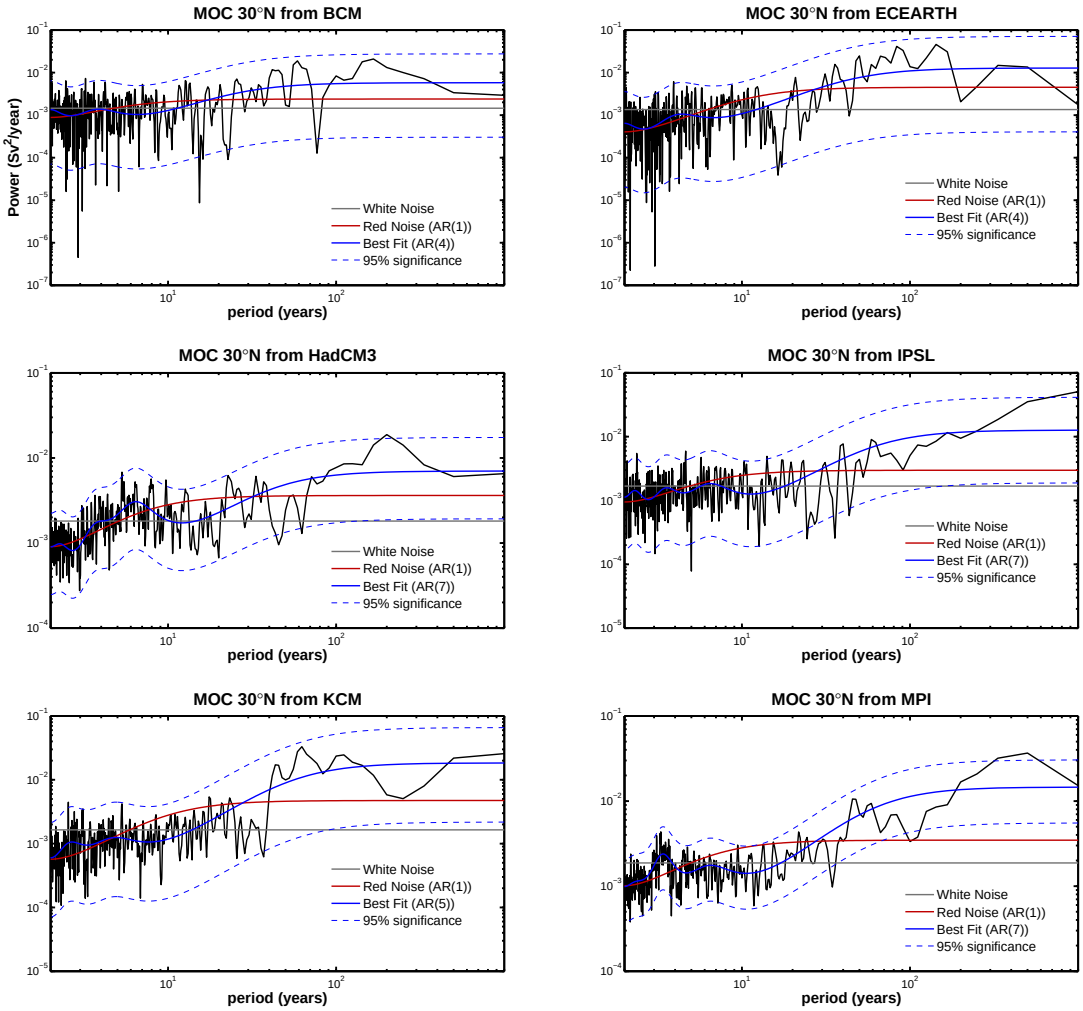

Figure 3.11: Power Spectrum of the AMOC at 30°N from several Thermohaline Circulation at Risk (THOR) models (http://www.eu-thor.eu/) (black) along with the theoretical white noise spectrum (gray), red noise (AR(1)) spectrum (red) and the best fit AR(p) spectrum (blue) along with the 95% confidence interval (dashed blue).

3.6.1 Appendix: Auto-Regressive Processes

Following chapter 3 in *Shumway et al.* [2000], an auto-regressive (AR) processes uses values from past time steps to compute the current time step, as shown in equation 3.2. To determine the order, q, of the AR process the partial auto-correlation function (PACF) is computed. The PACF at lag k is the correlation between x_t with x_{t+k} with the dependence on x_{t+1} to x_{t+k-1} removed from both x_t with x_{t+k}. The partial autocorrelation can be computed using the Durbin-Levinson iterative algorithm detailed in *Shumway et al.* [2000]. The last lag at which the PACF is significant at the 5% level is the order, q, which is for the best fit for the AR process. In contrast to the AR process the best fit for a weighted moving average process (like the integrated NAO used in this study) can be determined in the same way from the auto-correlation function. The coefficients for the AR process are calculated using the Yule-Walker equations (detailed in *Shumway et al.* [2000]) and a theoretical spectrum can be constructed using the following equation from *Von Storch and Zwiers* [2002]:

$$\Gamma(\omega) = \frac{\sigma^2}{|1 - \sum_{k=1}^{q} \alpha_k e^{-2\pi i k \omega}|}, \tag{3.3}$$

where, ω is the frequency and σ^2 is the variance for the time-series $x(t)$.

3.6.2 Acknowledgements

We would like to acknowledge the support from the DFG Emmy Noether-Programm, GEOMAR, the EU-THOR project and the HLRN computing facility.

Chapter 4

Multiple Timescales of Stochastically Forced North Atlantic Ocean Variability

J. V. Mecking (1*), N. S. Keenlyside (2), R. J. Greatbatch (1)

In preparation for submission

(1) Helmholtz Centre for Ocean Research Kiel (GEOMAR), Dsternbrooker Weg 20, 24105 Kiel, Germany
(2) Geophysical Institute and Bjerknes Centre, University of Bergen, Bergen, Norway

*corresponding author: jmecking@geomar.de.

4.1 Abstract

The North Atlantic Ocean forms an important part of the global climate system containing and carries the majority of the northward oceanic heat transport. Variability in the Atlantic Meridional Overturning Circulation (AMOC) and the subpolar gyre (SPG) is often an important element of mechanisms for multidecadal variability in the North Atlantic Ocean. The North Atlantic Oscillation (NAO), the dominant winter atmospheric pattern, has been shown in previous studies to have an immediate response in the ocean as well as to be able to generate multidecadal variability in the ocean. Through a 2000 year long ocean only model integration forced with the atmospheric patterns associated with a white noise NAO index, we were able to identify three distinct timescales of ocean variability. The first, an interannual timescale with variability shorter than 15 years, can be related to Ekman dynamics. Secondly, the multidecadal timescale, 15-65 years, is mainly concentrated in the subpolar gyre and is controlled by temperature variability. Finally, the centennial timescales, with variability longer than 65 years, can be attributed to the ocean being in a series of quasi-equalibrium states. It has been shown that the AMOC at 30°N and the SPG strength can be reconstructed by integrating the NAO index used to forced the ocean model. Applying the integrated NAO method to the filtered timeseries on the three different timescales produces different results for each timescale; the interannual timescale has the first coefficient of the integrated NAO fit being relatively large and the rest near zero; the integrated NAO coefficients from the multidecadal timescales show a sinusiondal pattern with a period of approximately 25 years; and the centennial timescale has positive coefficients all of approximately the same value for 75 years for the AMOC at 30°N and 45 years for the SPG strength. Summing the integrated NAO coefficients from the three filtered timescales leads to the coefficients from the unfiltered timeseries.

4.2 Introduction

With the current increasing concern over anthroprogenic climate change, it is becoming more important to understand the natural variability in the Earth's climate system. The ocean plays an important role in the global climate system, with the North Atlantic being responsible for the majority of oceanic northward heat transport (*Wunsch* [2005]). The typical conveyer belt schematic of the large scale global oceanographic circulation depicts both vertical and horizontal flows (*Broecker et al.* [1991]). Of particular interest in this study is the North Atlantic basin which has a near surface northward transport of warm and saline waters from the tropics, via the Gulf Stream and North Atlantic Current to the Labrador and Greenland Seas, where the water then increases in density and sinks to form the North Atlantic Deep Water (*Rahmstorf* [2002]). The North Atlantic Deep water then, through a deeper return flow, is transported southward. The meridional component of this circulation is referred to as the Atlantic Meridional Overturning Circulation (AMOC) (*Latif et al.* [2006]). The Gulf Stream along with North Atlantic Current form a more zonal component of the ocean circulation and are at the interface of the subpolar gyre (SPG) and the subtropical gyre. This study will mainly be concerned with multidecadal to centennial variability of the AMOC and and SPG.

The observational record of the sea surface temperature (SST) contains a multidecadal signal in the North Atlantic region with a period of approximately 75 years (*Kerr* [2000], *Enfield et al.* [2001] and *Knight et al.* [2005]). This multidecadal signal is often referred to as the Atlantic Multidecadal Variability (AMV) or the Atlantic Multidecadal Oscillation and can be seen as the fingerprint for multidecadal variability in the entire North Atlantic basin. Unfortunately, the observational record of SST only extends back to 1870 (*Rayner et al.* [2003]) making it difficult to determine whether or not the multidecadal signal in the SST is an internally generated oscillation or just coincidence. In order to gain better insight into the multidecadal

variability present in the Atlantic Ocean one needs to turn to proxy data and model output.

Within the existing proxy and model data various timescales of multidecadal variability have been shown ranging from 20 year timescales (e.g. model: *Born and Mignot* [2012] and proxy: *Chylek et al.* [2011]) to multidecadal and longer timescales (e.g. model: *Menary et al.* [2012] and proxy: *Kilbourne et al.* [2008]). It is not uncommon to have variability on multiple timescales present in the North Atlantic Ocean at the same time; again, this effect is not only seen in model data (e.g. *Alvarez-Garcia et al.* [2008] and *Delworth and Zeng* [2012]) but also in proxy data (e.g. *Saenger et al.* [2009] and *Chylek et al.* [2012]). However, in order to be able to decrypt the physics behind this variability one needs to turn to modelling studies. Modelling studies have data below the surface, important for understanding both the AMOC and SPG strength variability.

Several modeling studies have looked into explaining the mechanisms behind multidecadal variability in the North Atlantic (e.g. *Dijkstra et al.* [2006], *Born and Mignot* [2012] and *Medhaug et al.* [2012]). In many cases these mechanisms involve convection in the northern regions of the North Atlantic (*Delworth et al.* [1993], *Born and Mignot* [2012] and *Medhaug et al.* [2012]). In particular, the Labrador Sea is an important region for deep convection, as seen in both modelling studies (e.g. *Medhaug et al.* [2012]) and in observations (*Dickson et al.* [1996]). Unfortunately, coupled atmosphere-ocean models often have difficulty placing the convection in the correct locations, with the convection favoring the region south of Greenland and/or the Irminger Sea (*Born and Mignot* [2012], *Ba et al.* [2013]). Increase in convection in the northern North Atlantic regions often leads the changes in the strength of the AMOC by a few years (e.g. *Delworth et al.* [1993], *Medhaug et al.* [2012] and *Ba et al.* [2013]). *Delworth et al.* [1993] show variability in the SPG strength leading the changes in the AMOC by approximately 10 years. In the study of *Delworth*

and Greatbatch [2000], an ocean model was forced with a stochastic atmosphere and the ocean produced an almost linear response on the multidecadal and longer timescales to the stochastic atmosphere forcing. The paper *Sutton and Allen* [1997] show from observation data that there is a propagation of SST anomalies along the path of the Gulf Stream and then continuing along the North Atlantic Current with a time scale of 12-14 years. Similarly, this pathway of the SST anomalies has been traced by *Alvarez-Garcia et al.* [2008] in an ocean model simulation again having a decadal timescale. The decadal timescale is too long to be explained solely by advection of the mean surface currents suggesting that both subsurface currents and anomalous currents may be important. Several studies have shown that various North Atlantic atmospheric patterns are important in driving or exciting the multidecadal variability in the North Atlantic (e.g. *Eden and Jung* [2001], *Medhaug et al.* [2012] and *Langehaug et al.* [2012]), among these one of the more prominate atmospheric pattern is the North Atlantic Oscillation (NAO).

The NAO, the dominant atmospheric pattern in the winter North Atlantic (*Hurrell* [1995]), is thought to play an important role in driving multidecadal variability in the Atlantic Ocean (e.g. *Eden and Jung* [2001] and *Medhaug et al.* [2012]). The NAO measures the strength of the westerly winds blowing across the North Atlantic (*Greatbatch* [2000]). An index for the NAO is often defined as the wintertime sea level pressure difference between a station near the high pressure center (positive phase; often the Azores Island or Lisbon, Portugal) and the low pressure center (negative phase; typically near Iceland) or the principle component of the first empirical orthogonal function of the wintertime sea level pressure over the North Atlantic (*Hurrell et al.* [2003]). In an observational study, *Curry and McCartney* [2001], were able to relate the observed NAO index to the transport in the intergyre region of the North Atlantic through integrating the NAO index over several previous years. In *Visbeck et al.* [1998], the ocean was forced with the wind stress forcing related to the NAO with its strength varying on different periods with a maximum period of

64 years. The strongest variability in the SSTs was modelled when the ocean model was forced with a 12 year oscillation of the NAO wind stress. In the study by *Eden and Greatbatch* [2003], an ocean model was forced with an atmospheric forcing pattern with constant positive NAO index, showing that the model responded with a damped oscillation with a period of 12 years. In a related modelling study, *Eden and Willebrand* [2001] showed that the response of the ocean to a positive NAO forcing is initially dominated by the wind forcing and then after approximately 3-5 years the heat flux forcing becomes more important, leading to an initial spin down of the SPG and then about 3 years later the sign of the SPG response changes. Forcing an ocean model with monthly fluxes related to the observed NAO index, *Eden and Jung* [2001] showed that a multidecadal variations in SST similar to observed were generated. Also, this study showed that the SST response to the NAO forcing is not only a reflection of the heat fluxes applied to the ocean surface but also involves ocean dynamics.

Similar results were found in Chapter 3, and experiments were preformed using a white noise NAO index. The 2000 year long white noise NAO index is capable of generating multidecadal to centennial variability in the North Atlantic Ocean. The AMOC and the SPG strength both show a red noise response to the NAO forcing with variability increasing with period until 86 and 15 years, respectively. Successful reconstructions of the model AMOC at 30°N and the SPG strength were made by integrating the NAO forcing, on the one hand, and using auto regressive (AR) model on the other.

In this chapter the various timescales of variability seen in the stochastically forced model integration from Chapter 3 are described and further analyzed. Section 4.3 gives an overview of the model setup used in this study. Section 4.4, describes some of the properties of the integrated NAO fit to both the AMOC at 30°N and the SPG strength and demonstrates that the results can be divided into three different

timescales; an interannual, a multidecadal and a centennial timescale. Sections 4.5, 4.6 and 4.7 go into further detail on each of these three timescales, and the results are then summarized and discussed in section 4.8.

4.3 Model set-up

The Nucleus for European Modelling of the Ocean (NEMO) Ocean General Circulation Model (OGCM) version 3.1 is used (*Madec et al.* [1998] in this study. The OGCM is used with the tri-polar ORCA05 grid which has a horizontal resolution of approximately 0.5°, with slightly higher meridional resolution towards the poles, and 46 vertical levels varying from a 6m thickness at the surface to 550m at depth. The Drakkar parameter configuration (*The Drakkar Group* [2007]), which has been successfully used in previous modelling studies (see *Barnier et al.* [2006]), is used used in this study. A surface salinity restoring of 150 days to climatology is employed to avoid model drift, partial steps are used to increase bottom resolution and the *Gent and McWilliams* [1990] eddy parameterization is used. An interactive sea ice model, LIM2, is also included in this model set-up. The atmospheric forcing used in this modelling study is based on the 10 m temperature, 10 m winds, 10 m humidity, shortwave radiation, longwave radiation and precipitation from the COREv2 dataset (*Large and Yeager* [2004], *Large and Yeager* [2009]) .

The same atmospheric forcing, experimental set-up and model parameters as described in section 3.3 are used in this study. We focus on the stochastic forced (SF) model integration, which consists of the OGCM being forced solely by atmospheric forcing based on a monthly white noise NAO index, (see sections 3.3.2 and 3.3.3 for a detailed explanation). The SF forced integration is started from year 725 of a climatological model integration using normal year forcing from COREv2 data (*Large and Yeager* [2004], *Large and Yeager* [2009]) and then run for 2000 years using the white noise NAO forcing. As in Chapter 3, the first 150 years were omitted from

the analysis to avoid an influence from the shock when going from climatological forcing to interannually varying forcing.

The oceanic convection, an important component in mechanisms for the meridional overturning circulation (MOC) (*Dickson et al.* [1996]), is measured by means of the surface mixed layer depth, defined as the depth at which the potential density differs from the surface value by 0.1 kg/m^3. In our simulations the main convection regions in the North Atlantic region are the Labrador and Greenland Seas (Figure 4.1a). The Greenland Sea convection region is found right at the ice edge (Figure 4.1) and with the exception of approximately 5 years, the mixed layer depth throughout the SF model integration is always greater then 3000 m. The sea ice extent in the model matches closely the sea ice extent from the observationally based dataset, HadISST (*Rayner et al.* [2003]), (Figure 4.1b,c).

4.4 Model Results

As discussed in Section 4.2, both the Atlantic Meridional Overturning Circulation (AMOC) and the Subpolar Gyre (SPG) form important parts of the ocean circulation in the North Atlantic Basin. The Atlantic meridional streamfunction is defined as follows,

$$AMOC(y,z,t) = \int_{-H}^{z} \int_{west}^{east} v(x,y,z',t)dxdz', \tag{4.1}$$

where $v(x,y,z,t)$ is the northward component of the velocity in the Atlantic Basin and H is the ocean depth. From this, an AMOC index at 30°N is defined as the maximum overturning circulation at 30°N, with the maximum of the AMOC typically occurring at a depth of 793 m (Figure 4.2a). Some properties of the AMOC at 30°N were discussed in Section 3.4.2. In particular, there is an abrupt change in the power spectrum when going from the shorter to the longer timescales at a

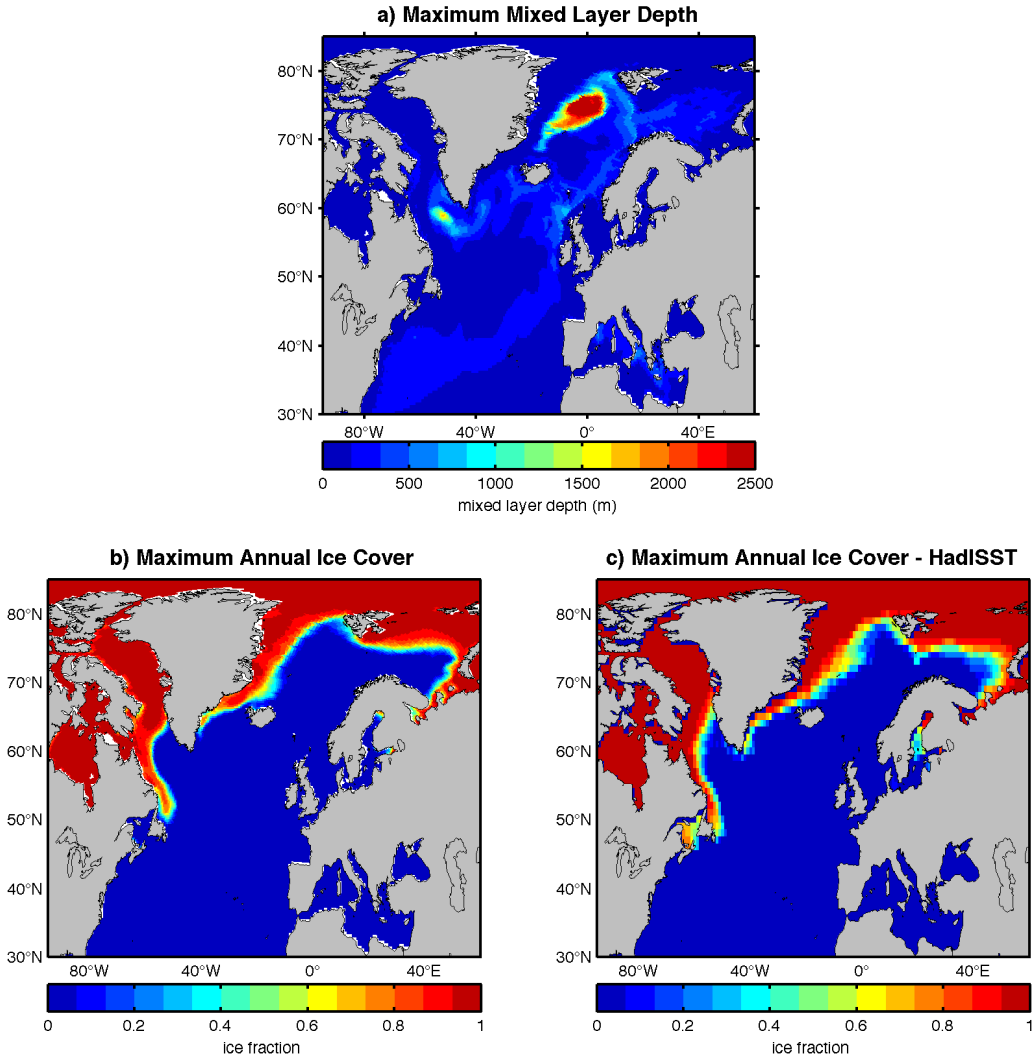

Figure 4.1: (a) Mean of annual maximum mixed layer depth from the SF model integration. (b) Mean of annual maximum ice fraction from the SF integration. (c) Mean of annual maximum ice fraction from HadISST data (*Rayner et al.* [2003]).

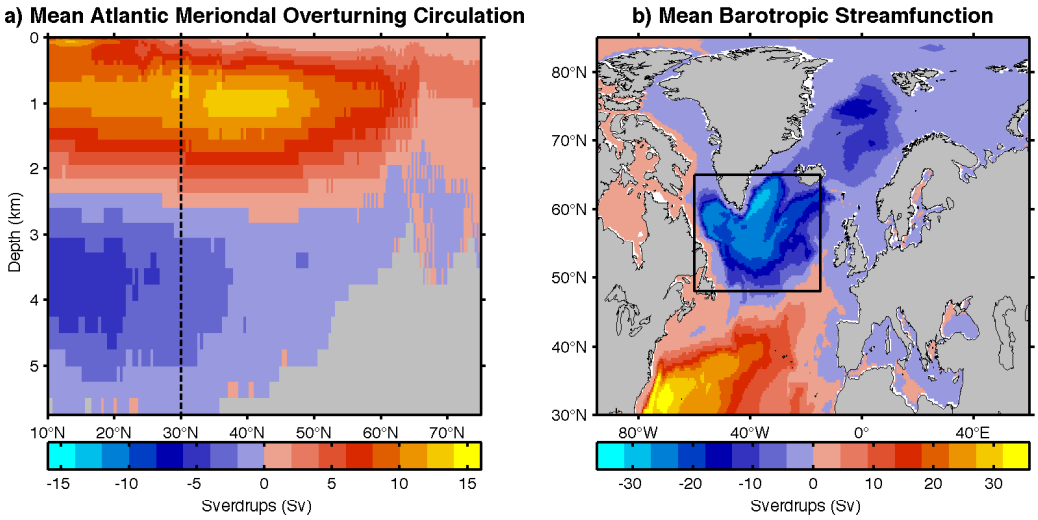

Figure 4.2: (a) Mean AMOC from the SF model integration. The dashed black line indicates where the AMOC at 30°N is measured. (b) Mean barotropic streamfunction from the SF model integration. The black box indicates the region used to compute the SPG strength.

frequency corresponding to approximately 65 years (Figure 4.3a); indeed, a first order autoregressive (AR(1)) process is not a good fit for AMOC at 30°N spectrum, which is often used as a significance test for red noise. The SPG strength in this study is defined as the negative area mean of the annual mean barotropic streamfunction averaged over the region 60°W to 15°W, 48°N to 65°N as in *Lohmann et al.* [2009] (Figure 4.2b), with positive values indicating a stronger gyre. As with the AMOC at 30°N, the SPG strength shows the properties of red noise, but with the difference that the transition to the long timescales of variability is not as abrupt (Figure 4.3b). The power spectrum of the SPG strength shows strong variability in the middle range timescales (15-65 years), which is almost non-existant in the power spectrum of the AMOC at 30°N. However, the power spectrum of the SPG strength shows a sharp drop in spectral power at approximately 65 years (Figure 4.3b).

From Chapter 3 we have seen that the AMOC at 30°N and the SPG strength can be reconstructed by integrating the NAO index as follows,

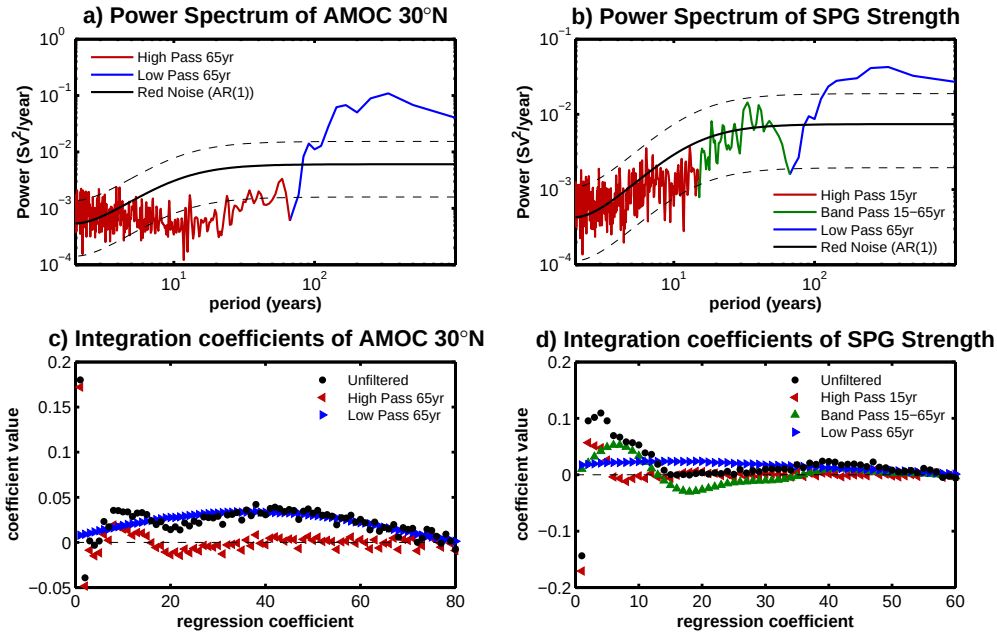

Figure 4.3: The power spectrum of (a) the AMOC at 30°N divided into periods of 65 years or less (red) and 65 years or more (blue) and (b) the SPG Strength, divided in periods of 15 years or less (red), 15-65 years (green) and 65 years and longer (blue). The AR(1) fit is shown in black with dashed lines indicated the 95% confidence interval. Coefficients from the integrated NAO fit are shown for (c) the AMOC at 30°N for unfiltered data (black), 65 year high pass filtered data (red) and 65 year low pass filtered data (blue) and (d) the SPG Strength for unfiltered data (black), 15 year high pass filtered data (red), 15-65 year band pass filtered data (green) and 65 year low pass filtered data (blue).

$$index(t) = \alpha_0 + \sum_{k=1}^{q} \alpha_k NAO(t-k+1) + \xi(t), \tag{4.2}$$

where q is the number of years of the NAO used to compute the index (either AMOC or SPG strength), with the α_k's computed using a linear regression method. The results show that the AMOC can be reconstructed using 53 previous years of the NAO with a correlation of 0.67 on decadal timescales (running mean of 11 years) and the SPG strength can be reconstructed using 10 previous years of data with a correlation of 0.61 on decadal timescales. However, the reconstruction of the SPG strength can be improved by extending the number of years of the NAO used to at least 50 years. On closer examination of the coefficients from integrating the NAO, three distinct behaviours become apparent (Figure 4.3c and d, black circles): 1) In both the AMOC and SPG Strength the coefficient for the NAO at lag 0 (i.e. α_1) is very large and in the case of the SPG Strength of opposite sign to the majority of the remainder of the coefficients. 2) In case of the SPG strength the first 12 coefficients are large relative to the remainder of the coefficients but this distinction is not as clear in the coefficients from the AMOC at 30°N. 3) The coefficients up to approximately 75 years for the AMOC and 50 years for the SPG strength are all relatively small and positive.

The combination of the power spectra and the properties of the integration coefficients of both the AMOC at 30°N and the SPG strength suggest dividing the time series into 3 different frequency bands; the interannual timescales (shorter than 15 years), the decadal timescales (15-65 years) and the multidecadal timescales (longer than 65 years). The timeseries were filtered using a fifth order butterworth filter to divide into the interannual, decadal and multidecadal time scales with a high pass filter with 15 year cut off, band pass filter with a 15-65 year band and a low pass filter with a 65 year cut off, respectively (Figure 4.4). The amplitude of the variability in the AMOC at 30°N clearly shows a weaker variability on the 15-65 year timescale

relative to the 65 year and longer timescale, while the amplitude variability of the SPG strength does not differ much between the 15-65 year timescale and the 65 year and longer timescale (Figure 4.4). Similar to the AMOC at 30°N, the mixed layer depth in the Labrador Sea also has a weaker variability on the 15-65 year timescale than on the 65 year and longer timescale (Figure 4.4).

Using the filtered timeseries to compute the integrated NAO fits, quite different behaviours on the different timescales is apparent (Figure 4.3c and d). On the interannual timescales both the AMOC at 30°N and the SPG strength have large values for the first few coefficients, with α_1 being the largest by far and of opposite sign for the AMOC and the SPG strength (Figure 4.3c and d, red triangles). For the long time scales the behavior of the integrated NAO coefficients are similar, all having relatively small, positive and of constant value, with the SPG strength requiring approximately 20 less coefficients (Figure 4.3c and d, blue triangles). For the SPG strength, the integrated NAO coefficients for the 15-65 year timescales show an interesting behavior, with the coefficients having a sinusoidal shape with a maximum at approximately α_8 and minimum at approximately α_{17} (Figure 4.3d, green triangles). The sinusoidal shape of the α's has the consequence that the power of timescales twice the period of the sinusoid in the integrated NAO coefficients are greatly reduced, explaining the drop at approximately 65 years in the power spectrum of the SPG Strength (Figure 4.3b). Summing the integrated NAO coefficients computed from the filtered timeseries gives the NAO coefficients from the unfiltered timeseries. In particular, in the SPG strength case, summing the integrated NAO coefficients from the 65 year low pass filtered timescales with the 15-65 year band pass filtered integrated NAO coefficients from α_{15} to α_{25} leads to these coefficients becoming zero.

The following sections focus on describing the properties of interannual timescale (15 years and shorter), the multidecadal timescale (15-65 years) and centennial

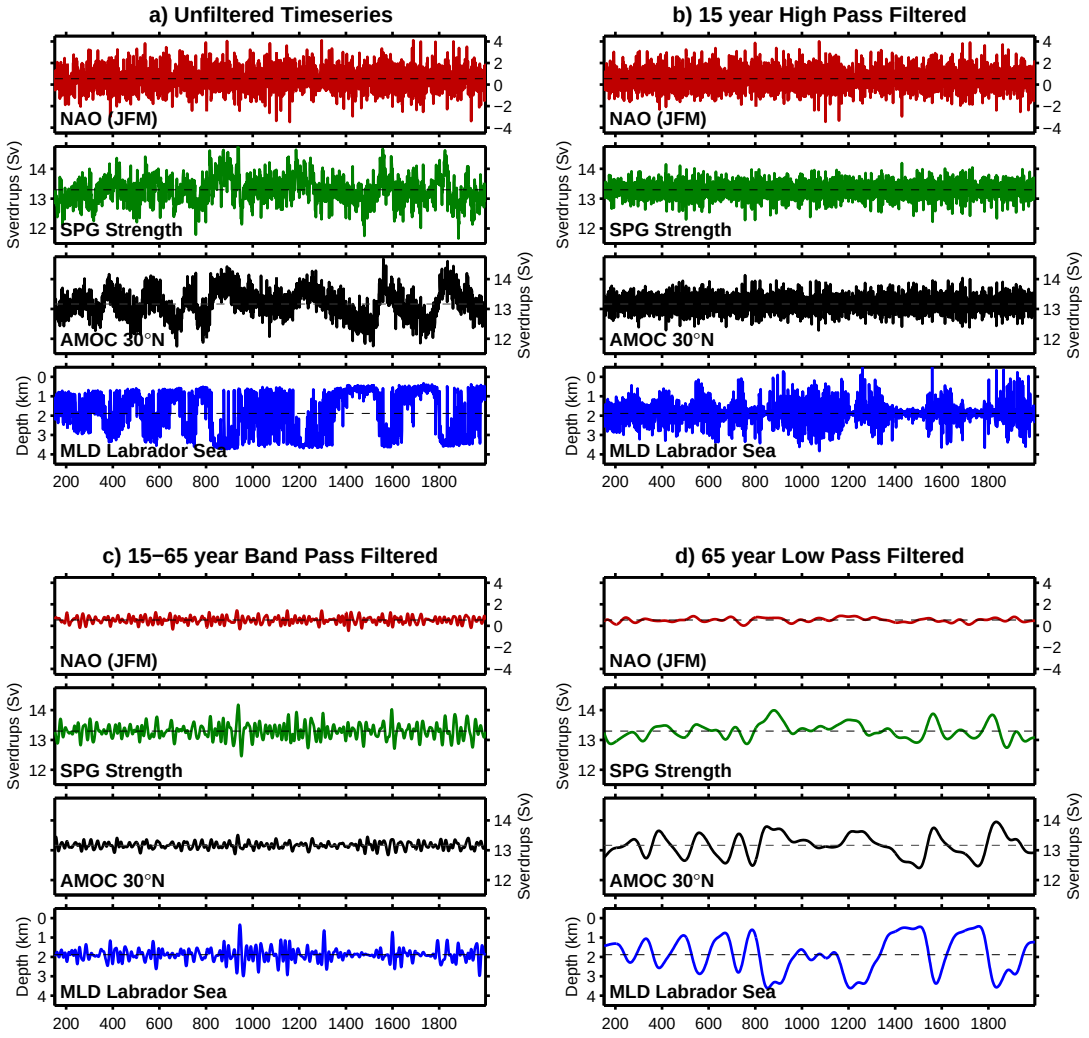

Figure 4.4: Timeseries of the winter (JFM) NAO (red), AMOC at 30°N (black), SPG Strength (green) and mixed layer depth in the Labrador Sea (Blue). The timeseries are (a) unfiltered, (b) filtered with a 15 year high pass filter, (c) 15-65 year band pass filter and (d) 65 year low pass filtered.

timescales (65 years and longer) in more detail.

4.5 Interannual Timescale

In this section the 15 year high pass filtered (referred to as the interannual) variability is investigated (Figure 4.4b). In the current model setup the model is forced with the 10 m temperature, winds and specific humidity, long- and shortwave radiation and precipitation as opposed to the fluxes directly. Therefore the heat, momentum and fresh water fluxes are computed by the ocean model and can vary with the state of the ocean. However, the heat flux forcing associated with the interannual timescales of the NAO does not differ much from what is expected from observations (*Visbeck et al.* [2003], Figure 4.5a). As expected, the positive minus negative NAO difference is associated with a large area of upward heat flux over the Labrador Sea and a narrow region from the east coast of Greenland up to Svalbard. According to *Visbeck et al.* [2003], the majority of this heat flux can be attributed to the sensible component of the heat flux. The winter wind stress curl associated with the positive minus negative NAO difference shows a mostly positive curl north of approximately 55°N, with the main exception being along the eastern coast of Canada. South of 55°N the wind stress curl is mostly negative (Figure 4.5b).

Computing the cross correlations between the 15 year high pass filtered NAO, AMOC at 30°N, SPG strength and mixed layer depth in the Labrador Sea shows that there are strong correlations in phase with the NAO index and the correlation quickly drops off there after (Figure 4.6). The AMOC at 30°N is positively correlated with the NAO with a significant correlation of 0.70 at 0 lag and also a positive correlation with the mixed layer depth in the Labrador Sea (Figure 4.6a). On lags of one year and longer, the correlation between the the NAO index and the AMOC at 30°N changes sign and becomes very small but remains significant (Figure 4.6a). The SPG strength and the NAO index (AMOC) has a significant negative correlation

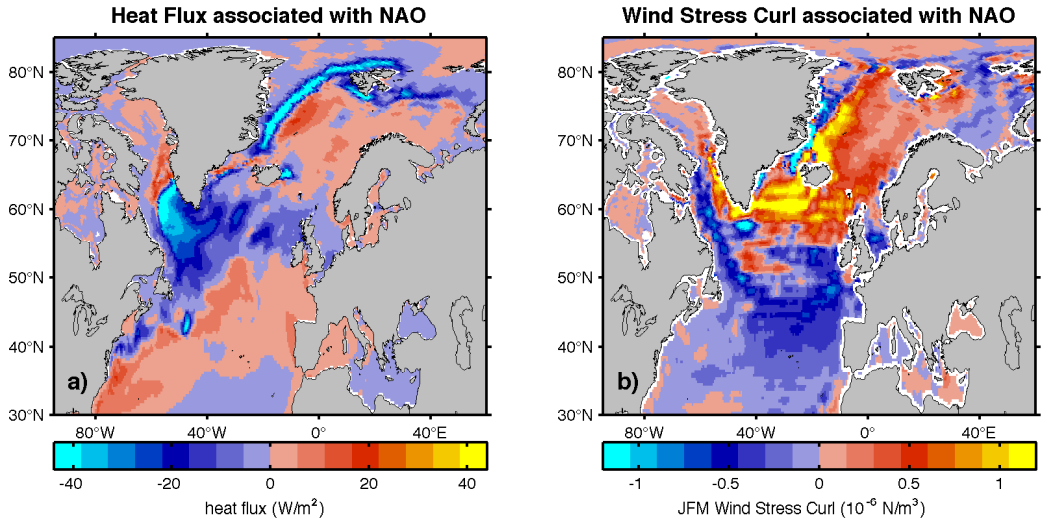

Figure 4.5: (a) The difference of the mean winter (JFM) downward heat flux in the years where the 15 year high pass filtered NAO index (Figure 4.4b) is larger than the mean NAO index by more than one standard deviation, from the mean years where the filtered NAO index is smaller than one standard deviation from the mean. (b) Same as (a) but for the wind stress curl. A 9-point smoothing has been applied to the wind stress curl.

of -0.74 at 0 lag, which again becomes very small and changes sign at larger lags (Figure 4.6b). This is similar to what is seen in *Eden and Willebrand* [2001] where the initial response of the SPG to the NAO changes sign after about 3 years. To go into more detail on the ocean response to the NAO forcing on interannual timescales we next investigate patterns of the barotropic streamfunction and the AMOC.

The barotropic streamfunction associated with the maximum in SPG strength has a large area of negative barotropic streamfunction (spin-up of the SPG) covering much of the North Atlantic (Figure 4.7c) and a weaker positive anomaly over the region surrounding Iceland. Comparing the anomalies in the barotropic streamfunction to the mean SPG (Figure 4.2a) shows that the spin-up of the SPG on the interannual timescales corresponds to an increase in the western part of the gyre only. In phase with the maximum in SPG strength we have a wind stress curl pattern which strongly resembles the negative of the pattern associated with a positive NAO

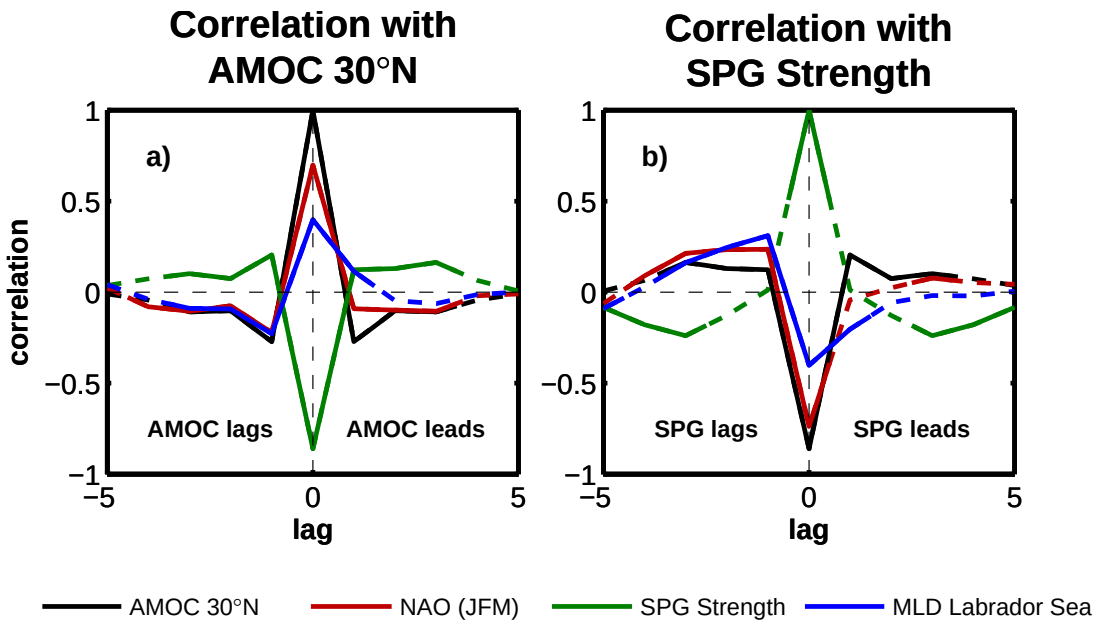

Figure 4.6: (a) Autocorrelation of the 15 year high pass filtered AMOC at 30°N (black) and cross-correlations of the 15 year high pass filtered AMOC at 30°N with the15 year high pass filtered NAO index (red), SPG strength (green) and the mixed layer depth in the Labrador Sea (blue). Correlations significant at 95% are shown with a solid curve while correlations not significant at the 95% level are shown with a dashed curve. (b) Same as (a) but with the SPG strength.

(Figure 4.4b, Figure 4.7d). From the response of the barotropic streamfunction to the wind stress curl is what is expected from the topographic Sverdrup relationship (Figure 4.7c&d). Three years before the maximum in the 15 year high pass filtered SPG strength the sign of the anomalies in the barotropic streamfunction and wind stress curl are very weak and change sign (Figure 4.7a-d) which is consistent with what is seen in the cross correlation analysis (Figure 4.6b). Three years after the maximum in barotropic streamfunction the wind stress curl has a signal similar to 3 years before and the barotropic streamfunction shows almost no signal (Figure 4.7e,f).

The AMOC pattern that is in phase with the 15 year high pass filtered AMOC at 30°N shows two cells of meridional overturning; one with a positive overturning centered at 30°N with a maximum at a depth of about 2.5 km and the other with a negative overturning centered at about 50°N and with maximum at a depth of about 0.5 km (Figure 4.8d). This overturning cell with Ekman transport in the surface layer is what is expected from the directly wind driven AMOC. To explain the double cell structure in the AMOC, we again turn to the wind stress curl. Since the 15 year high pass filtered AMOC at 30°N is positively correlated with the NAO (4.6a) we can compare with the wind stress curl pattern in Figure 4.5b. From Ekman pumping, $\rho w = f\hat{k} \cdot (\nabla \times \bar{\tau})$, where ρ is the density, w is the vertical velocity at the bottom of the Ekman layer and τ is the wind stress, we know that a positive (negative) wind stress curl will lead to Ekman pumping (sinking). From Figure 4.5b the positive wind stress curl centered 65°N coincides with the upwelling region at 65°N and the negative wind stress curl centered at 45°N coincides with the region between the two cells where water is sinking (Figure 4.8d). This is similar to *Eden and Willebrand* [2001] who found that the AMOC measured at 48°N has a negative correlation with the NAO index. As seen in the cross correlation analysis associated with the maximum in the AMOC at 30°N there is a maximum in mixed layer depth in the Labrador Sea (Figure 4.8e) and in the Greenland Sea of opposite

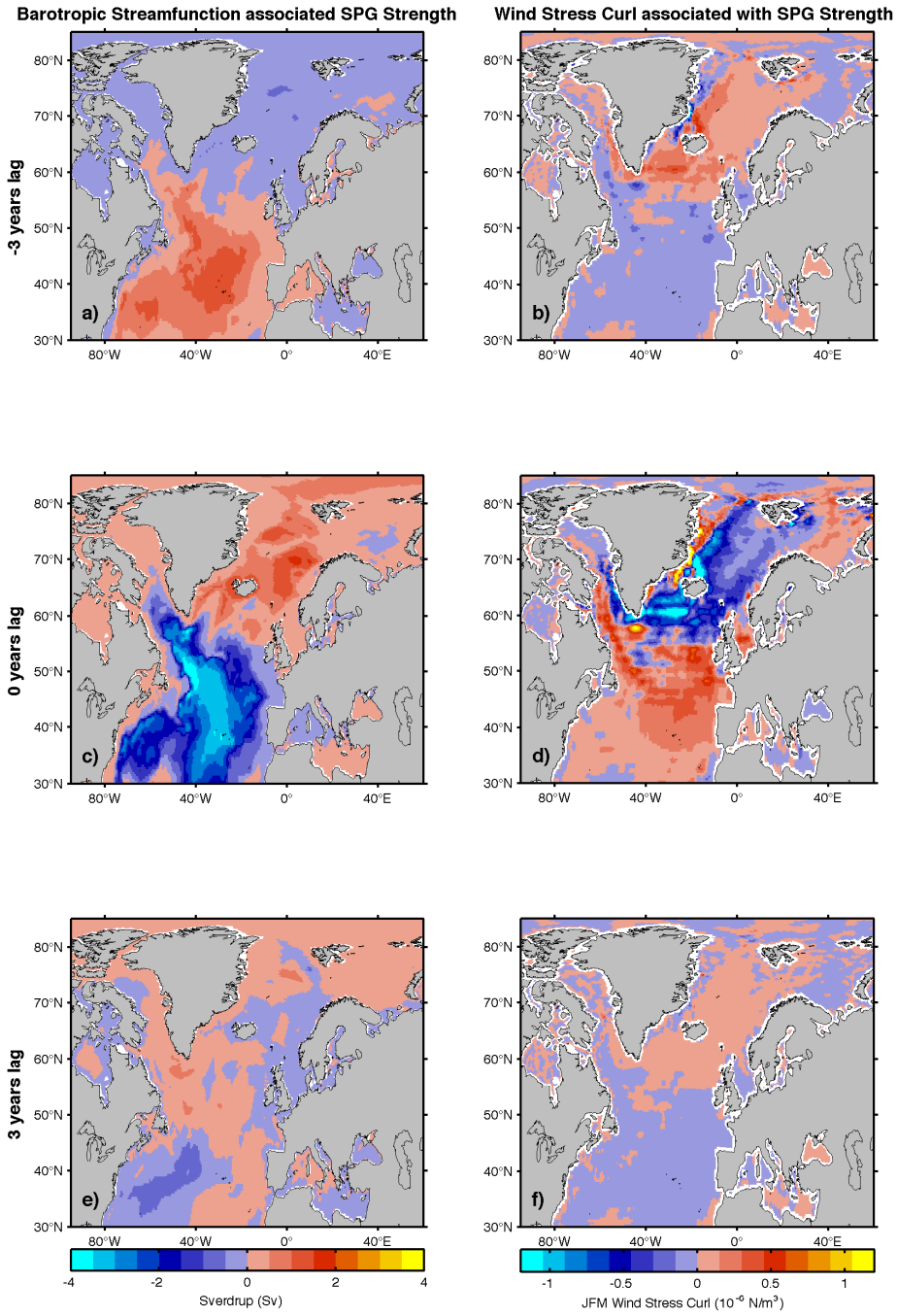

Figure 4.7: (a,c,e) The difference of the barotropic streamfunction in the years when the 15 year high pass filtered SPG strength (Figure 4.4b) is larger than the mean SPG strength by more than one standard deviation, from the years when the filtered SPG strength is smaller than one standard deviation from the mean. (b,d,f) Same as (a,c,e) but for the mean winter (JFM) wind stress curl. (a,b) The SPG strength lags by 3 years, (c,d) in phase with the SPG strength and (e,f) the SPG strength leads by 3 years. A 9-point smoothing has been applied to the wind stress curl.

sign (Figure 4.8e). The downward heat flux associated with a maximum in AMOC at 30°N (Figure 4.8f) shows a pattern similar to the downward heat flux from the NAO index (Figure 4.5a). The heat flux indicates a heat loss to the atmosphere over the Labrador Sea region which would lead to denser waters being formed in the Labrador Sea, hence increasing Labrador Sea convection. As indicated from the cross correlation analysis (Figure 4.6a), three years before and three years after the maximum in the AMOC at 30°N the signal is weak and of opposite sign (Figure 4.8).

For the interannual timescales it is clear that the SPG strength and the AMOC variability is strongly associated with the immediate response of the ocean to the wind stress through the Ekman dynamics. This is similar to what has already been seen in the results from *Eden and Willebrand* [2001].

4.6 Multidecadal Timescale

From the power spectrum (Figure 4.3a and b) and the filtered timeseries (Figure 4.4c) it is evident that the AMOC at 30°N does not have a very strong signal on the 15-65 year timescale but the SPG strength has a lot more prominent signal on these time scales. Similarly, the annual maximum mixed layer depth in the Labrador Sea does not show much variability on the 15-65 year timescale (Figure 4.4c). The autocorrelation of the AMOC at 30°N and the SPG strength show minima at -/+ 13 years lag, suggesting an oscillation with a period of approximately 26 years (Figure 4.9). The cross correlation between the AMOC at 30°N and the NAO index show a significant correlation with a maximum of 0.34 when the NAO leads by 8 years (Figure 4.9a). However, this correlation is not very large and we have seen in section 3.5.1 that the AMOC at 30°N has a closer relation an integral of the winter NAO index over many years as opposed to the NAO directly. The cross correlation of the SPG strength and the NAO has a maximum significant correlation of 0.69 with the

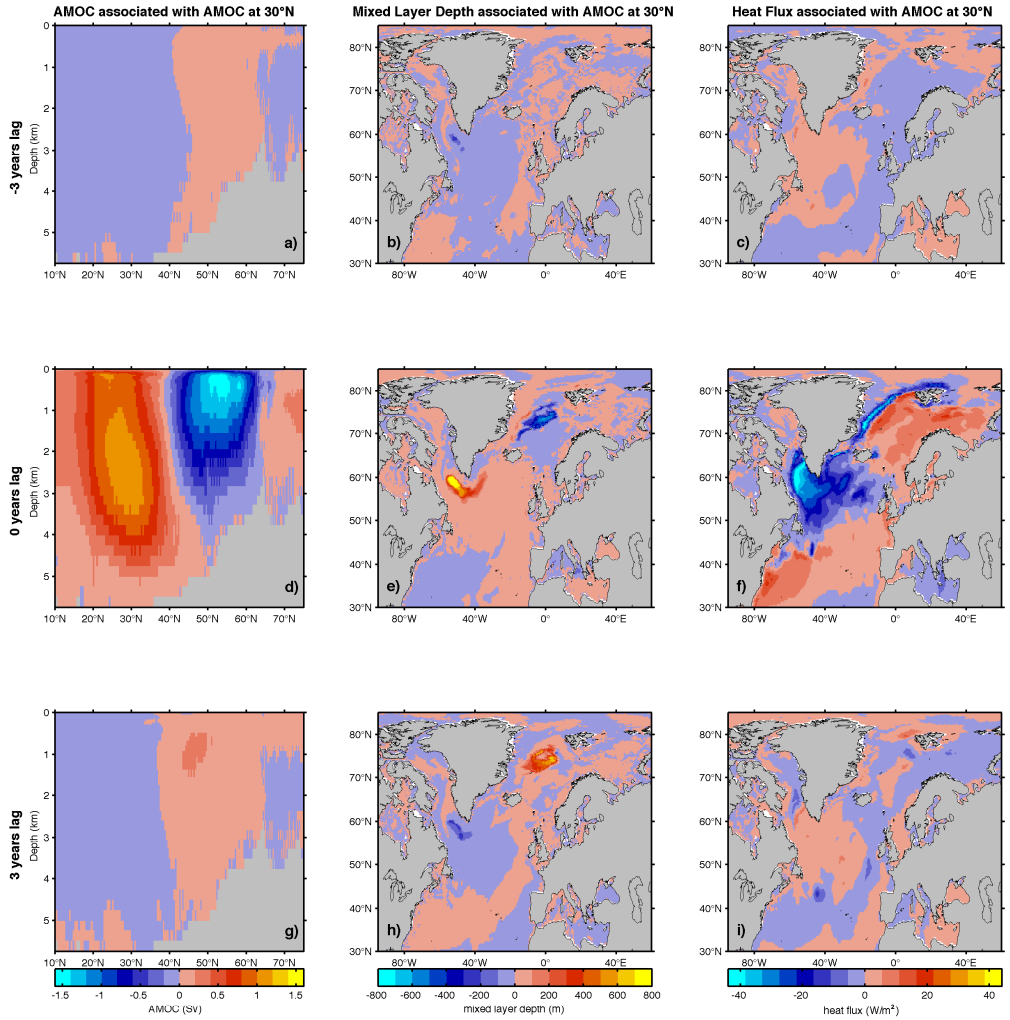

Figure 4.8: (a,d,g) The difference of the AMOC in the years where the 15 year high pass filtered AMOC at 30°N (Figure 4.4b) is larger than the mean AMOC at 30°N by more than one standard deviation, from the AMOC when the filtered AMOC at 30°N is smaller than one standard deviation from the mean. (b,e,h) Difference of the same years as (a,d,g) but for the annual maximum mixed layer depth. (c,f,i) Difference of the same years as (a,d,g) but for the annual mean heat flux. (a,b,c) The AMOC at 30°N lags by 3 years, (d,e,f) in phase with the AMOC at 30°N and (g,h,i) the AMOC at 30°N leads by 3 years.

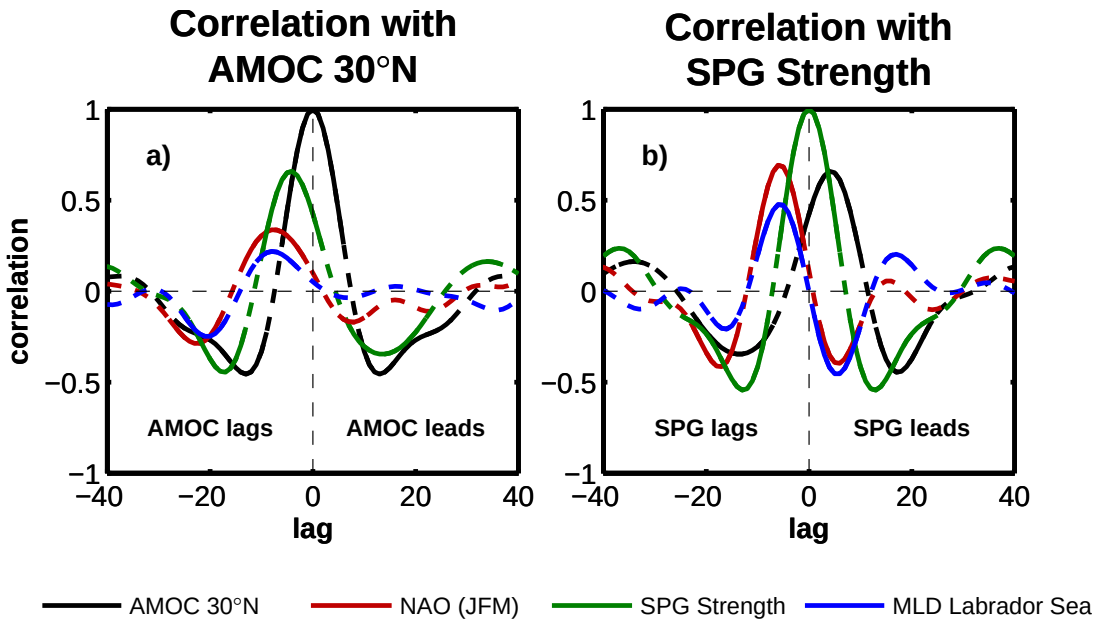

Figure 4.9: (a) Autocorrelation of the 15-65 year band pass filtered AMOC at 30°N (black) and cross-correlations of the 15-65 year band pass filtered AMOC at 30°N with the 15-65 year band pass filtered NAO index (red), SPG strength (green) and the mixed layer depth in the Labrador Sea (blue). Correlations significant at 95% are shown with a solid curve while correlations not significant at the 95% level are shown with a dashed curve. (b) Same as (a) but with the SPG strength.

NAO leading by 6 years (Figure 4.9a). Despite the AMOC at 30°N having a weak signal it lags the SPG strength by 4 years with a correlation of 0.66.

There is some variability present in the AMOC on multidecadal timescales. The standard deviation of the AMOC when filtered with a 15-65 year band pass filter shows that the area of strongest variability with a standard deviation of 0.4 Sv is centered at approximately 48°N and a depth of 2 km (Figure 4.10a). Creating a timeseries of the AMOC at 48°N, by taking a maximum of the AMOC at 48°N, shows that the timeseries has a power spectrum similar to the SPG strength (Figure 4.10b and Figure 4.3a) with stronger variability on the multidecadal timescale than the AMOC at 30°N. The cross correlation analysis shows that an increased AMOC at 48°N varies in phase with the SPG strength (Figure 4.10c) with a significant

correlation of 0.91 and leads variations in the AMOC at 30°N by lags 4 years with a significant correlation of 0.67. Also the 15-65 year band pass filtered NAO index leads the AMOC at 48°N by 5 years with a significant correlation of 0.69.

The spatial pattern of the barotropic streamfunction associated with the maximum SPG strength shows a negative anomaly of the barotropic streamfunction covering the area occupied by the SPG in the mean (Figure 4.11g). 14 years before the maximum and 14 years after the maximum in SPG strength, the pattern of the barotropic streamfunction that is has the opposite sign from the barotropic streamfunction in phase SPG strength (Figure 4.11a,g and m), again indicating an oscillatory behaviour with a period of approximately 28 years. The maximum AMOC at 48°N varies in phase with the SPG strength, and is part of a positive circulation cell explaining the standard deviation maximum in AMOC on these timescales (Figure 4.11i). Density in the center of the gyre is important for mechanisms for SPG strength variability; in the study *Born and Mignot* [2012] a maximum in density at the center of the SPG is in phase with the maximum in SPG strength. The density of the upper 191 m (upper 14 model levels and approximate mean mixed layer depth in that region) shows a maximum density in the center of the gyre region 7 years before the maximum in SPG strength occurs (Figure 4.11e). A density anomaly of the opposite sign appears 7 years after the maximum in SPG strength (Figure 4.11k) completing the oscillatory cycle. In phase with the maximum SPG there is also a small region of dense water south of Iceland that matches the negative anomaly of the barotropic streamfunction in that location (Figure 4.11g and h).

To further investigate the density signal in the center of the gyre a profile of the annual mean temperature, salinity and density is made in box C in Figure 4.12 and the upper 191 m is considered (the upper 14 model layers and the approximate depth of the mixed layer). Cross correlation analysis of the 15-65 year band pass filtered density shows that the density anomaly in box C occurs in phase with the

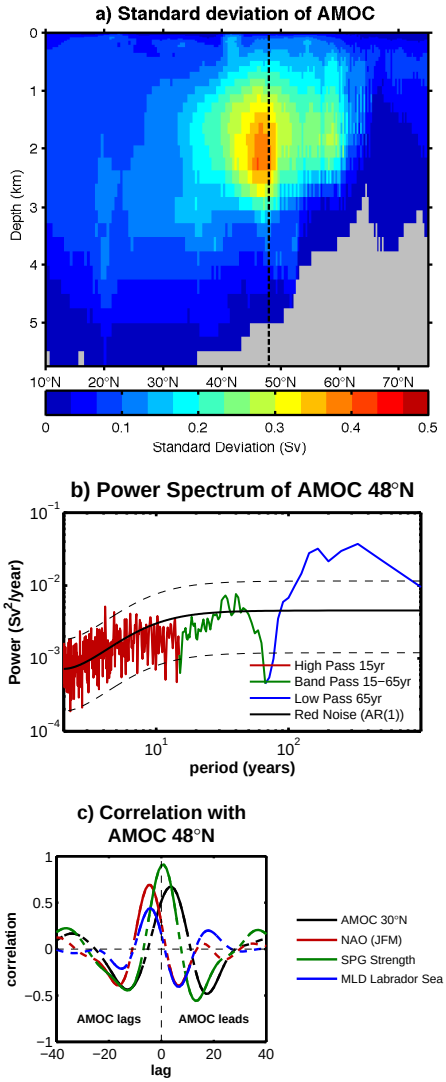

Figure 4.10: (a) Standard deviation of the 15-65 year band pass filtered AMOC. The dashed black line indicates the location used to calculate the AMOC at 48°N. (b) The power spectrum of the AMOC at 48°N divided into periods of 15 years or less (red), 15-65 years (green) and 65 years and longer (blue). The AR(1) fit is shown in black with dashed lines indicated the 95% confidence interval. (c) Cross-correlations of the 15-65 year band pass filtered AMOC at 48°N with the 15-65 year band pass filtered AMOC at 30°N (black), NAO index (red), SPG strength (green) and the mixed layer depth in the Labrador Sea (blue). Correlations significant at 95% are shown with a solid curve while correlations not significant at the 95% level are shown with a dashed curve.

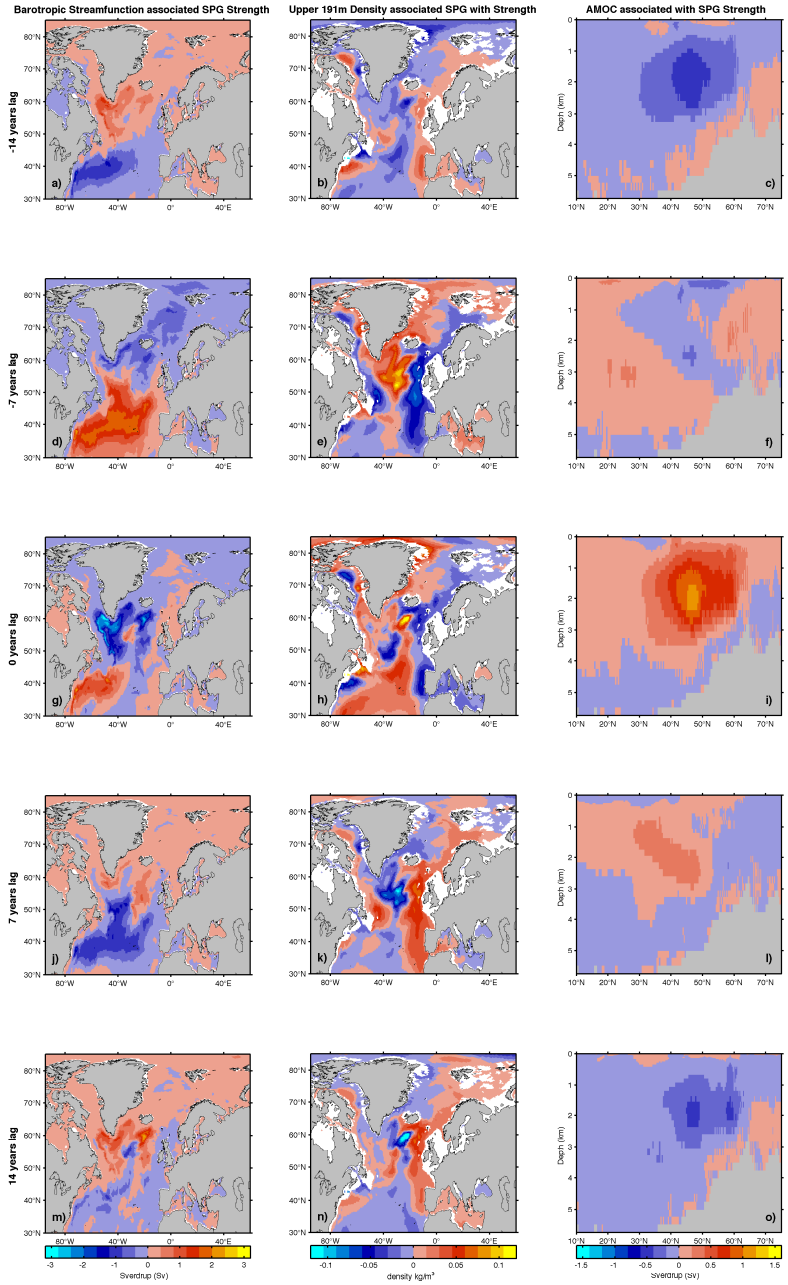

Figure 4.11: (a,d,g,j,m) The difference of the barotropic streamfunction in the years where the 15-65 year band pass filtered SPG strength (Figure 4.4c) is larger than the mean SPG strength by more than one standard deviation, from the barotropic streamfunction when the filtered SPG strength is smaller than one standard deviation from the mean. (b,e,h,k,n) Difference of the same years as (a,d,g,j,m) but for the annual mean of the density in the upper 191 m. (c,f,i,l,o) Difference of the same years as (a,d,g.j.m) but for the AMOC. (a,b,c) The SPG strength lags by 14 years, (d,e,f) the SPG strength lags by 7 years, (g,h,i) in phase with the SPG strength, (j,k,l) the SPG strength leads by 7 years and (m,n,o) the SPG strength leads by 14 years.

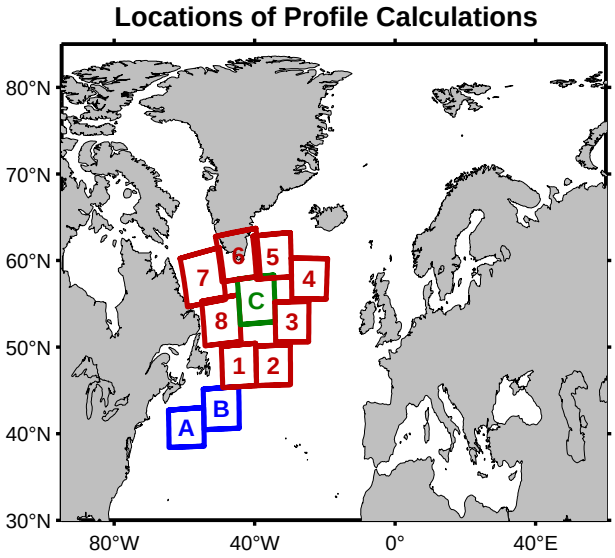

Figure 4.12: Location of boxes at which density profiles have been computed.

15-65 year band pass filtered NAO index with a correlation of 0.58 and leads the barotropic streamfunction by 3 years with a significant correlation of 0.73 (Figure 4.13a). The density variability on the 15-65 year timescales in the center of the SPG region is both dependent on the temperature and the salinity (Figure 4.13b) with the salinity contribution to the density being less important on the 15-65 year timescales when compared to the temperature based contribution; this can also be seen in their power spectra (Figure 4.13c and d). The lag between the maximum density in the center of the gyre region and the SPG strength is mainly confined to the mixed layer. However, the density anomaly reaches its maximum depth (about 150 m) in phase with the 15-65 year filtered SPG strength (Figure 4.14).

When examining the density anomalies associated with the 15-65 year band pass filtered SPG strength year by year it appears that the density anomalies are propagating around the SPG (not shown). In the studies of *Sutton and Allen* [1997] and *Alvarez-Garcia et al.* [2008], SST anomalies propagate along the Gulf Stream and

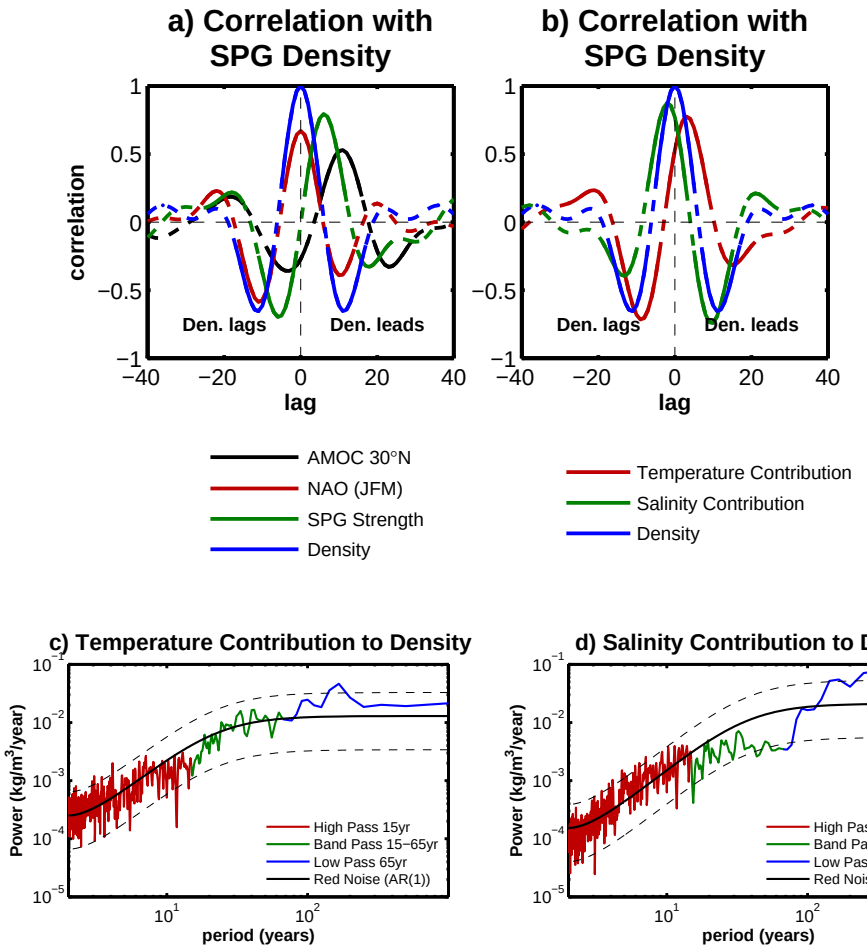

Figure 4.13: (a) Cross correlation of 15-65 year band pass filtered upper 191 m density in the center of gyre (box C, Figure 4.12) with AMOC at 30°N (black), JFM NAO index (red), SPG strength (green) and autocorrelation (blue). (b) Cross correlation of 15-65 year band pass filtered density in the center of the gyre with the temperature contribution to density (red), salinity contribution to density (green) and autocorrelation (blue). (c) The power spectrum of the temperature contribution to density in the center of the gyre divided into periods of 15 years or less (red), 15-65 years (green) and 65 years and longer (blue). The AR(1) fit is shown in black with dashed lines indicated the 95% confidence interval. (d) Same as (c) but for the salinity contribution to density.

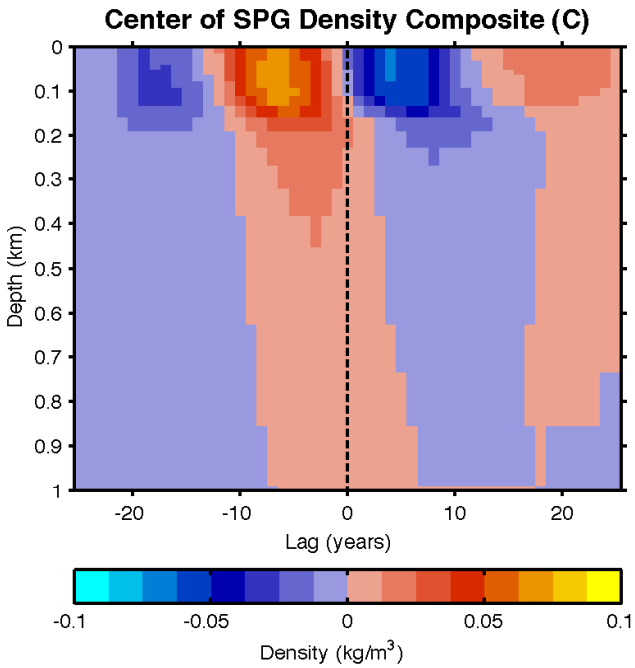

Figure 4.14: The difference of the density in box C (Figure 4.12) in the years when the 15-65 year band pass filtered SPG strength (Figure 4.4c) is larger than the mean SPG strength by more than one standard deviation, from the density in box C from the years where the filtered SPG strength is smaller than one standard deviation from the mean. A negative lags correspond to the density anomalies leading and positive lags correspond to the SPG strength leading.

then along the North Atlantic Current on multidecadal timescales. This propagation of SST anomalies is too slow to be associated with the mean currents, suggesting it has to either be related to currents below the surface, currents not in the strongest part of the Gulf Stream, anomalous advection or some other mechanism (*Sutton and Allen* [1997]). Here we have setup profiles along the path of the SPG (Figure 4.12, red boxes) as well as two boxes for profiles along the Gulf Stream (Figure 4.12, blue boxes). In all these boxes except box A, the density anomalies in the upper 191 m are mainly related to changes in temperature on the 15-65 year time scales; the salinity contribution does have a significant contribution on these time scales (not shown). Tracing the density anomalies around the SPG using the 15-65 year band pass filtered SPG strength shows that anomalies propagate around the SPG with a period of about 25 years (Figure 4.15). Density anomalies from box 1 make their way relatively slowly to box 4-6 taking approximately 15 years. This density anomaly takes another 10 years to go from box 6 back to box 1 to complete the cycle (Figure 4.15). The studies *Sutton and Allen* [1997] and *Alvarez-Garcia et al.* [2008] only take into consideration SST anomalies, for which the path along the Gulf Stream is also important. Here we considered the density anomalies in the upper 191m for which box A does not constribute to the path of the density anomalies (Figure 4.15). However, when only upper 50 m are taken into account, the density anomaly in box A occurs in phase with the density anomaly in box B, then making its way to box 1 (not shown).

The multidecadal (15-65 year) timescale shows strong variability in the SPG region with the SPG strength variability on these timescales being in phase with AMOC variability centered around 48°N. A density anomaly located in the upper 191 m at the center of the SPG leads the SPG strength by 5-7 years and when this anomaly reaches a its maximum depth (about 150 m) it becomes in phase with the SPG strength. This process has period of about 25-28 years and can be related to mainly temperature dominant density anomalies which make their way around the

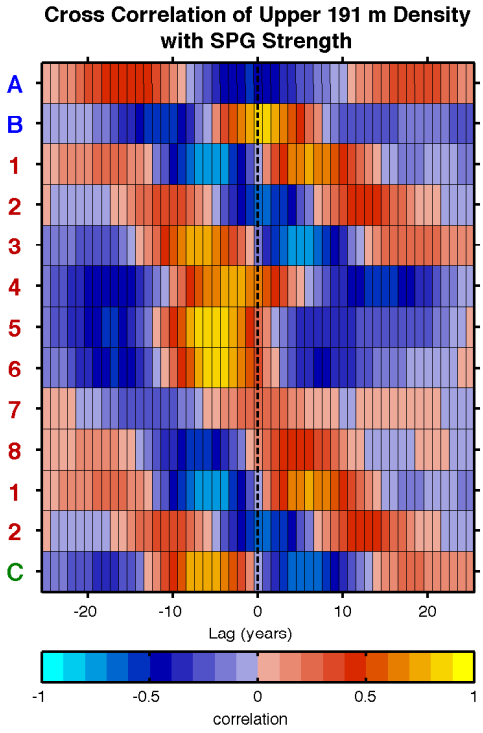

Figure 4.15: Cross correlation between the 15-65 year band pass filtered SPG strength and the density in the boxes defined in Figure 4.12.

SPG.

4.7 Centennial Timescale

The centennial timescale refers to timescales longer than 65 years (Figure 4.4d). The power spectra of both the AMOC at 30°N and the SPG strength show strong variability on the 65 year and longer timescales (Figure 4.3a&b). The flattening out of the spectrum on these timescales is an indication that the model is in a quasi-equalibrium state. From the work done in Chapter 3, we know that the signals on the long timescales are just a reflection of the low frequency signal in the white noise NAO index. On the long timescales the coefficients of the integrated NAO fit are all of a nearly constant value for about 75 years for the AMOC at 30°N and 45 years for the SPG strength before falling off to zero (Figure 4.3c and d). This provides additional evidence that the centennial timescale is in a quasi-equilibrium state. The 75 (45) years of coefficients for the NAO fit with a small positive value indicated that the AMOC (SPG strength) requires about 75 (45) years to adjust to the new equalibrium.

The cross correlation analysis of the 65 year low pass filtered data has the NAO leading the AMOC at 30°N (SPG strength) by 36 (15) years with a significant correlation of 0.68 (0.61) (Figure 4.16). In both cases this is about half the number of years for which the coefficients for the integrated NAO fit have a positive value. Furthermore, the cross correlation analysis of the 65 year low pass filtered timeseries shows no indication of a possible oscillatory behaviour; for all auto and cross correlation curves the largest correlation is positive and significant at 95% but none of the negative correlations are significant (Figure 4.16). The lack of a significant negative correlation in the autocorrelation curves adds to the evidence that the centennial timescale variability is in a quasi-equilibrium state. On the 65 year low pass filtered timescales, the mixed layer depth in the Labrador Sea has a strong signal (Figure

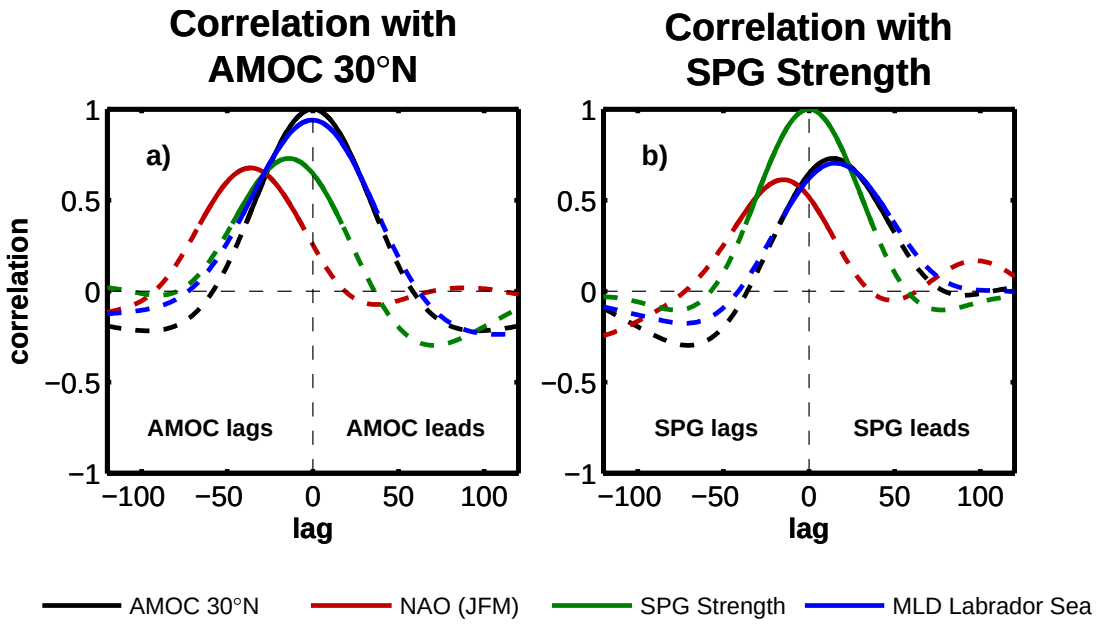

Figure 4.16: (a) Autocorrelation of the 65 year low pass filtered AMOC at 30°N (black) and cross-correlations of the 65 year low pass filtered AMOC at 30°N with the 65 year low pass filtered NAO index (red), SPG strength (green) and the mixed layer depth in the Labrador Sea (blue). Correlations significant at 95% are shown with a solid curve while correlations not significant at the 95% level are shown with a dashed curve. (b) Same as (a) but with the SPG strength.

4.4d); this signal is in phase with the AMOC at 30°N with a significant correlation of 0.94 (Figure 4.16a).

The mixed layer depth in the Labrador Sea plays an important role on the centennial timescales with the Labrador Sea being the main region of convection on these timescales (not shown). As in the study of *Ba et al.* [2013], the salinity dominates the mixed layer depth variability and the temperature only plays a minor damping role (Figure 4.17). The negative anomalies in the density reach the bottom of the ocean indicating the mixing of dense water to the surface, while the positive density anomalies appear to only occur in the top 3000 m (Figure 4.17). The contribution to the density from the salinity appears to be in phase with the AMOC at 30°N while the negative contribution to the density from the temperature slightly lags the

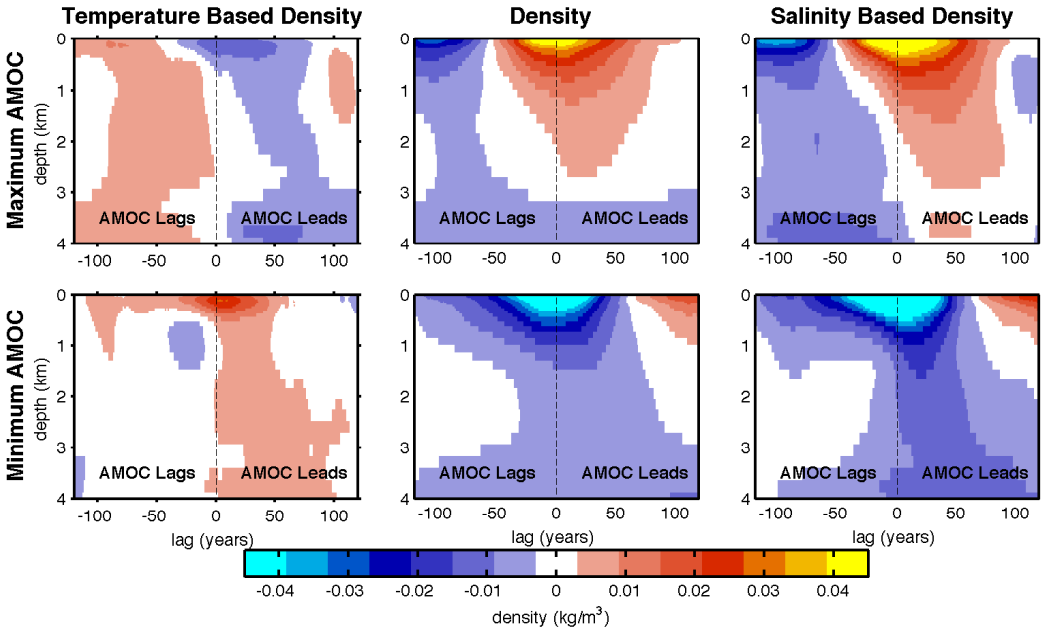

Figure 4.17: (a,b,c) The difference in density in the Labrador Sea convection region from the mean density in the years where the 65 year low pass filtered AMOC at 30°N (Figure 4.4d) is larger than the mean of AMOC at 30°N by one standard deviation. (d,e,f) Same as (a,b,c) but for when the AMOC at 30°N is smaller than one standard deviation from the mean. (a,d) show the temperature contribution to the density, (b,e) the full density and (c,f) the salinity contribution to the density.

maximum in AMOC by a few years (Figure 4.17).

The spatial pattern of the AMOC associated with the quasi-equalibrium states on the centennial timescales shows that the main area where there is strength in the AMOC increases and is centered at about 35°N and at a depth of 1.5 km, which is deeper than where the maximum in the AMOC is found in the mean AMOC (Figure 4.18a and 4.2a). The pattern of the AMOC suggests that the upper overturning cell strengthens and deepens during a persistent phase of positive AMOC at 30°N, while the lower, weaker overturning cell is only very marginally weakened (Figure 4.18a). The barotropic streamfunction associated with the maximum in SPG strength on the 65 year and longer timescales shows that the SPG spins up (Figure 4.18b) in situ with the exception of the corner just south of Iceland (this part of the SPG

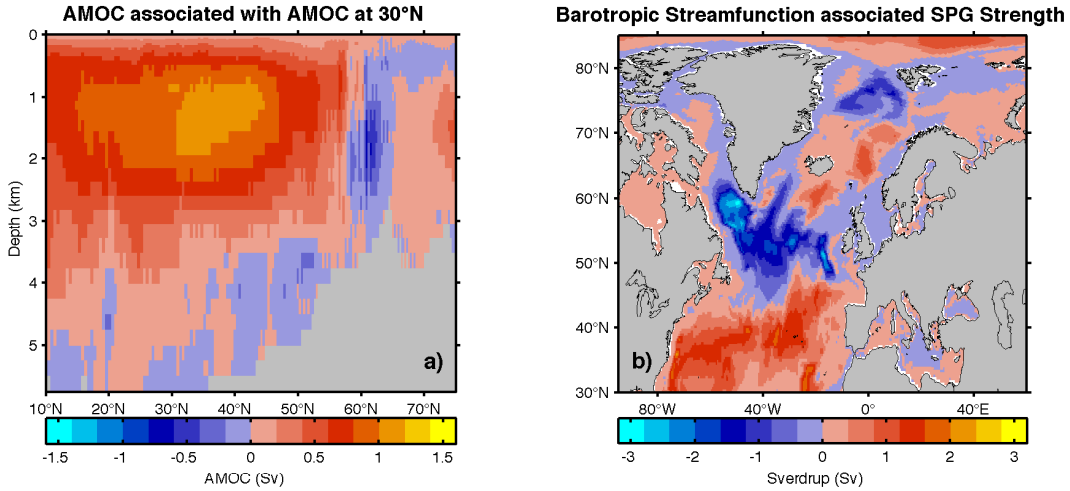

Figure 4.18: (a) The difference of the AMOC, in the years where the 65 year low pass filtered AMOC at 30°N (Figure 4.4d) is larger than the mean AMOC at 30°N by more than one standard deviation, from the AMOC from the years when the filtered AMOC at 30°N is smaller than one standard deviation from the mean. (b) Same as (a) but the barotropic streamfunction associated with the SPG strength .

seems to be dominated by the 15-65 year timescales (Figure 4.11g)).

On the centennial (65 year and longer) timescales there are several indicators that the ocean model is in a state of quasi-equalibrium, requiring around 45-75 years to set-up. Evidence for the quasi-equalibrium comes from the spectrum, the NAO integration coefficients (as noted earlier) and the cross-correlation analysis. As in the study of *Ba et al.* [2013], the salinity is the dominant factor for determining the density anomalies in the Labrador Sea.

4.8 Conclusions

This chapter continued the analysis of the 2000 year long stochastically forced (SF) model integration introduced in Chapter 3, describing the various timescales of variability. Further analysis of the integrated NAO technique identified different integration coefficients with different timescales. Through analysis of the power spectra of the AMOC at 30°N and the SPG strength the model output was divided into three different timescales: interannual (15 years and shorter), multidecadal (15-65 years) and centennial (65 years and longer). On the interannual timescales the first coefficient of the integrated NAO fit is the largest, suggesting a strong immediate response to the NAO. The response to the NAO forcing on these timescales is mainly driven by Ekman dynamics as in *Eden and Willebrand* [2001]. The SPG spins down for positive values of the NAO due to the topographic Sverdrup response to the wind forcing and the AMOC generates two anomalous overturning cells, a positive one centered at 30°N and a negative one centered at 52°N, these are mainly due to the effects of Ekman pumping and Ekman upwelling. The multidecadal (15-65 year) timescales have integrated NAO coefficients of the SPG strength that have the shape of approximately one period of a sinusoid. This multidecadal timescale is dominated by variability in the SPG with a period of around 25 years and can be related to density changes in the center of the gyre. The centennial timescale has integrated NAO coefficients that are all of positive and have nearly the same value. These integrated NAO coefficients are non-zero for the first 75 years in the reconstruction of the AMOC at 30°N and for the first 45 years of the SPG strength. Evidence from the centennial timescales suggests that the ocean model is in a quasi-equilibrium state on these timescales.

Using the method of integrating the NAO to investigate what is happening in an ocean model can be useful to gain insight on how the dynamics of the ocean model differ on the different timescales. This method could be applied to the results from

coupled atmosphere-ocean models and can be extended to include other atmospheric forcing patterns, for instance the East Atlantic Pattern or the Scandinavian pattern (*Barnston and Livezey* [1987]). This relatively simple method can be useful, without being computationally expensive, in making predictions as well as in inter-model comparisons. Another possible extension to this method could be to include some feedbacks between the atmosphere and ocean, leading to a dynamical system that is a simplified explanation of the ocean dynamics.

Chapter 5

Conclusions

5.1 Summary

With the increasing concern about climate change it is becoming more and more important to understand natural climate variability. The North Atlantic is a region that has a high potential for predictability on the decadal and longer timescales (*Boer* [2004]). Observational records of sea surface temperature (SST) on these timescales are relatively sparse especially at high latitudes but show a multidecadal signal in the North Atlantic. To gain better understanding of the multidecadal variability both proxy data and model output need to be considered. In this thesis multidecadal variability in the North Atlantic is investigated with a high latitude marine proxy (Chapter 2) and results from a global ocean model forced using the observed NAO index and a 2000 year long white noise NAO index are considered(Chapters 3 and 4).

Chapter 2 described an analysis of a coralline algae sample from the Aleutian Island chain, extending back to 1818 and is longer than the available instrumental record. The algal record, one of the first pieces of marine based proxies for this area, and the Mg/Ca ratio show a strong correlation of 0.85 to the February/March local SST on decadal timescales. The algal Mg/Ca also has a strong connection to the

Aleutian Low (Aleutian Low leading by 5 years) and provides one of the first marine based proxy evidence to link the atmospheric variability in the extra-tropical North Pacific to the North Atlantic (correlation of -0.87 to the JFM NAO index). Not only does the Algal Mg/Ca record provide a proxy for high latitude decadal atmospheric variability but it also proves to be a proxy for the AMV index on decadal timescales with a correlation of 0.6, significant at the 80% level.

The following two chapters try to answer the following questions: (i) Can multidecadal variability be generated by solely forcing the an ocean model with the NAO index? and (ii) Can an ocean model forced with a white noise NAO generate internal variability in the North Atlantic Ocean?

Chapter 3 begins, similar to the study *Eden and Jung* [2001] by forcing the OGCM, NEMO, with the observed NAO and was able to generate a multidecadal signal in the North Atlantic. The model shows a multidecadal signal similar to that found in the observations in the SSTs in the northern North Atlantic with a correlation of 0.73. Attention was then switched to a model integration forced with a 2000 year long white noise NAO index. The results show that the timescales of variability of the NAO index on long timescales can be directly seen in the resulting model data. The AMOC at 30°N and the SPG strength both respond to the NAO with a red noise spectrum but neither highlight any particular frequency of variability. The AMOC at 30°N and the SPG strength can be reconstructed by integrating 53 and 10 previous years of the NAO index respectively. Taking this idea further, the AMOC at 30°N and the SPG strength can also be reconstructed using a 7th order and a 5th order autoregressive (AR) process respectively, with the NAO index as the white noise forcing. Using AR processes to analyze the climate model output can be a useful tool for inter-model comparisons and prediction studies.

The following chapter, Chapter 4, examines the stochastically forced model integration in more details. From the power spectra of the AMOC at 30°N and the SPG

strength behaviour three different timescales are defined: an interannual timescale (15 years and shorter), a multidecadal timescale (15-65 years) and a centennial timescale (65 years and longer). The AMOC at 30°N does not have very strong power on the multidecadal timescale. The coefficients from the integrated NAO fit reflect the different beaviour on these different timescales. On the interannual timescale the first integrated NAO coefficient has a large value and the remaining are all near zero and the response of the ocean is mainly related to Ekman dynamics similar to *Eden and Willebrand* [2001]. On the multidecadal timescale the integrated NAO coefficients for the subpolar gyre strength reconstruction show a sinusoidal behavior with a period of about 25 years. On these multidecadal timescales the SPG strength is associated with density anomalies in the center of the subpolar gyre which lead a maximum in SPG strength by approximately 7 years. Similar to *Sutton and Allen* [1997] and *Alvarez-Garcia et al.* [2008] density anomalies mainly controlled by the temperature propagate around the subpolar gyre. These density anomalies are transported around the gyre circulating with a period of about 25-28 years. The variability on the centennial timescales, through evidence from the power spectra, integrated NAO coefficients and the cross correlation analysis show that ocean appears to be in a series of quasi-equalibrium states that require approximately 50 years to establish.

5.2 Outlook

Encrusting coralline algae have a common occurrence in mid- to high-latitudes and can live for a few centuries (*Halfar et al.* [2011]). Through their annual growth patterns, the coralline algae are well suited for high-resolution geochemical sampling (*Halfar et al.* [2007], *Williams et al.* [2010]) and have been shown to successfully reproduce both local temperature records *Hetzinger et al.* [2009] and salinity records (*Hetzinger et al.* [2013]). The sparsity of the available instrumental data in the mid-

to high-latitudes make coralline algae a valuable type of proxy to help increase the understanding of historical SST and surface salinity variability.

The statistical methods used in both chapters 3 and 4 give a nice and computationally inexpensive way to analyze ocean model data. The techniques used to investigate the NAO forced model integrations can easily be extended to examine more complex systems. For instance one can apply these methods to coupled atmosphere-ocean models and potentially include some coupled behaviour through a "dynamical systems like" setup. Also, in addition to the NAO, one can apply the same method of integrating the NAO to other atmospheric pattern like the East Atlantic Pattern or the Scandinavian Pattern (*Barnston and Livezey* [1987]). Through integrating the various time series from different atmospheric forcing patterns their relative importance can be measured from the integration coefficients. The simplicity and computational inexpensiveness of these analysis methods can easily be applied to model inter-comparision studies.

Bibliography

Adey, W., S. Lindstrom, M. Hommersand, and K. Müller (2008), The biogeographic origin of arctic endemic seaweeds: A thermogeographic view1, *Journal of Phycology*, *44*(6), 1384–1394.

Allan, R., and T. Ansell (2006), A new globally complete monthly historical gridded mean sea level pressure dataset (hadslp2): 1850-2004, *Journal of Climate*, *19*(22), 5816–5842.

Alvarez-Garcia, F., M. Latif, and A. Biastoch (2008), On multidecadal and quasi-decadal north atlantic variability, *Journal of Climate*, *21*(14), 3433–3452.

Ba, J., N. S. Keenlyside, W. Park, M. Latif, E. Hawkins, and H. Ding (2013), A mechanism for atlantic multidecadal variability in the kiel climate model, *Climate Dynamics*, pp. 1–12.

Barnier, B., G. Madec, T. Penduff, J. Molines, A. Treguier, J. Le Sommer, A. Beckmann, A. Biastoch, C. Böning, J. Dengg, et al. (2006), Impact of partial steps and momentum advection schemes in a global ocean circulation model at eddy-permitting resolution, *Ocean Dynamics*, *56*(5), 543–567, doi:10.1007/s10236-006-0082-1.

Barnston, A., and R. Livezey (1987), Classification, seasonality and persistence of low-frequency atmospheric circulation patterns, *Monthly Weather Review*, *115*(6), 1083–1126.

Bjerknes, J. (1964), Atlantic air-sea interaction, *Advances in geophysics*, *10*(1), 1–82.

Boer, G. J. (2004), Long time-scale potential predictability in an ensemble of coupled climate models, *Climate dynamics*, *23*(1), 29–44.

Böning, C. W., M. Scheinert, J. Dengg, A. Biastoch, and A. Funk (2006), Decadal variability of subpolar gyre transport and its reverberation in the north atlantic overturning, *Geophysical Research Letters*, *33*(21).

Born, A., and J. Mignot (2012), Dynamics of decadal variability in the atlantic subpolar gyre: a stochastically forced oscillator, *Climate dynamics*, *39*(1), 461–474, doi:10.1007/s00382-011-1180-4.

Broecker, W. S., et al. (1991), The great ocean conveyor, *Oceanography*, *4*(2), 79–89.

Bryden, H. L., H. R. Longworth, and S. A. Cunningham (2005), Slowing of the atlantic meridional overturning circulation at 25 n, *Nature*, *438*(7068), 655–657.

Chylek, P., C. Folland, H. Dijkstra, G. Lesins, and M. Dubey (2011), Ice-core data evidence for a prominent near 20 year time-scale of the Atlantic Multidecadal Oscillation, *Geophysical Research Letters*, *38*(13), L13,704, doi: 10.1029/2011GL047501.

Chylek, P., C. Folland, L. Frankcombe, H. Dijkstra, G. Lesins, and M. Dubey (2012), Greenland ice core evidence for spatial and temporal variability of the atlantic multidecadal oscillation, *Geophysical Research Letters*, *39*(9), doi: 10.1029/2012GL051241.

Cook, E. R. (2003), Multi-proxy reconstructions of the north atlantic oscillation (nao) index: A critical review and a new well-verified winter nao index reconstruction back to ad 1400, *Geophysical Monograph Series*, *134*, 63–79.

Cunningham, S. A., T. Kanzow, D. Rayner, M. O. Baringer, W. E. Johns, J. Marotzke, H. R. Longworth, E. M. Grant, J. J.-M. Hirschi, L. M. Beal, et al. (2007), Temporal variability of the atlantic meridional overturning circulation at 26.5 n, *science*, *317*(5840), 935–938.

Curry, R., and M. McCartney (2001), Ocean gyre circulation changes associated with the North Atlantic Oscillation, *Journal of Physical Oceanography*, *31*(12), 3374–3400.

Danabasoglu, G. (2008), On multidecadal variability of the atlantic meridional overturning circulation in the community climate system model version 3, *Journal of Climate*, *21*(21), 5524–5544.

D'Arrigo, R., R. Wilson, C. Deser, G. Wiles, E. Cook, R. Villalba, A. Tudhope, J. Cole, and B. Linsley (2005), Tropical-north pacific climate linkages over the past four centuries*, *Journal of Climate*, *18*(24), 5253–5265.

Delworth, T., and R. Greatbatch (2000), Multidecadal thermohaline circulation variability driven by atmospheric surface flux forcing, *Journal of Climate*, *13*(9), 1481–1495.

Delworth, T., and F. Zeng (2012), Multicentennial variability of the Atlantic meridional overturning circulation and its climatic influence in a 4000 year simulation of the GFDL CM2. 1 climate model, *Geophysical Research Letters*, *39*(13), L13,702, doi:10.1029/2012GL052107.

Delworth, T., S. Manabe, and R. Stouffer (1993), Interdecadal variations of the thermohaline circulation in a coupled ocean-atmosphere model, *Journal of Climate*, *6*(11), 1993–2011.

Deser, C., A. Phillips, and J. Hurrell (2004), Pacific interdecadal climate variability: Linkages between the tropics and the north pacific during boreal winter since 1900, *Journal of Climate*, *17*(16), 3109–3124.

Dickson, R., J. Lazier, J. Meincke, P. Rhines, and J. Swift (1996), Long-term coordinated changes in the convective activity of the North Atlantic, *Progress in Oceanography*, *38*(3), 241–295.

Dickson, R., T. Osborn, J. Hurrell, J. Meincke, J. Blindheim, B. Adlandsvik, T. Vinje, G. Alekseev, and W. Maslowski (2000), The Arctic Ocean response to the North Atlantic Oscillation, *Journal of Climate*, *13*(15), 2671–2696, doi: 10.1175/1520-0442(2000)013<2671:TAORTT>2.0.CO;2.

Dijkstra, H., L. Te Raa, M. Schmeits, and J. Gerrits (2006), On the physics of the Atlantic Multidecadal Oscillation, *Ocean Dynamics*, *56*(1), 36–50, doi: 10.1007/s10236-005-0043-0.

Dima, M., and G. Lohmann (2007), A hemispheric mechanism for the Atlantic Multidecadal Oscillation, *Journal of Climate*, *20*(11), 2706–2719, doi: 10.1175/JCLI4174.1.

Doblas-Reyes, F., I. Andreu-Burillo, Y. Chikamoto, J. García-Serrano, V. Guemas, M. Kimoto, T. Mochizuki, L. Rodrigues, and G. van Oldenborgh (2013), Initialized near-term regional climate change prediction, *Nature communications*, *4*, 1715.

Drinkwater, K., A. Belgrano, A. Borja, A. Conversi, M. Edwards, C. Greene, G. Ottersen, A. Pershing, and H. Walker (2003), The response of marine ecosystems to climate variability associated with the North Atlantic Oscillation, *Geophysical Monograph-American Geophysical Union*, *134*, 211–234.

dOrgeville, M., and W. Peltier (2007), On the pacific decadal oscillation and the atlantic multidecadal oscillation: Might they be related, *Geophysical Research Letters*, *34*(23), L23,705.

Eden, C., and R. J. Greatbatch (2003), A damped decadal oscillation in the north atlantic climate system, *Journal of climate*, *16*(24), 4043–4060.

Eden, C., and T. Jung (2001), North atlantic interdecadal variability: oceanic response to the North Atlantic Oscillation (1865-1997), *Journal of Climate*, *14*(5), 676–691, doi:10.1175/1520-0442(2001)014<0676:NAIVOR>2.0.CO;2.

Eden, C., and J. Willebrand (2001), Mechanism of interannual to decadal variability of the North Atlantic circulation, *Journal of Climate*, *14*(10), 2266–2280, doi: 10.1175/1520-0442(2001)014<2266:MOITDV>2.0.CO;2.

Eden, C., R. Greatbatch, and J. Lu (2002), Prospects for decadal prediction of the North Atlantic Oscillation (NAO), *Geophysical research letters*, *29*(10), 1466, doi:10.1029/2001GL014069.

Enfield, D., A. Mestas-Nunez, P. Trimble, et al. (2001), The atlantic multidecadal oscillation and its relation to rainfall and river flows in the continental U. S., *Geophysical Research Letters*, *28*(10), 2077–2080, doi:10.1029/2000GL012745.

Gent, P., and J. McWilliams (1990), Isopycnal mixing in ocean circulation models, *Journal of Physical Oceanography*, *20*(1), 150–155, doi:10.1029/2004GL019932.

Gilman, D., F. Fuglister, and J. Mitchell Jr (1963), On the power spectrum of red noise, *Journal of the Atmospheric Sciences*, *20*(2), 182–184.

Goldenberg, S., C. Landsea, A. Mestas-Nuñez, and W. Gray (2001), The recent increase in Atlantic hurricane activity: Causes and implications, *Science*, *293*(5529), 474–479, doi:10.1126/science.1060040.

Gray, S., L. Graumlich, J. Betancourt, and G. Pederson (2004), A tree-ring based reconstruction of the Atlantic Multidecadal Oscillation since 1567 AD, *Geophysical Research Letters*, *31*(12), L12,205, doi:10.1029/2004GL019932.

Greatbatch, R. (2000), The North Atlantic Oscillation, *Stochastic Environmental Research and Risk Assessment*, *14*(4), 213–242, doi:10.1007/s004770000047.

Greatbatch, R., and P. Rong (2006), Discrepancies between different Northern Hemisphere summer atmospheric data products, *Journal of Climate*, *19*(7), 1261–1273.

Greatbatch, R., and S. Zhang (1995), An interdecadal oscillation in an idealized ocean basin forced by constant heat flux, *Journal of Climate*, *8*(1), 81–91.

Grebmeier, J., J. Overland, S. Moore, E. Farley, E. Carmack, L. Cooper, K. Frey, J. Helle, F. McLaughlin, and S. McNutt (2006), A major ecosystem shift in the northern bering sea, *Science*, *311*(5766), 1461–1464.

Griffies, S., M. Winton, and B. Samuels (2004), The Large and Yeager (2004) dataset and CORE, *NOAA Geophysical Fluid Dynamics Laboratory PO Box*, *308*.

Griffies, S., A. Biastoch, C. Böning, F. Bryan, G. Danabasoglu, E. Chassignet, M. England, R. Gerdes, H. Haak, R. Hallberg, et al. (2009), Coordinated ocean-ice reference experiments (COREs), *Ocean Modelling*, *26*(1), 1–46, doi: 10.1016/j.ocemod.2008.08.007.

Griffies, S. M., and E. Tziperman (1995), A linear thermohaline oscillator driven by stochastic atmospheric forcing, *arXiv preprint ao-sci/9502002*.

Gulev, S. K., B. Barnier, H. Knochel, J.-M. Molines, and M. Cottet (2003), Water mass transformation in the north atlantic and its impact on the meridional circulation: Insights from an ocean model forced by ncep-ncar reanalysis surface fluxes, *Journal of climate*, *16*(19), 3085–3110.

Häkkinen, S. (1999), Variability of the simulated meridional heat transport in the north atlantic for the period 1951–1993, *Journal of Geophysical Research: Oceans (1978–2012)*, *104*(C5), 10,991–11,007.

Halfar, J., R. Steneck, B. Schöne, G. Moore, M. Joachimski, A. Kronz, J. Fietzke, and J. Estes (2007), Coralline alga reveals first marine record of subarctic north pacific climate change, *Geophysical Research Letters*, *34*(7), L07,702.

Halfar, J., B. Williams, S. Hetzinger, R. Steneck, P. Lebednik, C. Winsborough, A. Omar, P. Chan, and A. Wanamaker Jr (2011), 225 years of bering sea climate and ecosystem dynamics revealed by coralline algal growth-increment widths, *Geology*, *39*(6), 579–582.

Hasselmann, K. (1976), Stochastic climate models, *Tellus*, *28*(6), 31–762,896.

Hetzinger, S., M. Pfeiffer, W.-C. Dullo, N. Keenlyside, M. Latif, and J. Zinke (2008), Caribbean coral tracks atlantic multidecadal oscillation and past hurricane activity, *Geology*, *36*(1), 11–14.

Hetzinger, S., J. Halfar, A. Kronz, R. Steneck, W. Adey, P. Lebednik, and B. Schöne (2009), High-resolution mg/ca ratios in a coralline red alga as a proxy for bering sea temperature variations from 1902 to 1967, *Palaios*, *24*(6), 406–412.

Hetzinger, S., J. Halfar, J. Mecking, N. Keenlyside, A. Kronz, R. Steneck, W. Adey, and P. Lebednik (2012), Marine proxy evidence linking decadal north pacific and atlantic climate, *Climate Dynamics*, *39*(6), 1447–1455, doi:10.1007/s00382-011-1229-4.

Hetzinger, S., J. Halfar, T. Zack, J. Mecking, B. Kunz, D. Jacob, and W. Adey (2013), Coralline algal barium as indicator for 20th century northwestern north atlantic surface ocean freshwater variability, *Scientific Reports*, *3*.

Honda, M., H. Nakamura, J. Ukita, I. Kousaka, and K. Takeuchi (2001), Interannual seesaw between the aleutian and icelandic lows. part i: Seasonal dependence and life cycle, *Journal of climate*, *14*(6), 1029–1042.

Honda, M., S. Yamane, and H. Nakamura (2005), Impacts of the aleutian-icelandic low seesaw on surface climate during the twentieth century, *Journal of climate*, *18*(14), 2793–2802.

Hurrell, J. (1995), Decadal trends in the north atlantic oscillation: regional temperatures and precipitation, *Science*, *269*(5224), 676–678, doi:10.1126/science.269.5224.676.

Hurrell, J. (1996), Influence of variations in extratropical wintertime teleconnections on northern hemisphere temperature, *Geophysical Research Letters*, *23*(6), 665–668.

Hurrell, J., Y. Kushnir, G. Ottersen, and M. Visbeck (2003), *The North Atlantic Oscillation: climatic significance and environmental impact*, vol. 134, 1–34 pp., American Geophysical Union.

Jarosewich, E., and I. MacIntyre (1983), Carbonate reference samples for electron microprobe and scanning electron microscope analyses, *Journal of Sedimentary Research*, *53*(2), 677–678.

Jones, P., T. Jonsson, and D. Wheeler (1997), Extension to the north atlantic oscillation using early instrumental pressure observations from gibraltar and south-west iceland, *International Journal of Climatology*, *17*(13), 1433–1450.

Jones, P. D., T. J. Osborn, and K. R. Briffa (2003), Pressure-based measures of the north atlantic oscillation (nao): A comparison and an assessment of changes in the strength of the nao and in its influence on surface climate parameters, *Geophysical Monograph Series*, *134*, 51–62.

Jungclaus, J., H. Haak, M. Latif, and U. Mikolajewicz (2005), Arctic-North Atlantic interactions and multidecadal variability of the meridional overturning circulation, *Journal of climate*, *18*(19), 4013–4031, doi:10.1175/JCLI3462.1.

Keenlyside, N., M. Latif, J. Jungclaus, L. Kornblueh, and E. Roeckner (2008), Advancing decadal-scale climate prediction in the north atlantic sector, *Nature*, *453*(7191), 84–88.

Keenlyside, N. S., and J. Ba (2010), Prospects for decadal climate prediction, *Wiley Interdisciplinary Reviews: Climate Change*, *1*(5), 627–635.

Kerr, R. (2000), A north atlantic climate pacemaker for the centuries, *Science*, *288*(5473), 1984–1985, doi:10.1126/science.288.5473.1984.

Kilbourne, K., T. Quinn, R. Webb, T. Guilderson, J. Nyberg, and A. Winter (2008), Paleoclimate proxy perspective on caribbean climate since the year 1751: Evidence of cooler temperatures and multidecadal variability, *Paleoceanography*, *23*(3), PA3220, doi:10.1029/2008PA001598.

Knight, J., R. Allan, C. Folland, M. Vellinga, and M. Mann (2005), A signature of persistent natural thermohaline circulation cycles in observed climate, *Geophysical Research Letters*, *32*(20), 2–5, doi:10.1029/2005GL024233.

Köller, M., R. Käse, and P. Herrmann (2010), Interannual to multidecadal variability and predictability of North Atlantic circulation in a coupled earth system model with parametrized hydraulics, *Tellus A*, *62*(4), 569–578, doi:10.1111/j.1600-0870.2010.00450.x.

Kwon, Y., and C. Frankignoul (2012), Stochastically-driven multidecadal variability of the Atlantic meridional overturning circulation in CCSM3, *Climate dynamics*, *38*(5), 859–876, doi:10.1007/s00382-011-1040-2.

Langehaug, H., I. Medhaug, T. Eldevik, and O. Otterå (2012), Arctic/Atlantic exchanges via the subpolar gyre, *Journal of Climate*, *25*(7), 2421–2439, doi:10.1175/JCLI-D-11-00085.1.

Large, W., and S. Yeager (2004), *Diurnal to decadal global forcing for ocean and sea-ice models: the data sets and flux climatologies*, National Center for Atmospheric Research.

Large, W., and S. Yeager (2009), The global climatology of an interannually varying air–sea flux data set, *Climate Dynamics*, *33*(2), 341–364, doi:10.1007/s00382-008-0441-3.

Latif, M., and T. Barnett (1994), Causes of decadal climate variability over the north pacific and north america, *Science*, *266*(5185), 634–637.

Latif, M., and N. S. Keenlyside (2011), A perspective on decadal climate variability and predictability, *Deep Sea Research Part II: Topical Studies in Oceanography*, *58*(17), 1880–1894.

Latif, M., E. Roeckner, M. Botzet, M. Esch, H. Haak, S. Hagemann, J. Jungclaus, S. Legutke, S. Marsland, U. Mikolajewicz, et al. (2004), Reconstructing, monitoring, and predicting multidecadal-scale changes in the north atlantic thermohaline circulation with sea surface temperature, *Journal of Climate*, *17*(7), 1605–1614.

Latif, M., C. Böning, J. Willebrand, A. Biastoch, J. Dengg, N. Keenlyside, U. Schweckendiek, and G. Madec (2006), Is the thermohaline circulation changing?, *Journal of Climate*, *19*(18), 4631–4637, doi:10.1175/JCLI3876.1.

Lebednik, P. (1977), The corallinaceae of northwestern north america. i. clathromorphum foslie emend. adey, *Syesis*, *9*(1976), 59–112.

Liu, Z., L. Wu, R. Gallimore, and R. Jacob (2002), Search for the origins of pacific decadal climate variability, *Geophysical research letters*, *29*(10), 42–1.

Lohmann, K., H. Drange, and M. Bentsen (2009), A possible mechanism for the strong weakening of the North Atlantic subpolar gyre in the mid-1990s, *Geophysical Research Letters*, *36*(15), L15,602, doi:10.1029/2009GL039166.

Luterbacher, J., E. Xoplaki, D. Dietrich, P. Jones, T. Davies, D. Portis, J. Gonzalez-Rouco, H. Von Storch, D. Gyalistras, C. Casty, et al. (2001), Extending north atlantic oscillation reconstructions back to 1500, *Atmospheric Science Letters*, *2*(1-4), 114–124.

MacDonald, G., and R. Case (2005), Variations in the pacific decadal oscillation over the past millennium, *Geophysical Research Letters*, *32*(8), L08,703.

Madec, G., P. Delecluse, M. Imbard, C. Lévy, et al. (1998), Opa 8.1 ocean general circulation model reference manual, *Note du Pôle de modélisation, Institut Pierre-Simon Laplace*, *11*.

Mantua, N., S. Hare, Y. Zhang, J. Wallace, R. Francis, et al. (1997), A pacific interdecadal climate oscillation with impacts on salmon production, *Bulletin of the American Meteorological Society*, *78*(6), 1069–1080.

McCabe, G. J., M. A. Palecki, and J. L. Betancourt (2004), Pacific and atlantic ocean influences on multidecadal drought frequency in the united states, *Proceedings of the National Academy of Sciences*, *101*(12), 4136–4141.

Medhaug, I., H. Langehaug, T. Eldevik, T. Furevik, and M. Bentsen (2012), Mechanisms for decadal scale variability in a simulated Atlantic meridional overturning circulation, *Climate dynamics*, *39*(1–2), 77–93, doi:10.1007/s00382-011-1124-z.

Menary, M., W. Park, K. Lohmann, M. Vellinga, M. Palmer, M. Latif, and J. Jungclaus (2012), A multimodel comparison of centennial Atlantic meridional overturning circulation variability, *Climate dynamics*, *38*(11), 2377–2388, doi:10.1007/s00382-011-1172-4.

Moberly Jr, R. (1968), Composition of magnesian calcites of algae and pelecypods by electron microprobe analysis1, *Sedimentology*, *11*(1-2), 61–82.

Msadek, R., and C. Frankignoul (2009), Atlantic multidecadal oceanic variability and its influence on the atmosphere in a climate model, *Climate dynamics*, *33*(1), 45–62, doi:10.1007/s00382-008-0452-0.

Müller, W., C. Frankignoul, and N. Chouaib (2008), Observed decadal tropical pacific–north atlantic teleconnections, *Geophysical Research Letters*, *35*(24), L24,810.

Munk, W. H. (1950), On the wind-driven ocean circulation, *J. Meteor*, *7*(2), 79–93.

Ortega, P., E. Hawkins, and R. Sutton (2011), Processes governing the predictability of the Atlantic meridional overturning circulation in a coupled gcm, *Climate dynamics*, *37*(9), 1771–1782, doi:10.1007/s00382-011-1025-1.

Overland, J., and P. Stabeno (2004), Is the climate of the bering sea warming and affecting the ecosystem, *Eos*, *85*(33), 309–316.

Paillard, D., L. Labeyrie, and P. Yiou (1996), Macintosh program performs time-series analysis, *Eos Transactions*, *77*, 379–379.

Park, W., and M. Latif (2010), Pacific and atlantic multidecadal variability in the kiel climate model, *Geophysical Research Letters*, *37*, L24,702.

Park, W., and M. Latif (2011), Atlantic meridional overturning circulation response to idealized external forcing, *Climate Dynamics*, *39*(7–8), 1709–1726, doi: 10.1007/s00382-011-1212-0.

Rahmstorf, S. (2002), Ocean circulation and climate during the past 120,000 years, *Nature*, *419*(6903), 207–214.

Rayner, N., D. Parker, E. Horton, C. Folland, L. Alexander, D. Rowell, E. Kent, and A. Kaplan (2003), Global analyses of sea surface temperature, sea ice, and night marine air temperature since the late nineteenth century, *Journal of Geophysical Research*, *108*(D14), 4407, doi:10.1029/2002JD002670.

Saenger, C., A. L. Cohen, D. W. Oppo, R. B. Halley, and J. E. Carilli (2009), Surface-temperature trends and variability in the low-latitude north atlantic since 1552, *Nature Geoscience*, *2*(7), 492–495, doi:10.1038/ngeo552.

Schneider, N., A. J. Miller, and D. W. Pierce (2002), Anatomy of north pacific decadal variability, *Journal of climate*, *15*(6), 586–605.

Schwing, F., J. Jiang, and R. Mendelssohn (2003), Coherency of multi-scale abrupt changes between the nao, npi, and pdo, *Geophysical Research Letters*, *30*(7), 1406.

Shumway, R. H., D. S. Stoffer, and D. S. Stoffer (2000), *Time series analysis and its applications*, vol. 549, Springer New York.

Sigler, M., H. Harvey, J. Ashjian, M. Lomas, J. Napp, P. Stabeno, and T. Van Pelt (2010), How does climate change affect the bering sea ecosystem?, *Eos, Transactions American Geophysical Union*, *91*(48), 457.

Stommel, H. (1948), The westward intensification of wind-driven ocean currents, *Trans. Amer. Geophys. Union*, *29*(2), 202–206.

Sutton, R., and M. Allen (1997), Decadal predictability of north atlantic sea surface temperature and climate, *Nature*, *388*(6642), 563–567.

Sverdrup, H. U. (1947), Wind-driven currents in a baroclinic ocean; with application to the equatorial currents of the eastern pacific, *Proceedings of the National Academy of Sciences of the United States of America*, *33*(11), 318.

The Drakkar Group (2007), Eddy-permitting ocean circulation hindcasts of past decades, *Clivar Exchanges*, (12), 8–10.

Thompson, D., and J. Wallace (1998), The arctic oscillation signature in the wintertime geopotential height and temperature fields, *Geophysical Research Letters*, *25*(9), 1297–1300.

Timmermann, A., M. Latif, R. Voss, and A. Grötzner (1998), Northern hemispheric interdecadal variability: a coupled air-sea mode, *Journal of Climate*, *11*(8), 1906–1931.

Torrence, C., and G. Compo (1998), A practical guide to wavelet analysis, *Bulletin of the American Meteorological society*, *79*(1), 61–78.

Trenberth, K., and J. Hurrell (1994), Decadal atmosphere-ocean variations in the pacific, *Climate Dynamics*, *9*(6), 303–319.

Vellinga, M., and P. Wu (2004), Low-latitude freshwater influence on centennial variability of the atlantic thermohaline circulation, *Journal of Climate*, *17*(23), 4498–4511, doi:10.1175/3219.1.

Visbeck, M., H. Cullen, G. Krahmann, and N. Naik (1998), Ocean model's response to north atlantic oscillation-like wind forcing, *Geophysical Research Letters*, *25*(24), 4521–4524.

Visbeck, M., E. Chassignet, R. Curry, T. Delworth, R. Dickson, and G. Krahmann (2003), The ocean's response to north atlantic oscillation variability, *Geophysical Monograph-American Geophysical Union*, *134*, 113–146.

Von Storch, H., and F. W. Zwiers (2002), *Statistical analysis in climate research*, Cambridge University Press.

Walker, S. G. T. (1924), *Correlation in Seasonal Variations of Weather, IX: Further Study of World-weather*, Meteorological Office.

Wallace, J., and D. Gutzler (1981), Téléconnexions in the geopotential height field during the northern hemisphere winter, *Mon. Wea. Rev*, *109*, 784–812.

Williams, B., J. Halfar, R. Steneck, U. Wortmann, S. Hetzinger, W. Adey, P. Lebednik, and M. Joachimski (2010), Twentieth century δ 13 c variability in surface water dissolved inorganic carbon recorded by coralline algae in the northern north pacific ocean and the bering sea, *Biogeosciences Discuss*, *7*, 5801–5828.

Wunsch, C. (1999), The interpretation of short climate records, with comments on the north atlantic and southern oscillations, *Bulletin-American Meteorological Society*, *80*, 245–256, doi:10.1175/1520-0477(1999)080<0245:TIOSCR>2.0.CO;2.

Wunsch, C. (2005), The total meridional heat flux and its oceanic and atmospheric partition, *Journal of climate*, *18*(21), 4374–4380.

Wunsch, C. (2012), Covariances and linear predictability of the atlantic ocean, *Deep Sea Research Part II: Topical Studies in Oceanography*.

Wunsch, C., et al. (2002), What is the thermohaline circulation, *Science*, *298*(5596), 1179–1181.

Yeager, S., A. Karspeck, G. Danabasoglu, J. Tribbia, and H. Teng (2012), A decadal prediction case study: Late twentieth-century north atlantic ocean heat content, *Journal of Climate*, *25*(15), 5173–5189.

Zhang, R. (2008), Coherent surface-subsurface fingerprint of the atlantic meridional overturning circulation, *Geophysical Research Letters*, *35*(20).

Zhang, R., and T. Delworth (2006), Impact of atlantic multidecadal oscillations on india/sahel rainfall and atlantic hurricanes, *Geophysical Research Letters*, *33*(17), L17,712, doi:10.1029/2006GL026267.

Zhang, R., and T. Delworth (2007), Impact of the atlantic multidecadal oscillation on north pacific climate variability, *Geophys. Res. Lett*, *34*, L23,708.

Publications

1. **Mecking, J.V.**, N. Keenlyside, and R.J. Greatbatch (2013) Stochastically-forced multidecadal variability in the North Atlantic: A model study, Climate Dynamics, submitted.

2. Hetzinger, S., J. Halfar, T. Zack, **J.V. Mecking**, B. Kunz, D. Jacob, and W. Adey (2013), Coralline algal barium as indicator for 20th century northwestern north atlantic surface ocean freshwater variability, Scientific Reports, 3, doi:10.1038/srep01761.

3. Hetzinger, S., J. Halfar, **J.V. Mecking**, N. Keenlyside, A. Kronz, R. Steneck, W. Adey, and P. Lebednik (2012), Marine proxy evidence linking decadal north pacific and atlantic climate, Climate Dynamics, 39(6), 14471455, doi:10.1007/s00382-011- 1229-4.

Acknowledgments

First and most importantly, I would like to thank my supervisors Prof. Dr. Noel Keenlyside and Prof. Dr. Richard Greatbatch for their help and guidance. Especially, for their time and support when life got rough, deadlines approached too quickly or when I just needed encouragement.

Over the years I have had a lot of help, useful conversations and encouragements from colleges and friends from near and afar (via instant messenger). Special thanks goes to Dr. Steffen Hetzinger, Dr. Wonsun Park, Prof. Dr. Mojib Latif, Dr. Nour-Eddine Omrani, Dr. Vladimir Semenov and Dr. Markus Scheinert for fruitful conversations about my work and technical support with the ocean modelling. Dr. Jin Ba, Dr. Wan-Ling Tseng and Stephanie Gleixner for being the best officemates ever. Also, Ralf Hand, Alja Bielke and Stephanie Gleixner need a big thank you for all the help when the German language and bureaucracy was too difficult for me. Lastly, thanks to my entire research division at GEOMAR for the very friendly work environment.

This project received funding from the Deutsche Forschungsgemeinshaft under the Emmy Noether program. Also, thanks to the HLRN computing facility for allowing me to perform all my model experiments there and the friendly Dr. Matthias Läuter for his patience.

Finally, keeping sane during the almost five years wouldn't have been possible without friends to have fun with outside of work. In particular, a big thanks to all the people from Taekwondo at the Kang Center.

Erklärung

Hiermit erkläre ich, dass ich die vorliegende Dissertation, abgesehen von der Beratung durch meine akademischen Lehrer, selbstständig verfasst habe und keine weiteren Quellen und Hilfsmittel als die hier angegebenen verwendet habe. Diese Arbeit hat weder ganz, noch in Teilen, bereits an anderer Stelle einer Prüfungskommission zur Erlangung des Doktorgrades vorgelegen. Ich erkläre, dass die vorliegende Arbeit gemäß der Grundsätze zur Sicherung guter wissenschaftlicher Praxis der Deutschen Forschungsgemeinschaft erstellt wurde.

Kiel, May 11, 2013

(Jennifer Veronika Mecking)